The oxygen isotope composition of the country rock of the Koegel Fontein igneous complex

Dissertation presented for the degree of Master of Science

in the Department of Geological Sciences,

University of Cape Town

December 2017

By

Benjamin Whitehead

Supervised by

Chris Harris and Alastair Sloan

Declaration

I, Benjamin Whitehead, hereby declare that the work on which this dissertation/thesis is based is my original work (except where acknowledgements indicate otherwise) and that neither the whole work nor any part of it has been, is being, or is to be submitted for another degree in this or any other university.

I empower the university to reproduce for the purpose of research either the whole or any portion of the contents in any manner whatsoever.

Signature: ……

Date: December 2017

Acknowledgements

This project would not have been possible without the guidance and resources generously provided by my supervisors Chris Harris and Alastair Sloan and funding provided by the NRF through Chris Harris. Credit goes to Sherissa Roopnarain for analysing a large portion of my samples in the stable isotope lab at the UCT Department of Geological Sciences, Silvio Elias, whose sand-driving skills were invaluable on one of the field trips and Simon Schorn, who helped out with the calculation and interpretation of pseudosections. I would like to thank Coenie de Beer, who supplied detailed unpublished geological maps and gave me advice at the Council for Geoscience. Branko Corner was very helpful and supplied geophysical filter products in the form of geotiffs files and guided me on how to interpret them. I would also like to thank Hartwig Frimmel for dialogue about glaciations and Pan-African deformation in the field area. I am grateful to Adele and Albie Pool, who provided accommodation at their wonderful Koëlfontein cottage and I thank Farmer Braam for access to his property.

Abstract

The Koegel Fontein Complex is a Cretaceous anorogenic complex located in southern Namaqualand, west of Bitterfontein, South Africa. The complex comprises a large granite intrusion (the Rietpoort Granite), a series of NW-striking quartz porphyry dykes, and numerous other minor igneous bodies. A breccia plug, and the quartz porphyry dykes have $\delta^{18}O$ values as low as -4.1‰, and these are believed to be the result of selective dehydration and melting of previously ^{18}O-depleted rock (Curtis et al., 2013; Olianti and Harris, 2018). This thesis investigates the oxygen isotope composition of the country rock of the Koegel Fontein Complex, which consists of Namaqua-Natal Belt granulite facies rock and minor remnants of overlying Gariep Supergroup metasedimentary rock. The Brak Fontein Shear Zone (BFSZ) is investigated as a protolith for low $\delta^{18}O$ (<6 ‰) units of the Koegel Fontein Complex.

Geological mapping combined with oxygen isotope data of the country rock confirms that ^{18}O-depletion occurred prior to the emplacement of the Koegel Fontein Complex and is localised in the ~545 Ma BFSZ. Generation of rock with $\delta^{18}O$ values as low as -4 ‰ requires a combination of high temperature water-rock interaction, a high water-rock ratio and very low $\delta^{18}O$ values in the alteration fluid. Deformation in the BFSZ coincides with the Pan-African Orogeny and a 549-545 Ma global glaciation, and it is reasonable to assume that ambient meteoric water had a very low $\delta^{18}O$ value, perhaps as low as -30 ‰. Assuming a possible $\Delta_{rock\text{-}water}$ range from 0.5 to 2.8, a $\delta^{18}O$ value of 8‰ for the rock before alteration, a $\delta^{18}O$ value of -2‰ for the rock after alteration, a $\delta^{18}O$ value of -30‰ for the fluid before fluid-rock exchange and exchange at a temperature range of 400°C to 700°C, a water-rock ratio of ~0.31 to ~0.40 is required to create the observed ^{18}O-depletion in the BFSZ. The calculated water-rock ratio suggests that a significant amount of meteoric water passed through the BFSZ, into the brittle-ductile transition zone.

A cold climate only coincides with a suitable tectonic setting during the Pan-African Orogeny, suggesting that the ^{18}O-depletion is syn-tectonic. Furthermore, strong recrystalisation and annealing after deformation and a lack of brittle overprint or cross-cutting fractures and/or veins suggest a low permeability in the BFSZ after the Pan-African deformation. Therefore ^{18}O-depletion in the BFSZ must have occurred during the Pan-African Orogeny and may be evidence for the infiltration of meteoric water into the ductile crust, possibly requiring variable strain rates or seismic pumping.

Table of Contents

1. Project Overview

1.1. Introduction

The Koegel Fontein Complex is a Cretaceous igneous complex which was emplaced into Proterozoic country rock of the Namaqua-Natal Metamorphic Belt along the west coast of South Africa (Figure 2). The youngest unit of the Koegel Fontein Complex, the Rietpoort Granite, is presumed to form a lopolith-shaped intrusion with a diameter of 20 km (Curtis et al., 2011). Dykes, quartz veins and a breccia plug of the Koegel Fontein Complex cross-cut its country rock and roof pendant, but are in turn cross-cut by the Rietpoort Granite. Previous work done on the Koegel Fontein Complex yielded an abundance of rocks with negative $\delta^{18}O$ values among felsic dykes of the complex, a breccia plug, Cretaceous veins and in its country rock (Curtis et al., 2013). Rocks with $\delta^{18}O$ values below 6‰, the $\delta^{18}O$ value of the Mantle are considered low $\delta^{18}O$ value rocks. It was suggested that low $\delta^{18}O$ magmas formed by selective melting of low $\delta^{18}O$ rock which was hydrothermally during a ~547 Ma global glaciation (Olianti and Harris, 2018).

Figure 1. The view down Brakfonteinkloof at the Northern Cape – Western Cape boundary. The field area's rolling hills and arid shrubs are typical for the west-coast of South Africa. Taken at 30.972064°S 17.877799°E facing west.

Evidence for a low $\delta^{18}O$ protolith may be found in ^{18}O-depletion in the country rock of the Koegel Fontein Complex. The country rock is primarily made up of granitic gneiss and subordinate supracrustals of the Namaqua-Natal Belt and minor outcrops of metasedimentary rocks of the Gariep Supergroup. In the study area the Gariep Supergroup and the Namaqua-Natal Belt basement where mineralogically and texturally overprinted by the ~545 Ma Pan-African Orogeny. A west-dipping shear zone, from here on called the Brak Fontein Shear Zone (BFSZ), is cross-cut by the Koegel Fontein Complex and may be associated with ^{18}O-depletion.

The aims of this project are to use oxygen isotope geochemistry in combination with geological constraints to:

- Investigate the spatial distribution and variation in $\delta^{18}O$ values in the different country rock types surrounding the Koegel Fontein Complex.
- Investigate the relationship between ^{18}O-depletion and the BFSZ.
- Investigate the probable cause(s) of low $\delta^{18}O$ values, including constraining the water/rock ratio and source of the fluid, as well as the timing and temperature of the fluid-rock interaction event(s).

1.2. Regional Geology

The field area is located approximately 50 km west of Bitterfontein at the boundary of the Northern and the Western Cape. The geology of the area is comprised of Mokolian (2050-900 Ma) rocks belonging to the Namaqua-Natal Metamorphic Belt, Namibian (900-542 Ma) rocks belonging to the Gariep and Vanrhynsdorp Groups, Cretaceous igneous rocks including 130-135 Ma regional dolerite dykes (Trumbull et al., 2007) and the ~135 Ma Koegel Fontein Complex (Curtis et al., 2011), the Paleogene, ~50 Ma Sandkopsdrif Complex and the Neogene (24 Ma-present) West Coast Group (Table 1 and Figure 2). A brief description of the geology of the field area follows. A more detailed description can be found in the 3017 Garies map explanation (de Beer, 2010).

The 2200-1000 Ma Namaqua-Natal metamorphic belt follows the coastline from southern Namibia to Natal through Namaqualand and the Karoo, where it is covered by the Cape and Karoo supergroups. The field area is situated in the Bushmanland Terrane, where granulite facies metamorphism occurred during the Namaqua-Natal Orogeny (Bial et al., 2015). The oldest rocks are metasedimentary rocks of the Kamiesberg Group. The Little Namaqualand Suite contains granitic gneisses. The Spektakel Suite is a syn- to post-tectonic granitic phase

of the Namaqua-Natal Belt and therefore shows little metamorphic and textural overprint from the Namaqua-Natal Orogeny. The Namaqua-Natal Metamorphic Belt is characterised by ductile deformation and five known deformation events (de Beer, 2010). D1 is poorly preserved and has been strongly overprinted. During the main D2 deformation event, a dominant S2 fabric with a shallowly dipping to subhorizontal orientation developed. The S1 fabric was transposed into parallelism to S2 by isoclinal F2 folding. During D3 the S2 fabric was folded into ENE-trending, open F3 folds. The F3 folds were then folded during D4 deformation by NW-striking F4 folds. The dominant S2 fabric is folded by F3 and F4 to form a dome and basin interference pattern, however F3 is dominant. D4 was accompanied by subhorizontal, ductile, metre wide shear zones. D5 is extension related to post-orogenic collapse, believed to be have resulted in the intrusion of the Spektakel Suite.

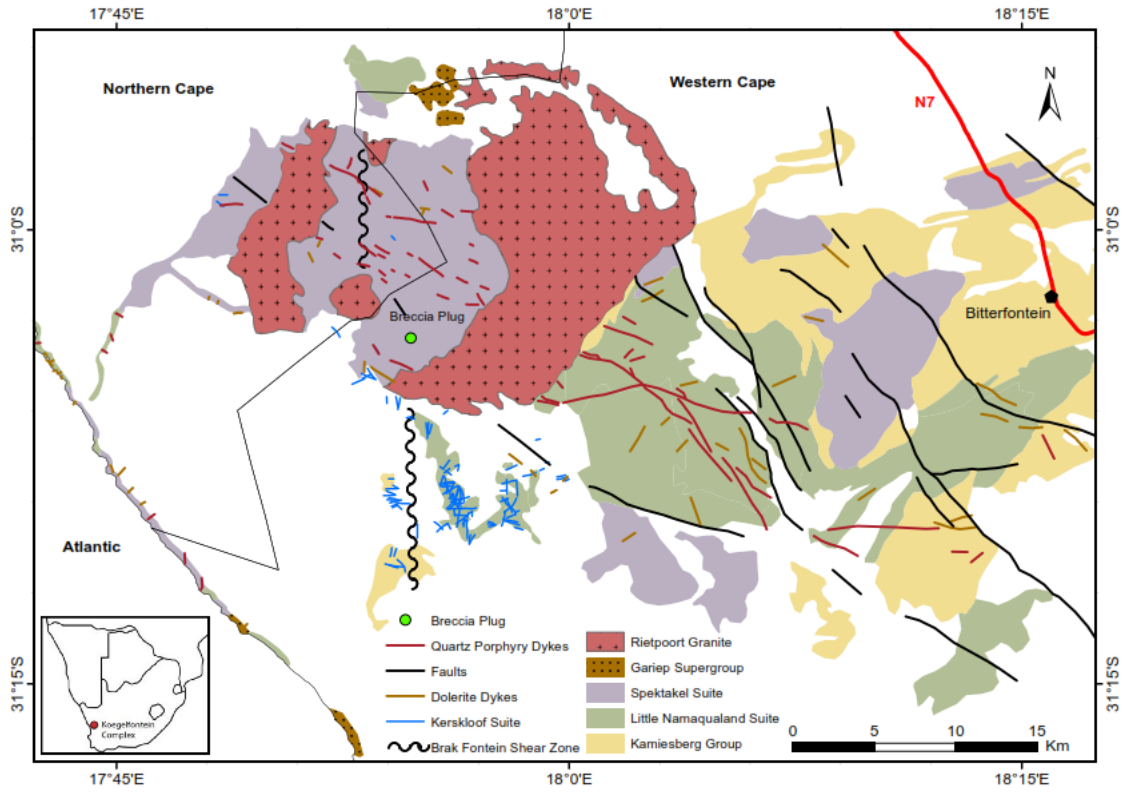

Figure 2. Simplified geology of the study area. The Kamiesberg Group, Little Namaqualand Suite and Spektakel Suite are the oldest and most abundant units in the field area and form part of the Namaqua-Natal Metamorphic Belt. Gariep Supergroup sediments were deposited unconformably before the field area experienced Pan-African deformation. The moderately west-dipping Brak Fontein Shear Zone is cross-cut by the Rietpoort Granite. During extension in the Cretaceous, regional dolerite dykes as well as the Kerskloof Suite dykes, quartz porphyry dykes, a breccia plug and the Rietpoort Granite of the Koegel Fontein Complex were emplaced. The Rietpoort Granite pluton forms the youngest and largest unit of the Koegel Fontein Complex and is interpreted to be lopolith-shaped intrusion with a roof pendant. Compiled from 3017 Garies, 3018 Loeriesfontein and 3118 Calvinia (de Beer, 2010, 2001; Macey and Minnaar, 2010).

Table 1. Simplified geological sequence of the field area. Gaps in the geological record are represented by horizontal double lines. The ages are taken from [(1)] the 3017 Garies map explanation (de Beer, 2010)*, [(2)]* Curtis et al. (2011)*, [(3)]* Trumbull et al. (2007) *and [(4)]* Fölling and Frimmel (2002)*.*

Age	Volcanic and Sedimentary Rocks	Intrusive Rocks	
Neogene	**West Coast Group**		
Paleogene		**Sandkopsdrif Complex**	
Cretaceous		**Koegel Fontein Complex:** *Rietpoort Granite (133.9 ± 1 Ma)[(2)]* *Kruisvlei Quartz Porphyry (133.9 ± 1 Ma)[(2)]* *Breccia Plug* *Kerskloof Bostonite* *Rooivleitjie Granite* *Sandkop Syenite (144.4 ± 2 Ma)[(2)]*	
		False Bay Dolerite Suite (130 – 135 Ma)[(3)]	↙*Cape Orogeny (~260 Ma)*
Namibian	***Giftberg Group*** **(Gariep Supergroup)** *Aties Formation* *Widouw Formation (555 ± 28 Ma)[(4)]* *Karoetjes Kop Formation*		↖*Pan-African Orogeny (~545 Ma)*
Mokolian	**Namaqua-Natal Belt**		
	Kamiesberg Group (~1.1 - ~1.3 Ga)[(1)]	*Spektakel Suite (~1.08 - ~1.03 Ga)[(1)]* *Little Namaqualand Suite (~1.15 Ga)[(1)]*	←*Namaqua Natal Orogeny (~1030 Ma)*

Following the Namaqua-Natal Orogeny, the Gifberg Group of the Gariep Supergroup was deposited into the Adamastor Ocean, on top of the Namaqua-Natal Basement. The Gifberg Group contains various sedimentary rocks including a basal diamictite (Karoetjes Kop Formation) and an overlying cap carbonate sequence (Widouw Formation). Diamictites and cap carbonates can be evidence for global glaciations as described by Hoffman and Schrag (2002). Diamictites and cap carbonates along the western margin of southern Africa are recognised as evidence for a ~750 Ma Sturtian and a ~580 Ma Marinoan glaciation (Fölling and Frimmel, 2002; Frimmel et al., 2002). Glacial pavements, striated clasts and diamictites in the Klein Karas Mountains are evidence for the 549-545 Ma Vingerbreek glaciation, which is believed to have caused a eustatic sea level fall and a regional unconformity (Germs and Gaucher, 2012). The Widouw Formation has been correlated with the 555 ± 28 Ma Bloeddrif Member (Fölling and Frimmel, 2002).

During the Pan-African Orogeny peak conditions were reached at 545 ± 2 Ma, when SW-directed oblique collision of the Rio de la Plata Craton with the Kalahari Craton resulted in west-directed thrusting and north-striking sinistral strike-slip shear zones (Frimmel and Frank, 1998). In the study area the Namaqua-Natal Belt basement was tectonically and mineralogically overprinted. Pan-African re-foliation is accompanied by the formation of chlorite/ biotite-garnet ± epidote schist in the Mesklip Gneiss and garnet-biotite-muscovite ± kyanite ± staurolite schist in metapelites of the Kamiesberg Group (de Beer, 2010). Frimmel and Frank (1998) $^{40}Ar/^{39}Ar$-dated cleavage forming muscovite in the south of the field area, near the Salt River. The cleavage is described as a crenulation cleavage orientated at ~275/45, which formed in granitic gneisses and metapelites of the Namaqua-Natal Belt due to Pan-African deformation. Ages of 495 – 506 Ma were determined, however these ages may represent cooling below the closure temperature of 410-430°C for muscovite and may post-date cleavage formation.

The 290 – 220 Ma Cape Orogeny is unlikely to have affected the field area significantly. The Cape Fold Belt is exposed ~100 km south of the field area. Temperatures of up to 300°C were reached in the base of the Cape Supergroup ~500 km to the SW (Frimmel et al., 2001). Closer to the field area however, the peak metamorphic temperatures and deformation are expected to be significantly lower. It is unlikely that the Cape Orogeny had a significant thermal or tectonic effect on the field area.

As the breakup of Gondwana initiated in the Cretaceous, the western edge of the Kalahari Craton experienced WSW-directed extension. Rifting and associated magmatism utilised Pan-African structures (Will and Frimmel, 2013). This led to the emplacement of ~132 Ma dolerite dyke swarms (Trumbull et al., 2007) and the emplacement of the Koegel Fontein Complex (Curtis et al., 2013, 2011).

The youngest geological units in the field area are the Paleogene Sandkopsdrif Complex and the Neogene West Coast Group. The Sandkopsdrif Complex is a carbonatite plug and REE prospect, which occurs in the north of the field area. Most of the field area is covered by coastal deposits of the West Coast Group. To the south of the study area, the West Coast Group contains economic occurrences of heavy mineral sands.

1.3. The Koegel Fontein Complex

During the breakup of Gondwana various anorogenic complexes of the Paraná-Etendeka igneous province were emplaced between 137 Ma and 124 Ma along the western margin of southern Africa and the eastern margin of South America between along NE-trending parallel lineaments over the Tristan plume (Milner et al., 1995; Trumbull et al., 2004). Alternatively, the Cretaceous anorogenic complexes may have formed along rift-related transform faults during early break up of Gondwana (Marsh, 1973). The 25 km wide, ~134 Ma Koegel Fontein Complex is the southernmost Cretaceous anorogenic complex, located ~1000 km south of the closest Damaraland complex. The Koegel Fontein Complex is comprised of a variety of mafic and felsic intrusive rocks, described by Curtis et al. (2011). Apart from various plugs and dykes, the main lithological units of the complex are the Kerskloof Suite bostonite dykes, Kruisvlei Suite quartz porphyry dykes and the Rietpoort Granite. The Rietpoort Granite is the largest unit of the Koegel Fontein Complex and was interpreted to form a lopolith-shaped pluton with a diameter of ~20km. The pluton surrounds and underlies a piece of its Namaquan country rock. The Kerskloof Suite dykes are compositionally a bostonite, which is synonymous with subvolcanic trachyte. The Kerskloof Suite intruded at 144 Ma followed by the intrusion of regional dolerite dykes. The dolerite dykes are cross-cut and therefore predate the quartz porphyry dykes. The quartz porphyry dykes and the Rietpoort granite were determined to have an age of 134 Ma, however the quartz porphyry dykes do not cross-cut the Rietpoort Granite making the main granitic pluton the youngest lithological unit of the Koegel Fontein Complex.

While the magmas of the Cretaceous Damaraland complexes generally have $\delta^{18}O$ values near and above the mantle value of 5.5‰ (Harris, 1995), the Koegel Fontein Complex has many rock types with $\delta^{18}O$ values ranging from >9 ‰ to -4.1 ‰ in both mineral grains and bulk rock samples (Curtis et al., 2013). The Rietpoort Granite and most samples of the country rock were found to have normal $\delta^{18}O$ values of 6 – 9 ‰. Low bulk rock $\delta^{18}O$ values (<5.5 ‰) in the country rock, dolerite dykes and Kerskloof Suite dykes were attributed to hydrothermal alteration. Direct evidence of hydrothermal activity is given by low $\delta^{18}O$ quartz veins and a breccia pipe which are constrained to be Cretaceous due to cross cutting field relationships (Olianti and Harris, 2018). Quartz porphyry dykes contain euhedral, unzoned and unaltered quartz phenocrysts with $\delta^{18}O$ values ranging from 8‰ to -2‰ (Harris, unpublished data). It was suggested that ^{18}O-depletion initially occurred during a ~547 Ma global glaciation and that low $\delta^{18}O$ rock was then selectively dehydrated and melted during the emplacement of the Koegel Fontein Complex, forming Cretaceous low $\delta^{18}O$ rocks (Olianti and Harris, 2018).

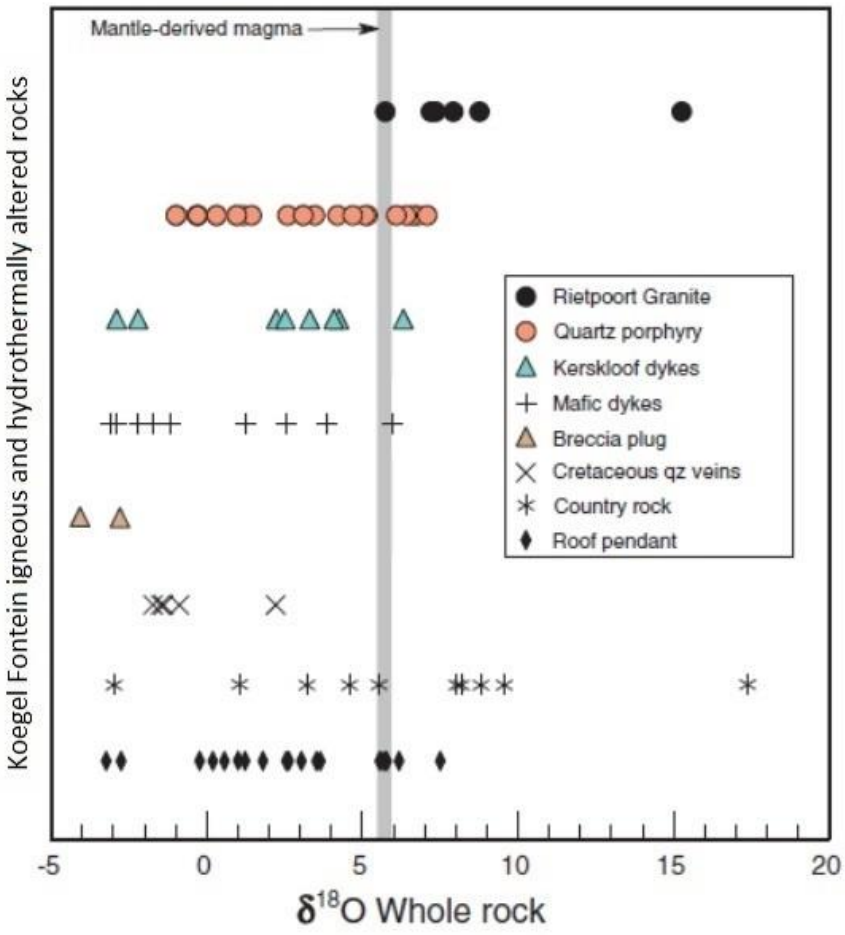

Figure 3. The $\delta^{18}O$ values of selected rock types (Curtis et al., 2013). *The country rock, roof pendant, Kerskloof Suite and mafic dykes were ^{18}O depleted due to Cretaceous hydrothermal alteration. The Cretaceous quartz veins and breccia pipe formed as a result of low $\delta^{18}O$ volatile release during the emplacement of the Koegel Fontein Complex. The Rietpoort Granite has normal $\delta^{18}O$ values. Low $\delta^{18}O$ values in euhedral, magmatic, isotopically unzoned and unaltered quartz grains in the quartz porphyry dykes are a result of selective melting of previously ^{18}O-depleted rock. The country rock has a wide range of $\delta^{18}O$ values. This project investigates low $\delta^{18}O$ country rock as a protolith for Cretaceous low $\delta^{18}O$ fluid and magma.*

2. Geological Investigation

2.1. Maps

The field area is approximately 35 km by 35 km large. It mostly lies on private property and is largely covered Neogene cover. The area is located on the edges of the 1:250 000 maps 3017 Garies, 3018 Loeriesfontein and 3118 Calvinia (de Beer, 2010, 2001; Macey and Minnaar, 2010) and the topographic maps 3017DC, 3017DD, 3018CC, 3117BA&BB and 3118AA (Chief Directorate: Surveys and Mapping, 2003a, 2003b, 2003c, 2003d, 1970). The maps of the 1:250 000 geological series do not have the necessary detail for this study and so unpublished field maps and filters of airborne geophysical data were used to create a geological map of the Koegel Fontein Complex, (Figure 4) and a geophysical interpretation map (Figure 5). I also produced a 1:5 000 map of the BFSZ (Figure 6).

2.1.1. Koegel Fontein Complex 1:50 000

An overview of the field area is given by the map Koegel Fontein Complex 1: 50 000 (Figure 4). The map is based on the hand drawn field maps 3017DD and 3117BA, which were previously mapped by and are provided by Coenie de Beer from the Council for Geoscience (de Beer. pers com, 2017). The original field maps have previously been compiled into the 1:250 000 map, 3017 Garies (de Beer, 2010), however detail was lost in the process. The hand-drawn field maps were digitised and compiled into an overview map of the field area (Figure 4). Unlike the original field maps, the digital map has the same colour coding and lithological codes as the official 3017 Garies map. As few changes were made to the content of the original field maps as possible during digitisation. The only deliberate change to the map is the addition of the breccia plug (Kb) which was mapped correctly in the original hand drawn field map but was incorrectly labelled in the official 3017 Garies map. The map shows the location of various Namaqua-Natal gneisses and schists, minor outcrops of the Vanrhynsdorp and Gariep Supergroup and various plugs, dykes and plutons related to the Koegel Fontein Complex or regional Cretaceous rifting and magmatism. N to NW-trending shear zones cross-cut the country rock of the Koegel Fontein Complex, including the roof pendant of the complex. The regional fabric of the country rock is moderately-to-steeply west-dipping inland, and shallowly-to-moderately west-dipping at the coast (Figure 4).

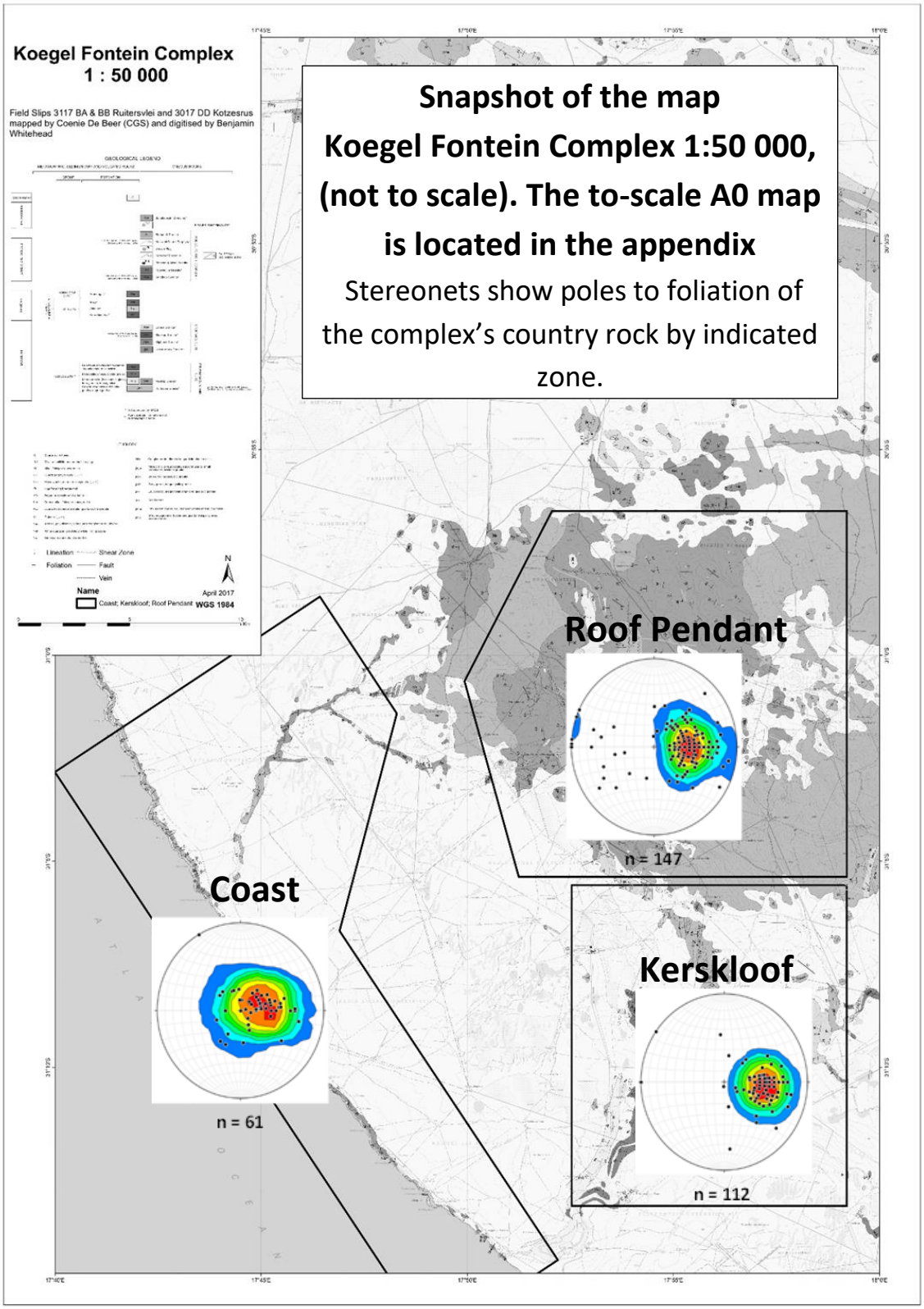

Figure 4. Snapshot of the map Koegel Fontein Complex 1:50 000 (not to scale) digitised from the unpublished field maps 3017DD Kotzesrus and 3117BA & BB Ruitersvlei. The actual map is located in the appendix and is scaled at 1:50 000 when printed out on an A0-sized sheet. The field maps were mapped by Coenie de Beer for the CGS. The map was digitised using ArcMap10.1 using the geographic coordinate system WGS_1984.

2.1.2. Aeromagnetic Interpretation 1:750 000

Geophysical data from magnetic surveys was used to map out regional features in the field area and to place the local geology in a regional context. Branko Corner from Manica Minerals provided geotiffs files showing various filtered products of magnetic data as well as part of a Bouguer gravity survey. Onshore, the filtered products are based on a magnetic survey done by the Council for Geoscience (CGS) while lower resolution EMAG2 (satellite-airborne-marine derived) data extends offshore (Maus et al., 2009). The CGS dataset is based on a magnetic survey flown with a 1 km line spacing and is gridded at 500 m. EMAG2 data has a lower resolution, being gridded at 3500m.

In order to facilitate interpretation of geophysical magnetic data, the magnetic susceptibility of the different lithologies was measured. The magnetic susceptibility of a material is the materials ability to amplify or to weaken a surrounding magnetic field. The magnetic susceptibility (x_v) is a unitless factor relating the magnetic field strength (H) to the magnetisation of a material (M) with the relationship $M = x_v H$. The magnetic susceptibility of various lithological units was measured using a hand held susceptibility meter. The mean of 8 measurements per sample was taken as the magnetic susceptibility of that sample. Variations in magnetic susceptibility between samples of the same lithological unit are statistically described using the mean and standard deviation in Table 2.

Table 2. The magnetic susceptibility of relevant lithological units in the field area. Note the high standard deviation in the BFSZ. The mean and standard deviation per sample is given in Table 7 in the appendix.

Lithological Unit	**Samples**	**Mean x_v**	**Standard Deviation**
Jakkalshoek Granite	8	1.80	1.70
BFSZ	9	3.97	6.34
Rietpoort Granite	4	1.59	0.90
QP Dyke	2	1.62	1.27
Breccia Plug	3	0.85	0.46

The magnetic susceptibility gives an indication as to which lithologies will show as high anomalies and which lithologies will show remnant anomalies in the aeromagnetic data. The provided magnetic data uploaded to ArcMap and an interpretation map was drawn over the geophysical data layers (Figure 5). Of various filters of the magnetic data provided by Branko Corner, the most useful were the first vertical derivative (1VD) and the reduction to the pole (RTP) filters. The 1VD filter was predominantly used to identify shallow features, as the derivative emphasises changes in the magnetic field, while the RTP filter was used to identify deeper and larger features, because it shows the regional magnetic variations, corrected to lie at the actual position of the geology by simulating a vertical magnetic field.

The geophysical interpretation maps are given in Figure 5. Lines and polygons were drawn over the aeromagnetic data to facilitate the geophysical interpretation. By comparison with the geological map, dyke-like features, fault-like features and a magnetic fabric could be distinguished. Linear features with internally consistent magnetisation and sharp edges were labelled as dyke-like features. Linear features which disrupt the surrounding fabric were labelled as fault-like features. In the north of the field area linear, subparallel features visible in 1VD were labelled as magnetic fabric and may represent lithological boundaries. A NNE-trending broad magnetic swath is identifiable in the RTP filter of the EMAG2 in the SW of the Koegel Fontein Complex. This feature is classified as a lineament on the geophysical interpretation map.

Various anomalous bodies were identified in the aeromagnetic data. The Rietpoort Granite outline is identifiable in 1VD by having an internally homogenous magnetisation with a sharp and well defined boundary which forms a magnetic high. This feature lies on the mapped position of the Rietpoort Granite. Anomalous bodies with a magnetic high visible in 1VD are classified as short-wavelength high. A large magnetic high extends to the SW from the Koegel Fontein Complex and is identifiable in the RTP filter. This feature was classified as a long wavelength magnetic high. Features which show a lower magnetisation with respect to their surroundings have a remnant magnetisation. The following general deductions can be made from the geophysical interpretation (Figure 5):

- Comparison with the geology shows that the magnetic fabric in the northern section of the area is likely due to lithological variation and the arcuate nature of the magnetic fabric is a manifestation of folding.
- ESE to SE-striking dyke and fault-like features occur along the coastline. These features may form part of a set of Neoproterozoic (Pan-African) faults, Cretaceous rift-related and coast-parallel normal faults, or Neoproterozoic faults which were reactivated as normal faults in the Cretaceous, as indicated in the 3017 Garies map explanation (de Beer, 2010). Cretaceous dykes intruded orthogonal to the extensional direction and/or intruded along pre-existing structures (Will and Frimmel, 2013).
- A set of N-striking fault-like features dominate the NE part of the map and occur south of the Rietpoort Granite. These features are coincident with faults mapped in the 1:250 000 geological maps which were interpreted as Neoproterozoic (Pan-African) faults in the 3017 Garies map explanation (de Beer, 2010).

- The Cretaceous Koegel Fontein Complex lies in the centre in the aeromagnetic interpretation:
    - The Rietpoort outline corresponds exactly with the position of the exposed Rietpoort Granite pluton. The roof pendant is clearly visible in the 1VD filter, as would be expected for a homogenous rock type exposed at the surface.
    - The WSW-striking lineament terminates at the Rietpoort Granite. This Lineament has the orientation of a Cretaceous transform fault (Marsh, 1973). Interpretation of this lineament remains speculative, because it was not found in the field and because it does not correspond to any features on the geological map.
    - The long-wavelength high magnetic anomaly extends from the position of the Rietpoort Granite to the SW. This feature may be a magnetic phase of the Koegel Fontein Complex, Jakkalshoek Granite or mineralisation in the Jakkalshoek Granite.
    - There is no evidence for mafic underplating. Mafic rocks are expected to create a high gravity anomaly, however there is a low in the Bouguer gravity data.
- The BFSZ is located at one of the N-striking fault-like features to the south of the Rietpoort Granite.

Figure 5 (see the following pages). A geophysical interpretation map of aeromagnetic data. The geophysical interpretation is overlaid onto various base maps. A: The first vertical derivative (1VD) filter. Lighter shades of grey indicate a stronger response. B: The reduction to pole (RTP) filter. A spectrum of blue to red indicates a low to high magnetic response C: Bouguer Gravity filter. Blue to red indicates a low to high Bouguer anomaly. D: The 1:250 000 geological maps for comparison.

A

Geophysical Interpretation:

Shallow Magnetic Anomalies
CGS RTP 1VD

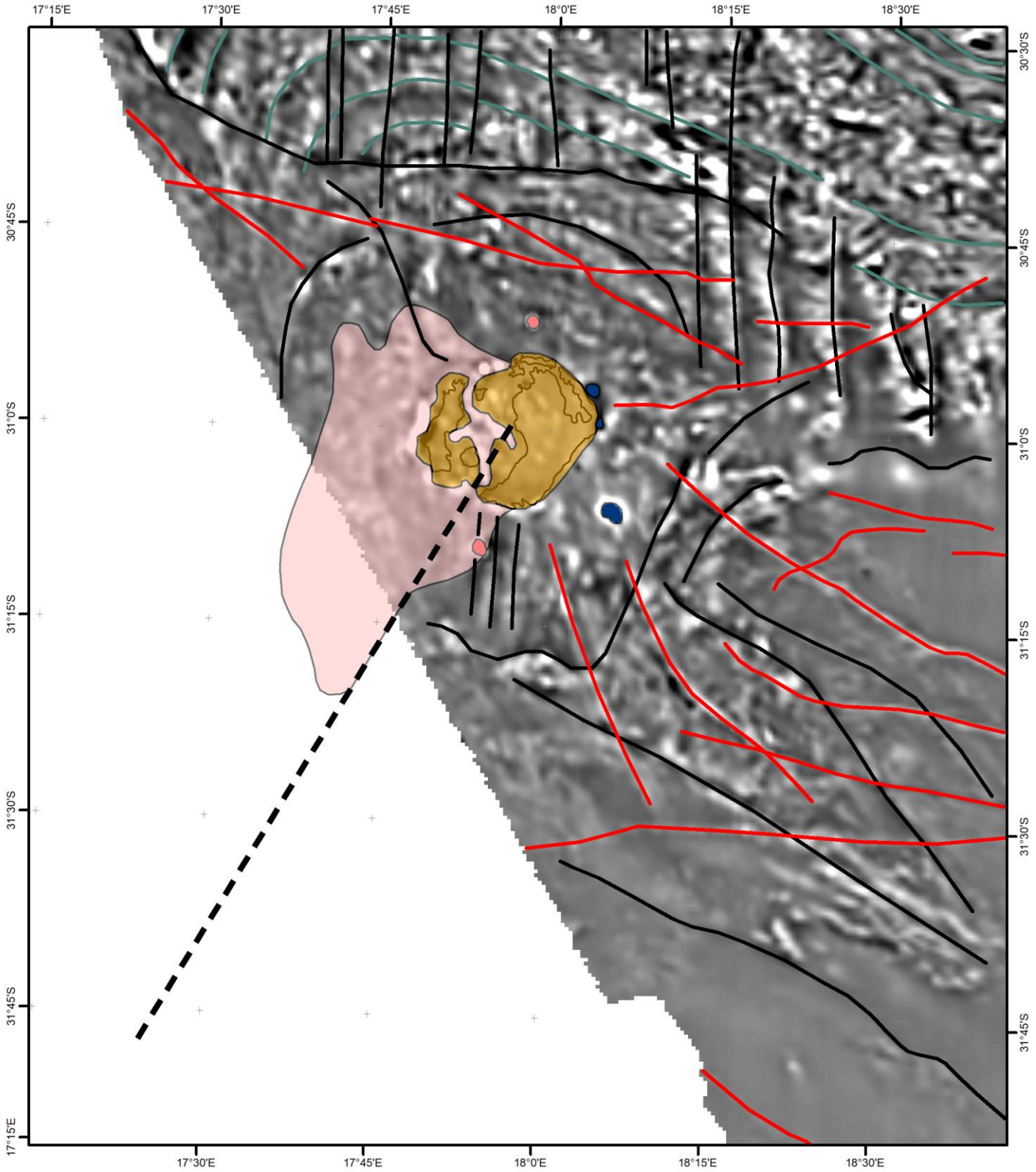

Lineament
Fault-like Feature
Dyke-like Feature
Magnetic Fabric
Rietpoort Granite Outline
Long-Wavelength Magnetic High
Short-Wavelength Magnetic High
Remanent Magnetisation

N

WGS 1984
UTM 33° S

0 5 10 20 30 40
km

B

Geophysical Interpretation:

Deep Magnetic Anomalies
EMAG2 & CGS RTP Sun300

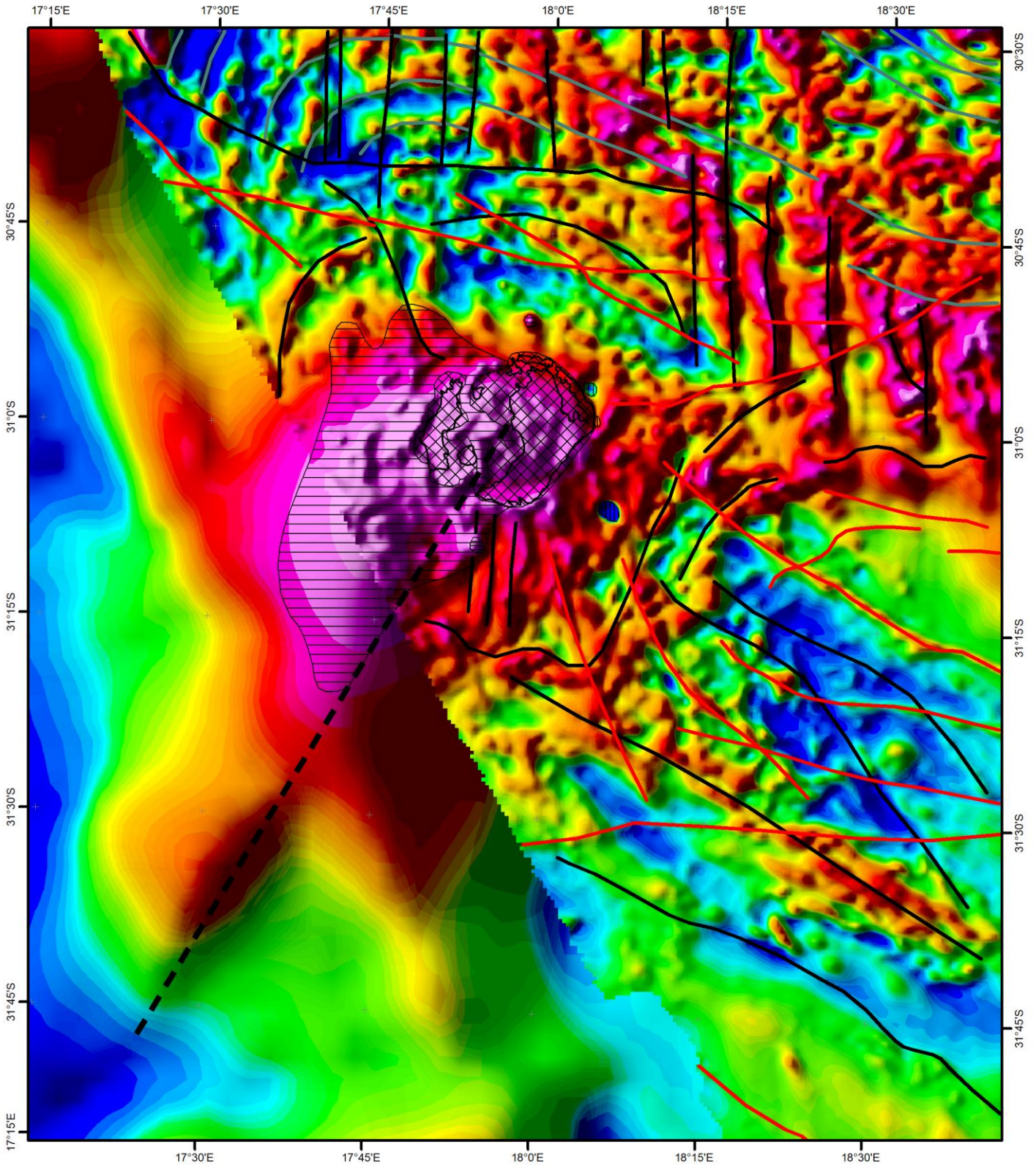

Lineament
Fault-like Feature
Dyke-like Feature
Magnetic Fabric
Rietpoort Granite Outline
Long-Wavelength Magnetic High
Short-Wavelength Magnetic High
Remanent Magnetisation

N

WGS 1984
UTM 33° S

0 5 10 20 30 40
km

C

Geophysical Interpretation:

Bouguer Gravity Anomalies
Residual Sun300
Note the Artificial High along the Continental Margin

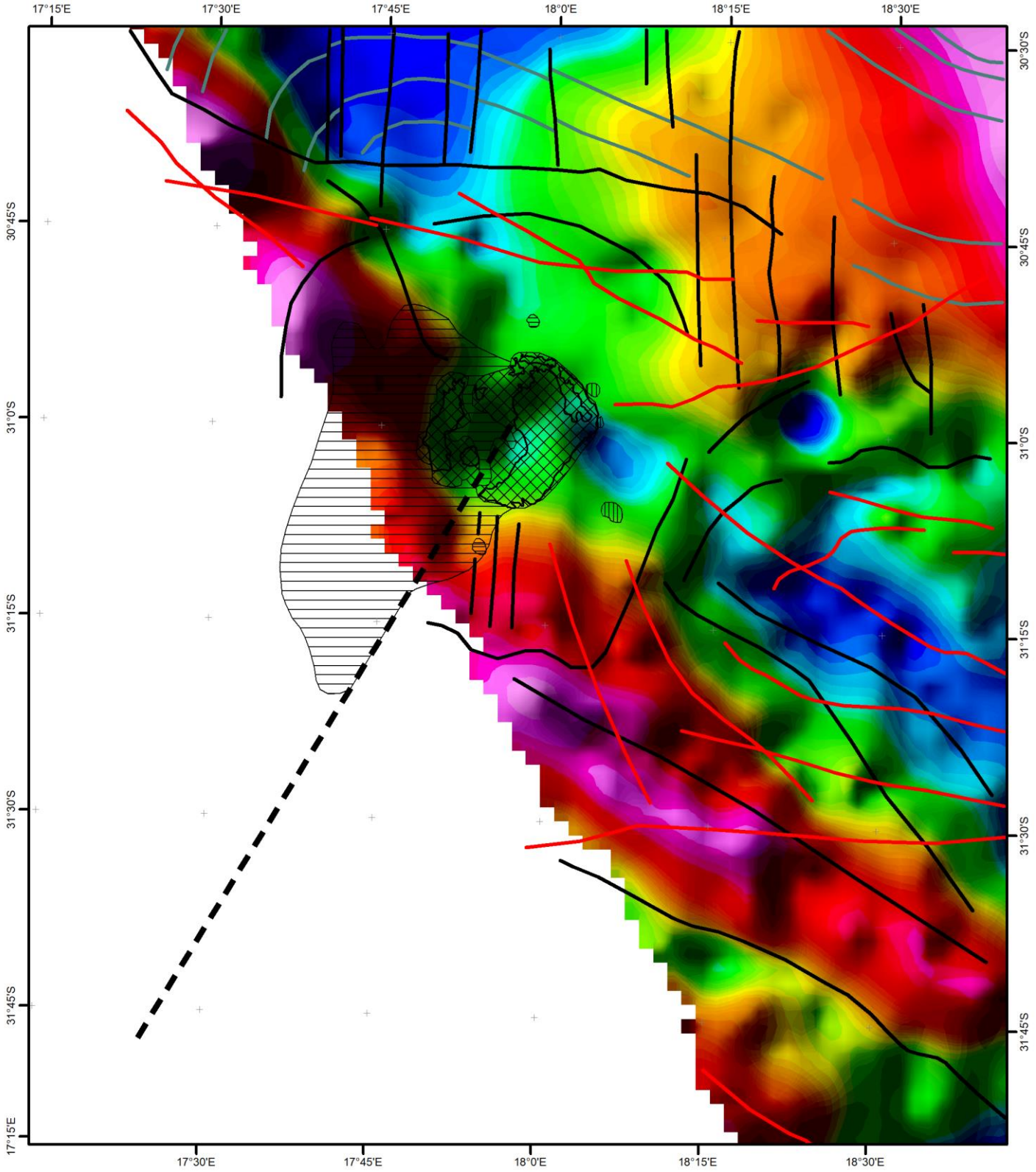

D

Geophysical Interpretation:

Comparison to Mapped Geology
3017 Garies, 3018 Loeriesfontein and 3118 Calvinia

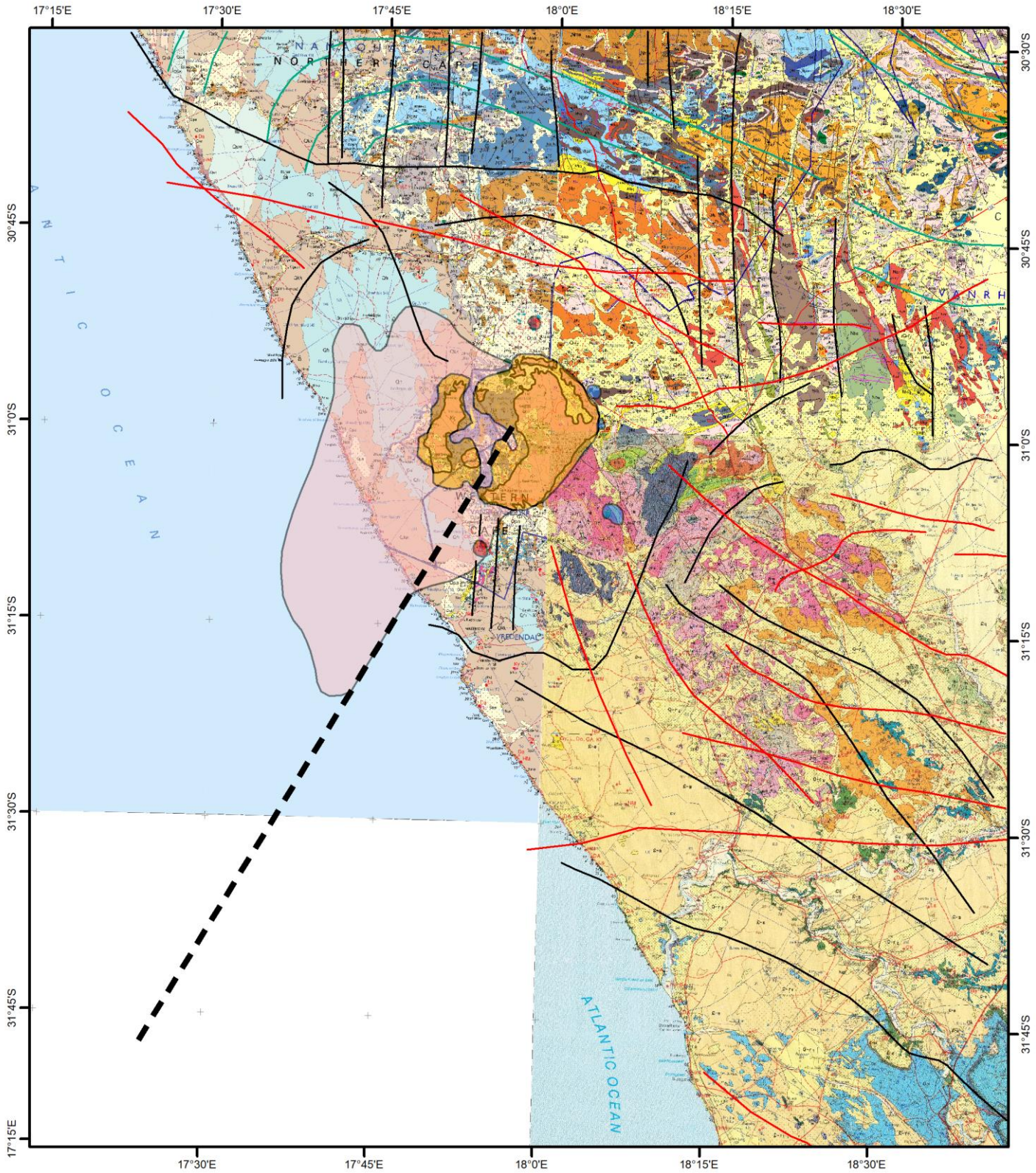

- Lineament
- Fault-like Feature
- Dyke-like Feature
- Magnetic Fabric
- Rietpoort Granite Outline
- Long-Wavelength Magnetic High
- Short-Wavelength Magnetic High
- Remanent Magnetisation

N

WGS 1984
UTM 33° S

0 5 10 20 30 40
km

2.1.3. Brak Fontein Shear Zone 1:5 000

The BFSZ is a north-striking area of variable strain initially discovered in the roof pendant of the Rietpoort Granite. The Jakkalshoek Granite is intensely deformed as described in section 2.2.3. A section of more or less continuous exposure was chosen for structural mapping along a river bed at approximately 17.88000°E; 30.97500°S. A strip map was drawn across the shear zone (Figure 6) and samples were taken for $\delta^{18}O$ analysis. Granitic gneiss (the Jakkalshoek Granite), mylonite, subordinate quartzite and quartz porphyry dykes were differentiated on the map. Structural data is displayed using foliation symbols and form lines. Figure 6 shows a west dipping mylonitic fabric confined by wall rock of Jakkalshoek Granite. The shear zone contains low strain areas where lenses of relatively undeformed Jakkalshoek Granite are preserved. The BFSZ is cross cut by younger quartz porphyry dykes. Strain is highly heterogeneous and the map only serves as a simplification of the complex deformation in the area. Variations in the bulk fabric on the 10m length scale were mapped, however 5-1 cm variation can observed within high-strain mylonitic zones.

Brak Fontein Shear Zone 1:5 000

17°52'40"E 17°52'50"E 17°53'0"E 17°53'10"E 17°53'20"E 17°53'30"E

30°58'20"S 30°58'30"S 30°58'40"S 30°58'50"S 30°59'0"S

river channel

180 m 200 m 220 m 240 m 260 m

Poles to Foliation (n = 35)
Lower hemisphere equal area projection

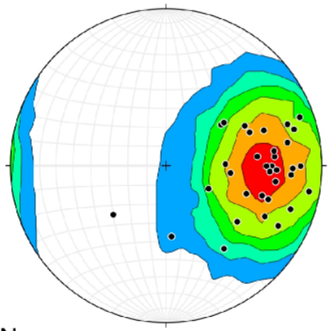

N

WGS 1984

- Foliation
- Form Lines
- Quartzite
- Granitic Gneiss
- Mylonite
- Quartz Porphyry Dyke

0 50 100 200 300 m

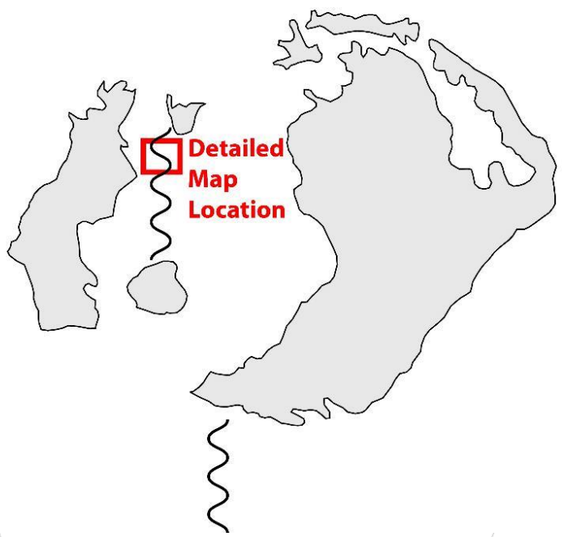

Figure 6. Brak Fontein Shear Zone 1:5 000. A section along Brakfonteinkloof was chosen for mapping due to more or less continuous exposure. A strip map with form lines was compiled. Form lines indicate the orientation of the mylonitic fabric. Foliation readings of the mylonite are given on the map.

2.2. Field Observations

In the following section field observations are reported with emphasis on the country rock of the Koegel Fontein Complex. The Namaqua-Natal Metamorphic Belt, the Gariep Supergroup, the BFSZ and Cretaceous quartz veins and igneous rocks are described. My field observations corresponded closely with the official lithologies described on the 3017 Garies map (de Beer, 2010) and the unpublished field maps (de Beer. pers com, 2017).

2.2.1. Namaqua-Natal Metamorphic Belt

The country rock of the Koegel Fontein Complex is predominantly made up of the Namaqua-Natal Metamorphic Belt. Various gneisses of the Namaqua Natal Metamorphic Belt are often mineralogically and texturally similar. This makes their distinction in the field difficult. In the study area the Namaqua-Natal Belt is predominantly made up of Hunboom Gneiss (Ɲhb) and the Mesklip Gneiss (Ɲme) of the Little Namaqualand Suite, metaquartzite (Mkq) and schist (Mks) of the Kamiesberg Group and the Jakkalshoek Granite (Ɲjk) of the Spektakel Suite. Metasedimentary rocks of the Kamiesberg Group were observed in cliffs along the Salt River (Figure 7). The Kamiesberg Group is comprised of interlayered schist, quartzite and micaceous quartzite. Along the Salt River a bed-parallel, west-dipping foliation is primarily defined by biotite and muscovite. Kyanite and garnet occurs within the Kamiesberg Group at 31.165513°S, 17.923119°E.

The Mesklip Gneiss (Figure 8) was primarily observed in Kerskloof (to the south of the Rietpoort Granite pluton), but is was also observed along the Groot-Goeraprivier and the Ruitersvlei Mouth along the coast. The Mesklip Gneiss has a cleavage defined primarily by biotite and muscovite. Along Kerskloof and the Groot-Goeraprivier, pegmatite veins intruded parallel to the foliation. These pegmatite veins typically have a quartz core and feldspar margins. The Mesklip Gneiss is highly strained along Kerskloof, as evidenced by strongly flattened feldspar augen. At the Ruitersvlei Mouth the Mesklip Gneiss displays round, ~1cm augen. The Jakkalshoek Granite (Figure 9) occurs in the roof pendant of the Rietpoort Granite and along the coast south of 31°5’S. It is a light grey granitic gneiss defined by ~2 cm feldspar augen. In low strain areas the granitic gneiss can have little to no foliation, resembling a granite. High strain areas are characterised by bands of quartz and biotite which wrap around sheared and flattened feldspar augen. The Jakkalshoek Granite forms the immediate wall rock of the BFSZ within the roof pendant.

Figure 7. Metasedimentary rocks of the Kamiesberg Group observed along the Salt River, south of the Rietpoort Granite Pluton. A: Interbedded schist and metaquartzite forms cliffs along the Salt River (31.18000036°S, 17.91070174°E facing south). B: Example of a biotite-rich schist (31.180439°S, 17.908509°E). C: An example of a micaceous quartzite (31.180462°S, 17.908739°E).

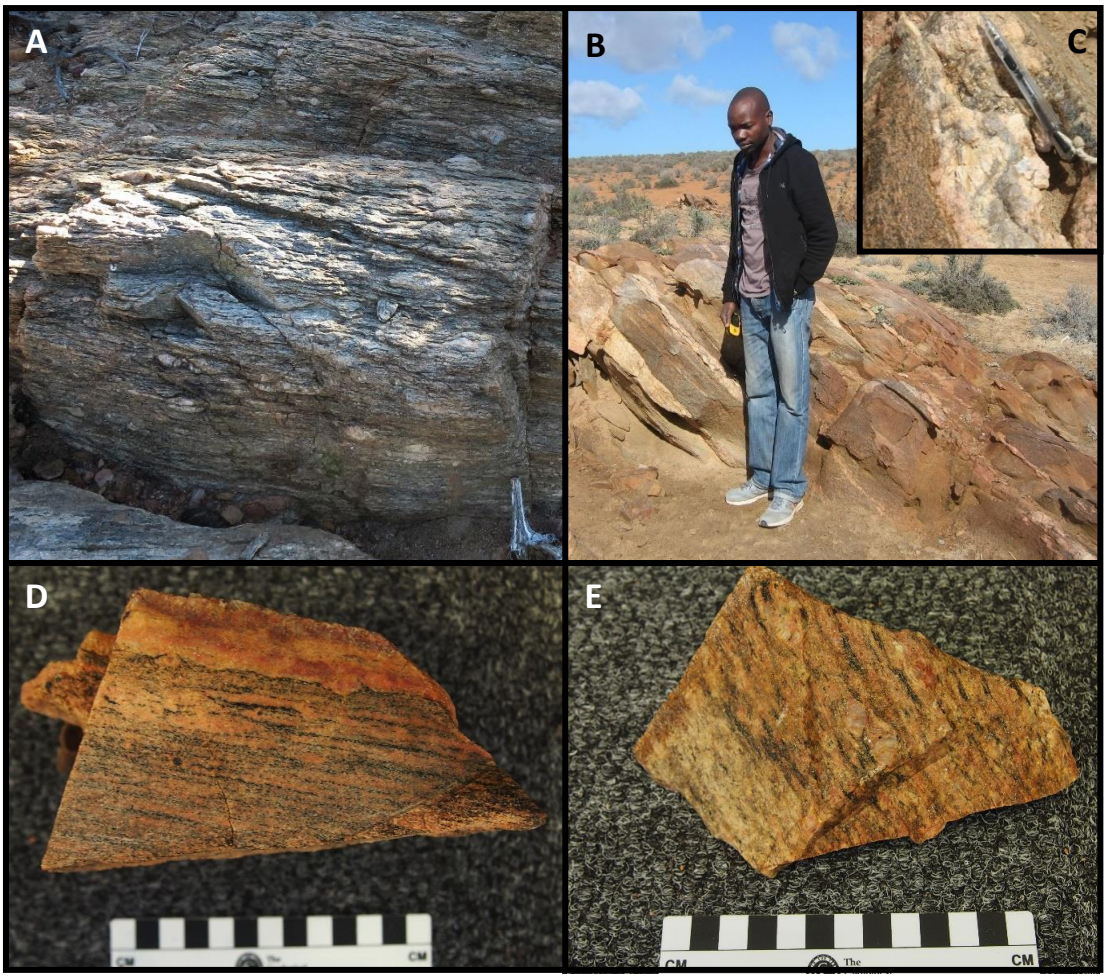

Figure 8. Pictures of the Mesklip gneiss which forms part of the Little Namaqualand Suite. The Mesklip Gneiss was predominantly observed in Kerskloof south of the Rietpoort Granite pluton and north of the Salt River. A: Mesklip Gneiss located in the north of Kerskloof (31.11247843°S, 17.92477705°E facing west). B: Silvio Elias and Pegmatite veins which intruded along the foliation of the Mesklip Gneiss at the Groot – Goeraprivier (31.188245°S, 17.925451°E, C facing south). C: A close-up picture of a pegmatite vein with feldspar margins and a quartz centre (same location as B). D: The Mesklip Gneiss in the Kerskloof area is highly strained and the feldspars are flattened (same location as B). E: Example of Mesklip Gneiss with round augen occurring at the coast (31.104685°S, 17.732433°E).

Figure 9. A: Examples of the Jakkalshoek Granite of the Spektakel Suite. Biotite and quartz bands wrap around large feldspar augen forming a foliation. A: A gneissic pavement located in the roof pendant of the Rietpoort Granite pluton (30.971930°S, 17.877126°E facing east). B and C: Examples of the Jakkalshoek Granite located along the coast (31.169326°S, 17.773236°E and 31.147433°S, 17.755041°E respectively).

2.2.2. Gariep Supergroup

In the study area outcrops of the Gariep Supergroup are sparse, presumably because they were eroded away to expose the Namaqua-Natal Belt basement. The Gariep Supergroup is exposed at the Salt River Mouth, where folded beds of marble, tillite and clastic sediments can be found along the beach. The contact between the Jakkalshoek Formation of the Namaqua-Natal Belt and the Karoetjes Kop Formation of the Gariep Supergroup occurs at 31.201456°S, 17.797824°E (Figure 10). The actual contact is not exposed and may therefore be either a tectonic or a sedimentary contact. Foliations are west dipping and lineations are west plunging on either side of the contact, suggesting that the Namaqua-Natal Belt was strongly overprinted by the Pan-African Orogeny in the area.

The Karoetjes Kop Formation was studied at 31.201456°S, 17.797824°E. It is a glacial diamictite with poorly sorted matrix supported clasts (Figure 11A). The west plunging lineation is visible when looking east, onto the foliation plane and is a result of stretched out clasts and (Figure 11B). The Widouw Formation occurs stratigraphically above the Karoetjes Kop Formation. A west-verging synform occurs at 31.23547°S, 17.83899°E (Figure 12). Shale and marble beds are folded isoclinally. The synform's western limb is overturned.

Figure 10. The contact between the Gariep Supergroup and the Namaqua-Natal Belt (31.201456°S, 17.797824°E). The contact is not exposed. It could either be either a sedimentary or a tectonic contact. Parallel west-dipping lineations and west-plunging foliations occur on either side of the contact, suggesting that the Namaqua-Natal Belt experienced strong Pan-African overprint.

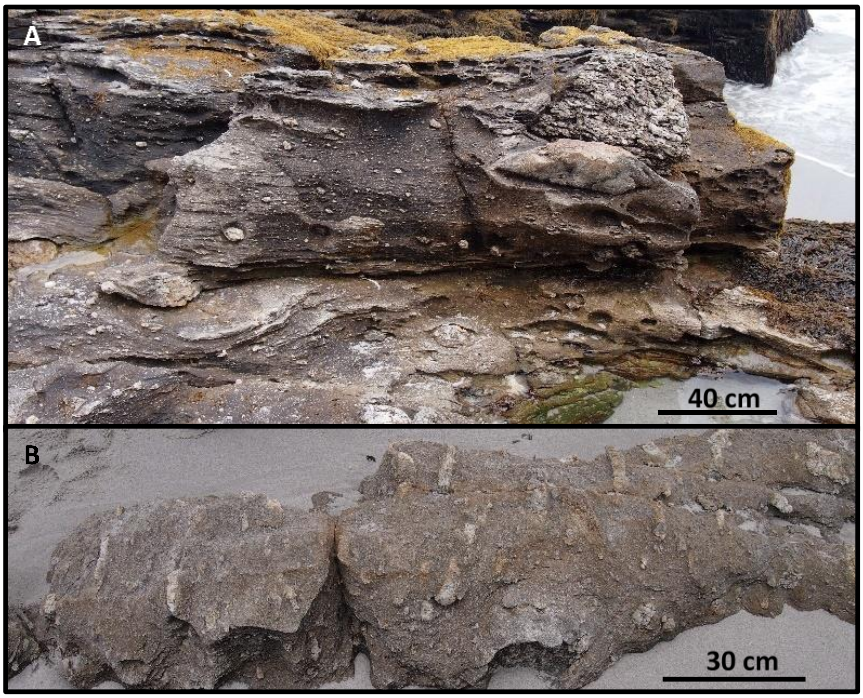

Figure 11. Glacial diamictite of the Karoetjes Kop Formation of the Gariep Supergroup (31.201456°S, 17.797824°E). A: A variety of poorly sorted clasts are matrix supported. A west-dipping foliation is developed (picture taken facing west). B: Clasts are stretched out to form a west plunging lineation which lies on the foliation plane (picture taken facing east).

Figure 12. Folded marble and shale beds occur in the Widouw Formation (Gariep Supergroup) north of the Salt River Mouth (31.23547°S, 17.83899°E). A: An east-verging, isoclinal synform with an overturned western limb (picture taken facing south). B: Close-up of the marble and shale in the overturned limb (picture taken facing west).

2.2.3. Brak Fontein Shear Zone

The Brak Fontein Shear Zone (BFSZ) was predominantly studied inside area covered by Figure 6. The best known exposure of the shear zone occurs in the Jakkalshoek Granite in the Roof Pendant of the Rietpoort Granite. In the BFSZ the Jakkalshoek Granite is deformed extensively. The different stages of deformation, from undeformed gneiss to mantled, or stretched out porphyroclasts to obliterated feldspar porphyroclasts are illustrated in Figure 13. Initially ductile deformation is taken up by the quartz, forming bands which wrap around feldspar augen. The more competent feldspar porphyroclasts become increasingly isolated in their finer grained mylonitic matrix. Eventually the feldspar porphyroclasts start to deform, becoming flattened out before being obliterated.

Field observations indicate strong strain partitioning within the shear zone (Figure 14). Evidence for strain softening is given in sharp contacts between shear bands and wall rock as well as low strain lenses of augen gneiss within the shear zone. Smaller isolated low strain lenses can develop a shape resembling a mantled porphyroclast. Feldspar porphyroclasts occur in some parts of the shear zone (Figure 15). When the porphyroclasts are mantled, they are either Φ-clasts or σ-clasts. The σ-clasts indicate a sinistral shear sense. Abundant small folds defined by the mylonitic fabric and veins can be observed in the BFSZ. These folds generally exhibit a strong asymmetry that further supports a sinistral displacement (Figure 16). Some larger, less strongly verging folds were also observed.

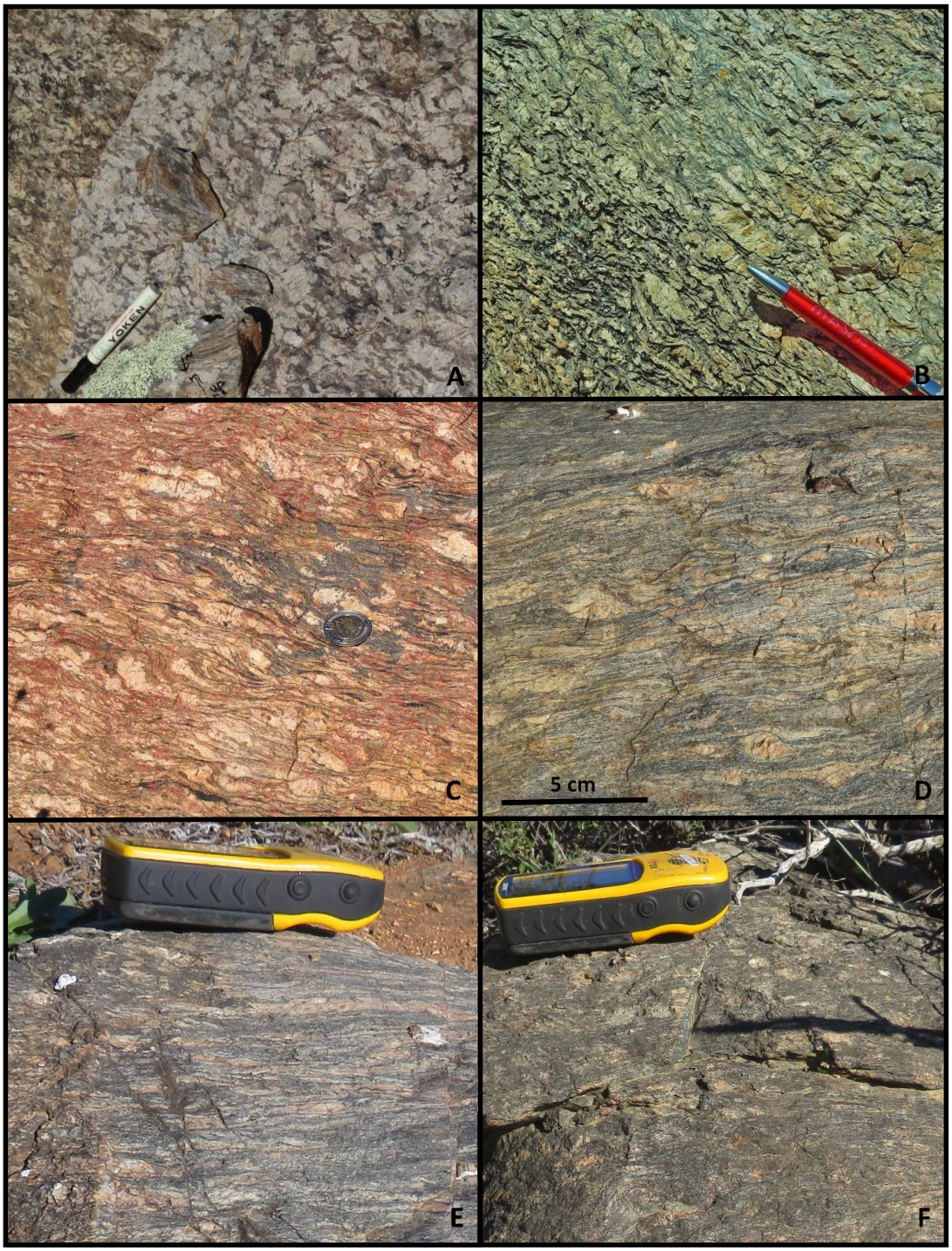

Figure 13. The appearance of the BFSZ with increasing strain. A: The undeformed wall rock is a granitic augen gneiss with large feldspar porphyroclasts. B to D: First the quartz matrix behaves ductilely, forming quartz bands which wrap around the brittle feldspar porphyroclasts with increasing strain. E to F: With increased strain and/ or temperature the feldspars become ductile and smear out, eventually becoming completely obliterated. A: 30.971930°S, 17.877126°E facing east; B: 30.97674868°S, 17.88895648°E; C: 30.97669328°S, 17.8839384°E; D, E and F: 31.01434495°S, 17.88326852°E facing west.

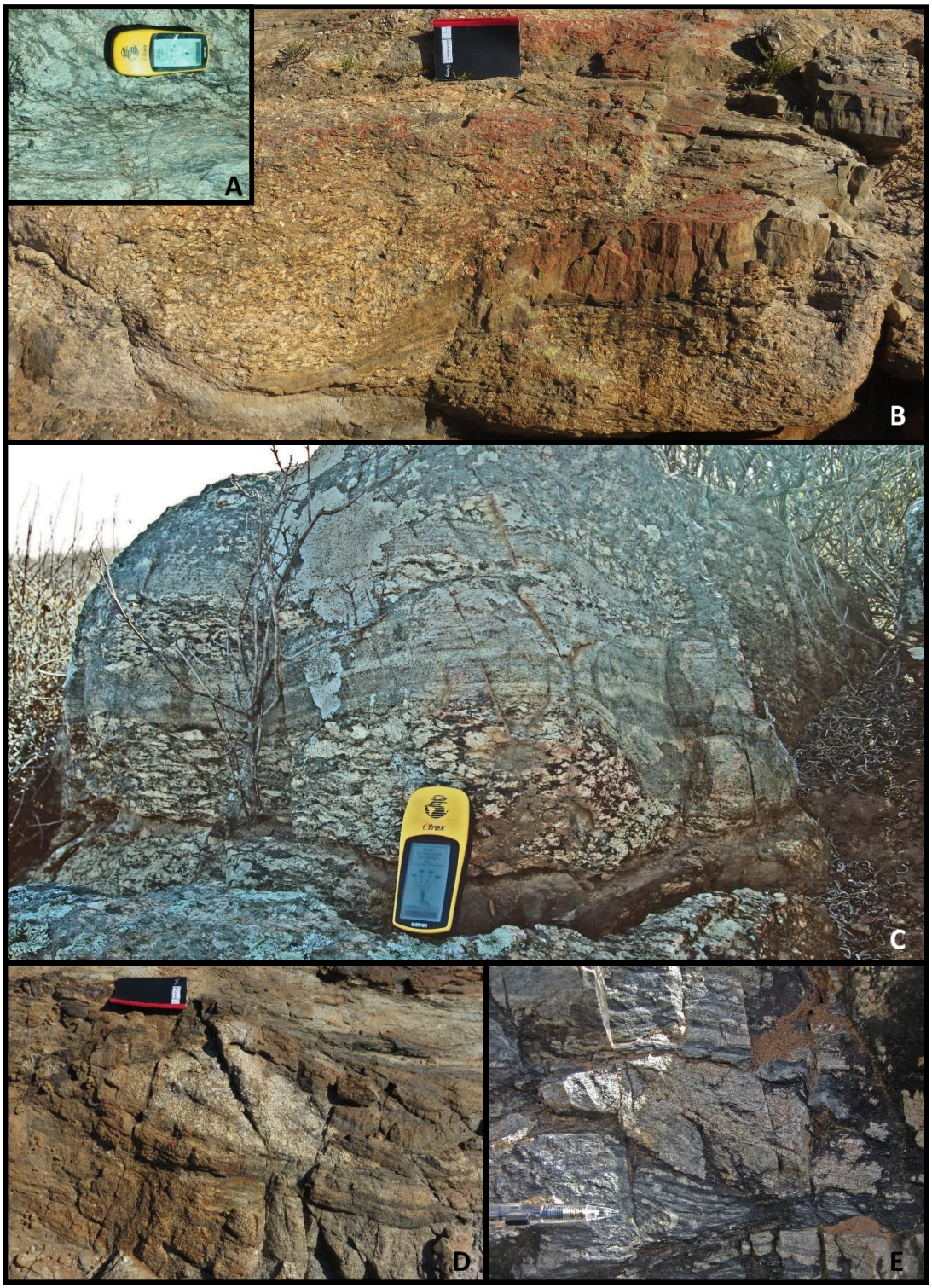

Figure 14. Illustration of strain partitioning in the BFSZ. After the initial development of a shear band (A), the deformation is strongly partitioned into the strain softened shear zone, creating sharp contacts between the shear band and its wall rock (B). C: Multiple shear bands can develop and wrap around low strain zones. D: With sufficient deformation the shear bands merge and isolated low strain lenses remain. E: These low strain lenses are more competent and smaller low strain lenses can deform in a porphyroclast-like fashion. A: 31.01537434°S, 17.88399791°E; B: 30.972851°S, 17.880097°E facing west; C: 31.01508264°S, 17.88361704°E; D: 30.973287°S, 17.880361°E facing west; E: 30.98112655°S, 17.88789047°E facing west.

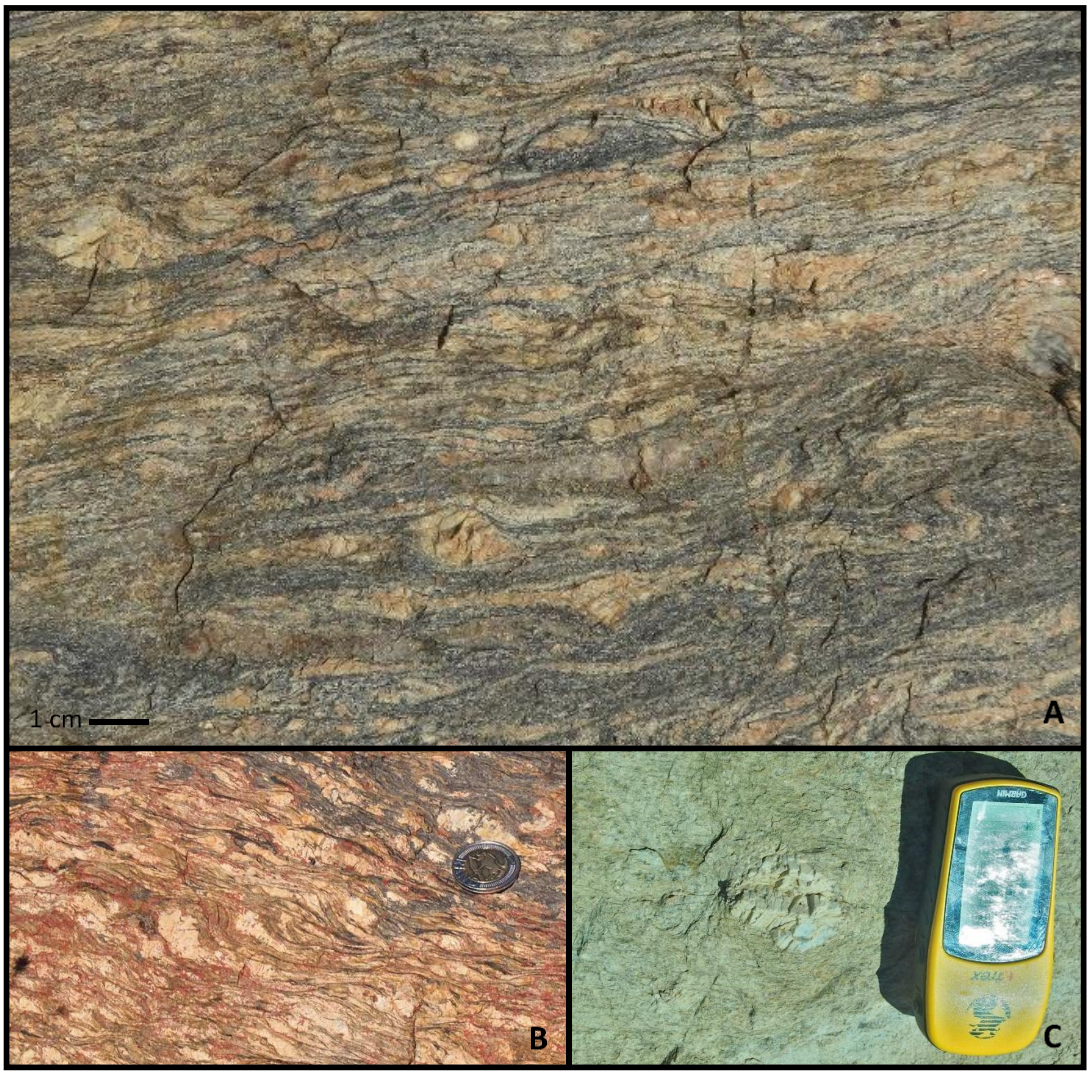

Figure 15. Porphyroclast in the BFSZ. In some sections of the shear zone, where conditions seem favourable, Φ-clasts and σ-clasts are present. A: A good example of shear indicators. S-folds and σ-clasts indicate a sinistral sense of shear. B: Less deformed feldspar porphyroclasts are less deformed and σ-clasts display sinistral displacement. C: An example of a Φ-clast preserved in a fine grained mylonite. A: 31.01434495°S, 17.88326852°E facing west; B: 30.97669328°S, 17.8839384°E; C: 31.01579695°S, 17.88392943°E.

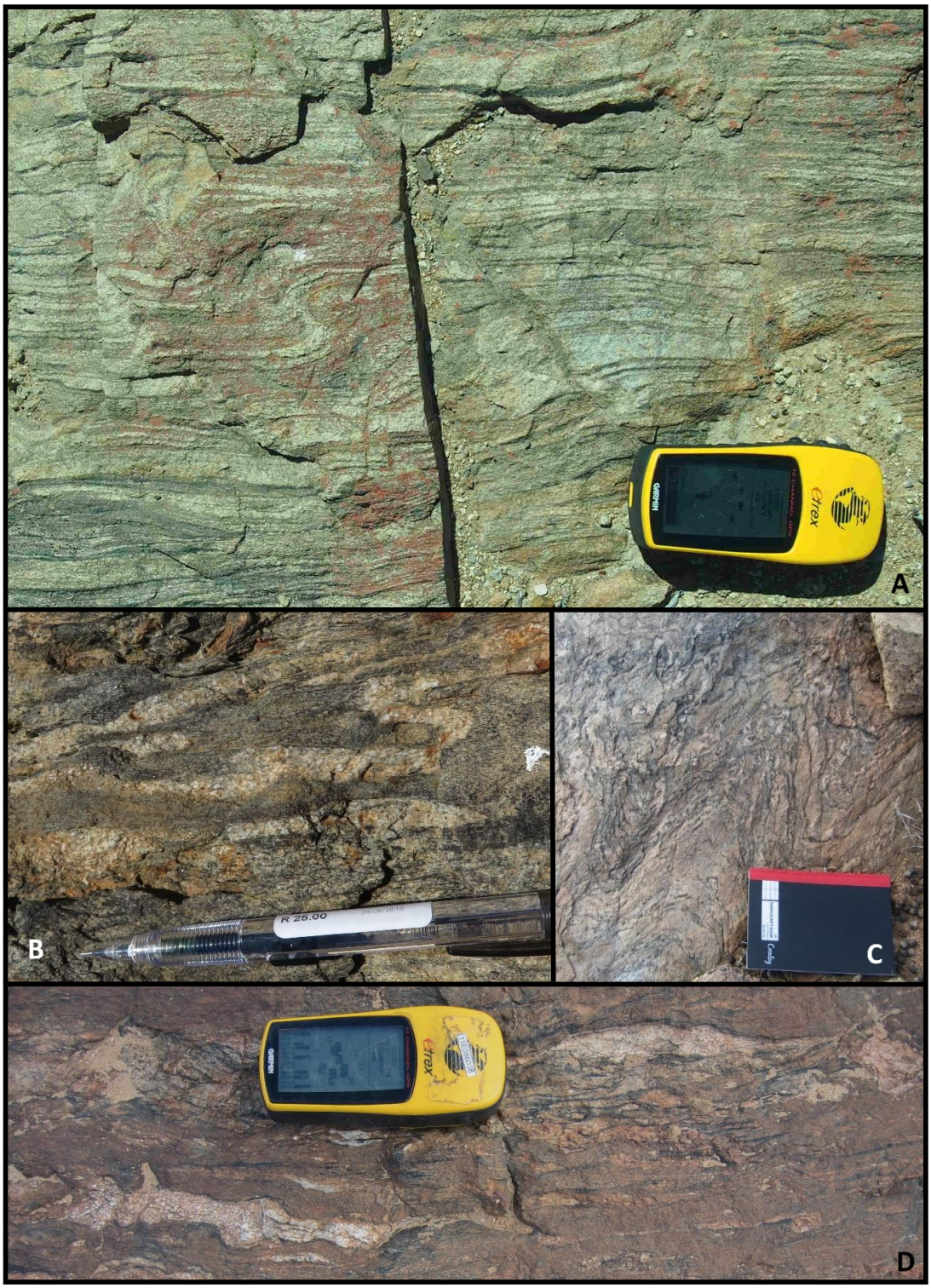

Figure 16. Folds indicating displacement in the BFSZ. A: An example of s-folds indicating sinistral displacement. B: A folded melt vein indicating sinistral displacement. C: Example of folds which are larger and verge less than usual. D: Unfolded melt veins for comparison with B. A: 30.97686896°S, 17.88587445°E facing west; B: 30.973994°S, 17.880786°E facing west; C: 30.98071986°S, 17.88793389°E facing NNE; D: 30.97988117°S, 17.8879675°E.

2.2.4. Cretaceous Igneous Rocks and Veins

Vuggy quartz veins and dykes of the Koegel Fontein Complex as well as regional dolerite dykes crosscut the BFSZ and its wall rock. In parts of the roof pendant a felsic intrusive rock cross cuts the Namaquan gneiss and the BFSZ in dykes and irregularly shaped intrusions (Figure 17). This rock is fine grained with sharp contacts to its country rock and may display flow banding. In thin section this rock contains spherulites, which are identifiable by being round features with radial extinction. This lithology was interpreted as an aplite, because spherulites give evidence for devitrification and fast cooling. A quartz porphyry dyke belonging to the Kruisvlei Suite intruded the Jakkalshoek Granite at 31.01072°S; 17.01567°E (Figure 18 A, B and C). This dyke is worthy of mention due to strongly developed flow banding on the edges of the dyke. A near vertical lineation is developed on the flow bands, which may indicate flow direction. Flow bands occur on ~1.5m margins on either side of the ~7m broad dyke. Another noteworthy quartz porphyry dyke intruded a shear zone at 31.01013°S; 18.00645°E (Figure 18 D and E). This dyke is ~20m wide. The fabric of the shear zone is parallel to the dyke's orientation. A strong lineation is developed in the shear zone. The igneous contact between the Rietpoort Granite and its country rock, the Jakkalshoek Granite was observed at 30.96481°S, 17.89127°E (Figure 19). The contact is a sharp, igneous contact and no faulting or brecciation was observed in the Jakkalshoek Granite.

Cretaceous quartz veins occur throughout the field area (Figure 20). They are identifiable by being vuggy and having euhedral quartz crystals that project into the centre of the vein. These quartz veins are generally less than 5 cm thick, often occur in brittle structures like joint sets and faults and in many cases cut the Cretaceous dykes. There are clearly distinct from the massive Pan-African or older quartz veins in outcrop which are usually several meters thick and can be traced for tens of kilometers. The timing of these veins is well constrained by cross cutting relationships in a particular outcrop, located at 31.00236°S, 17.01122°E. Here a dolerite dyke is cross cut by a vuggy quartz vein which is cross cut by a quartz porphyry dyke of the Koegel Fontein Complex. Regional dolerite dykes intruded between approximately 130 Ma and 135 Ma (Trumbull et al., 2007), followed by the low $\delta^{18}O$ veins, followed by intrusion of quartz porphyry dykes at 133.9 ± 1.3 Ma (Curtis et al., 2011). This restricts the emplacement of the vuggy quartz veins to 130-135 Ma.

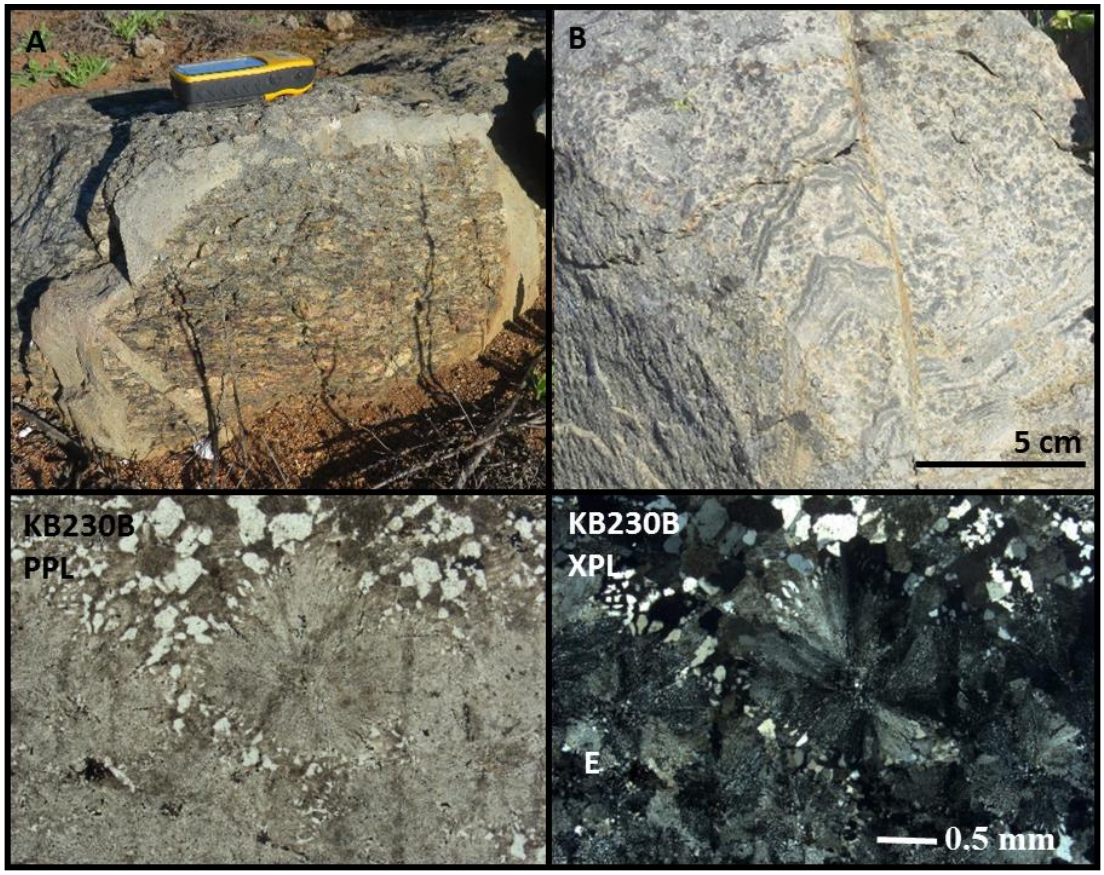

Figure 17. A: A felsic, fine grained rock intruded into the roof pendant including the BFSZ. This rock cross cuts the roof pendant gneiss and the BFSZ with sharp intrusive contacts. B: Flow banding and spherulites in the same lithology. KB230B: Thin sections confirm that round, radially extinguishing features are spherulites which result due to devitrification. Devitrification in conjunction with the location, in the roof pendant of the Rietpoort Granite, indicate that this rock is most likely quenched granite. A: 31.01583567°S, 17.8832629°E; B: 30.91406395°S, 17.88022254°E; KB230B: 30.91406395°S, 17.88022254°E.

Figure 18. A: Example of a felsic dyke with strongly developed flow banding. B: A near vertical lineation is developed on the margin of individual flow bands. C: The dyke is approximately 7m broad and intrudes Namaquan gneiss. D: A quartz porphyry dyke which intruded into a shear zone. E: Lineation in shear zone. A, B and C: 31.162777°S, 17.767901°E; D and E: 31.099357°S, 18.065645°E. 340/47

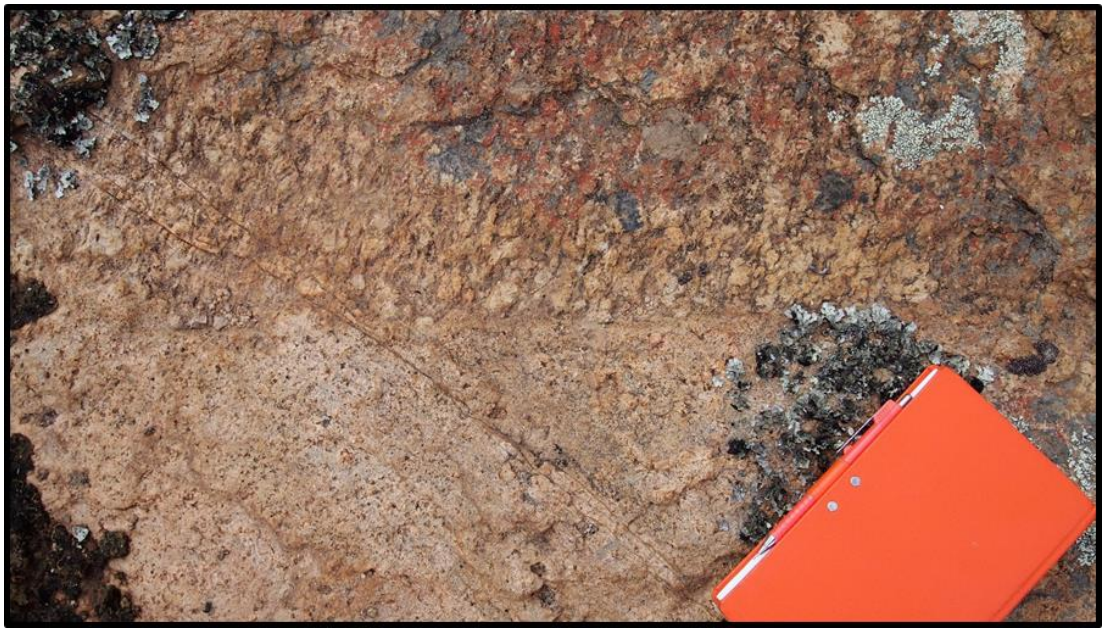

Figure 19. Igneous contact between the Rietpoort Granite (top half of picture) and its country rock, the Jakkalshoek Granite (lower half of picture) in the roof pendant (30.96480858°S, 17.89126989°E). No faulting or brecciation of the Jakkalshoek Granite is visible.

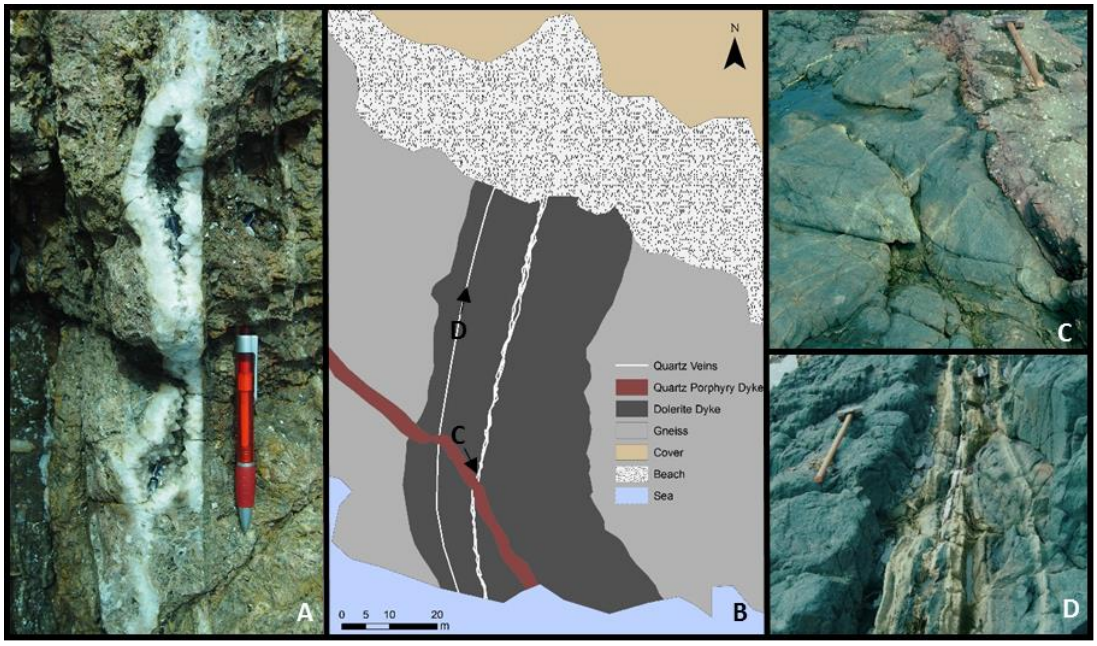

Figure 20. Disseminated, vuggy quartz veins occur throughout the field area. The veins are generally less than 10 cm thick and may follow brittle features such as joint sets or faults. A: The veins have open spaces and euhedral quartz grains. B: Sketch map of a field locality showing good cross cutting relationships. A Cretaceous dolerite dyke is cross cut by a vuggy vein which is cross cut by a quartz porphyry dyke. Therefore the age of these veins is well constrained to 130-135 Ma. A: 31.14719502°S, 17.7548151°E; B: 31.13569538°S, 17.74456638°E; C and D are indicated on B with arrows representing view direction.

2.3. Petrography of the Brak Fontein Shear Zone

Thin sections of the BFSZ and its wall rock were made in order to constrain the temperature and nature of deformation. Orientated thin sections were made in order to determine a sense of displacement. The mineralogy of the BFSZ and its wall rock consists predominantly of quartz (~30%), feldspar (~55%), biotite (~10%) and opaque minerals (~5%), making geothermobarometry difficult. The wall rock Jakkalshoek Granite (Figure 21) has feldspar phenocrysts with a mottled, altered appearance. Poorly defined bands of quartz and bands of biotite with opaque minerals occur. With increasing strain (Figure 22), the feldspar grains are flattened and sheared out and the quartz and biotite-opaque shear bands become closer spaced. Deformation textures are not visible in the quartz grains as these are strongly recrystallized. Typically the feldspar grains become flattened and stretched out, consistent with regime 2 or 3 deformation (Tullis, 2002). No obvious asymmetry was observed in the biotite. Rare observations in the BRSZ include folds in thin section scale, a single thin section with mantled porphyroclasts, rare garnets and a cross-cutting chlorite alteration (Figure 23). The mylonite of the BFSZ was recrystallized and annealed soon after deformation and there is no evidence for a later ductile overprint, which suggests that permeability after deformation, in the dormant BFSZ, was very low.

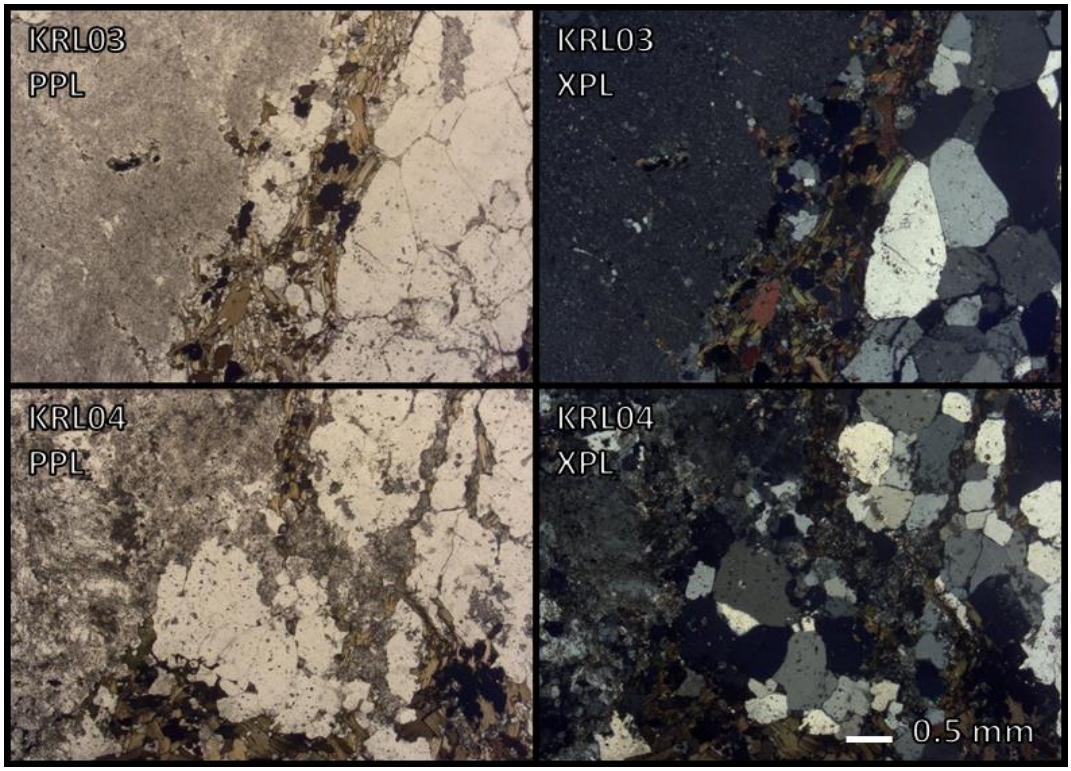

Figure 21. Jakkalshoek Granite in the wall rock of the BFSZ. Texturally and mineralogically the Jakkalshoek Granite is fairly consistent. Two representative thin sections are shown. The mineralogy is made up of feldspars, quartz, biotite and opaque minerals. A poorly developed fabric consisting of quartz and biotite bands wraps around large, strongly altered feldspar grains. KRL03: 31.0233°S, 17.92749°E; KRL04: 31.02233°S, 17.91772°E.

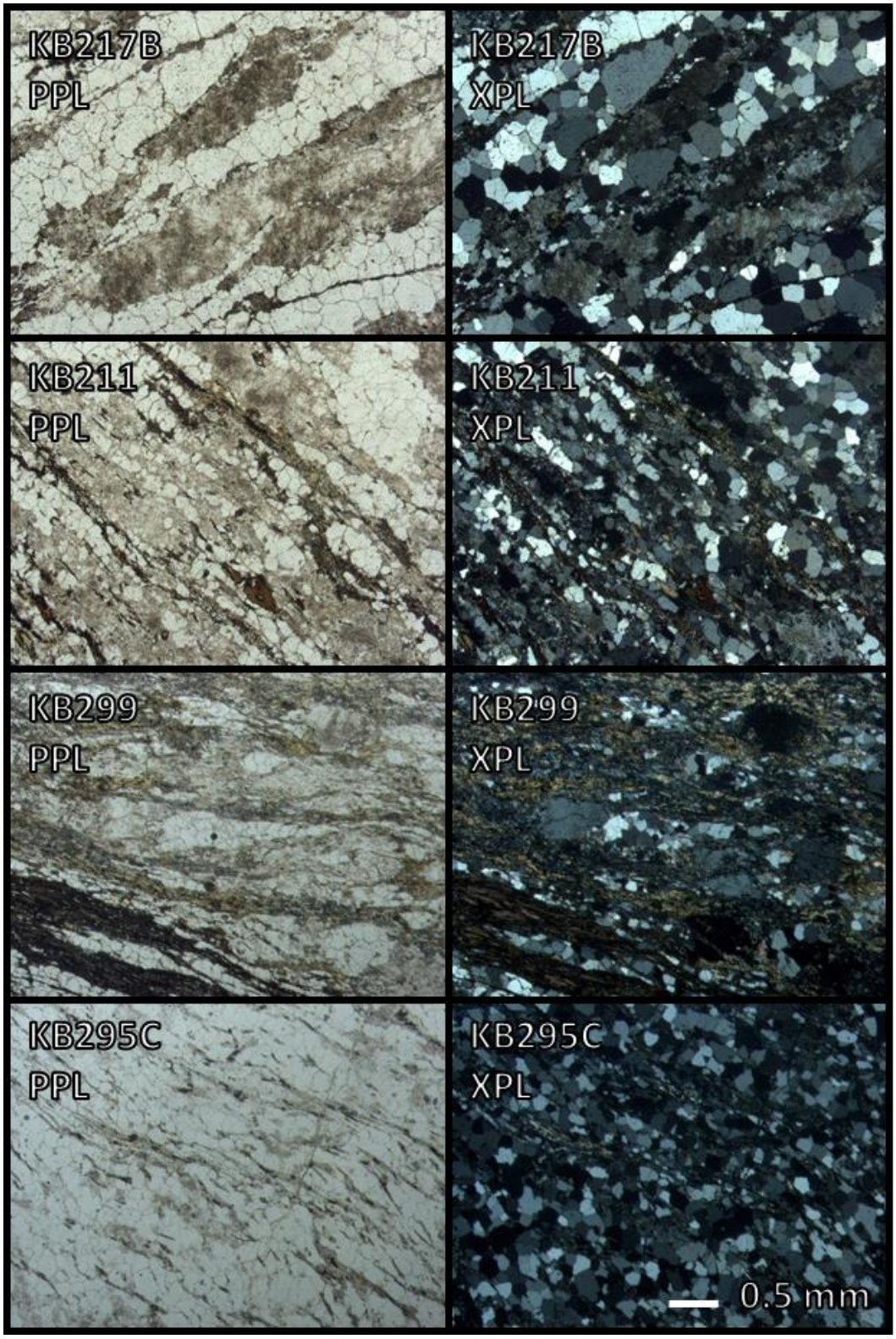

Figure 22. Representative textures and mineralogy of the BFSZ in the roof pendant. As the Jakkalshoek Granite is deformed, shear bands of quartz and feldspar develop and the feldspar grains become progressively flattened with increasing strain. Generally no shear indicators are visible in thin sections. KB217B: 30.97700391°S, 17.88797152°E; KB211: 30.97686896°S, 17.88587445°E; KB299: 30.97389883°S, 17.88063769°E; KB295C: 30.97502268°S, 17.88410981°E.

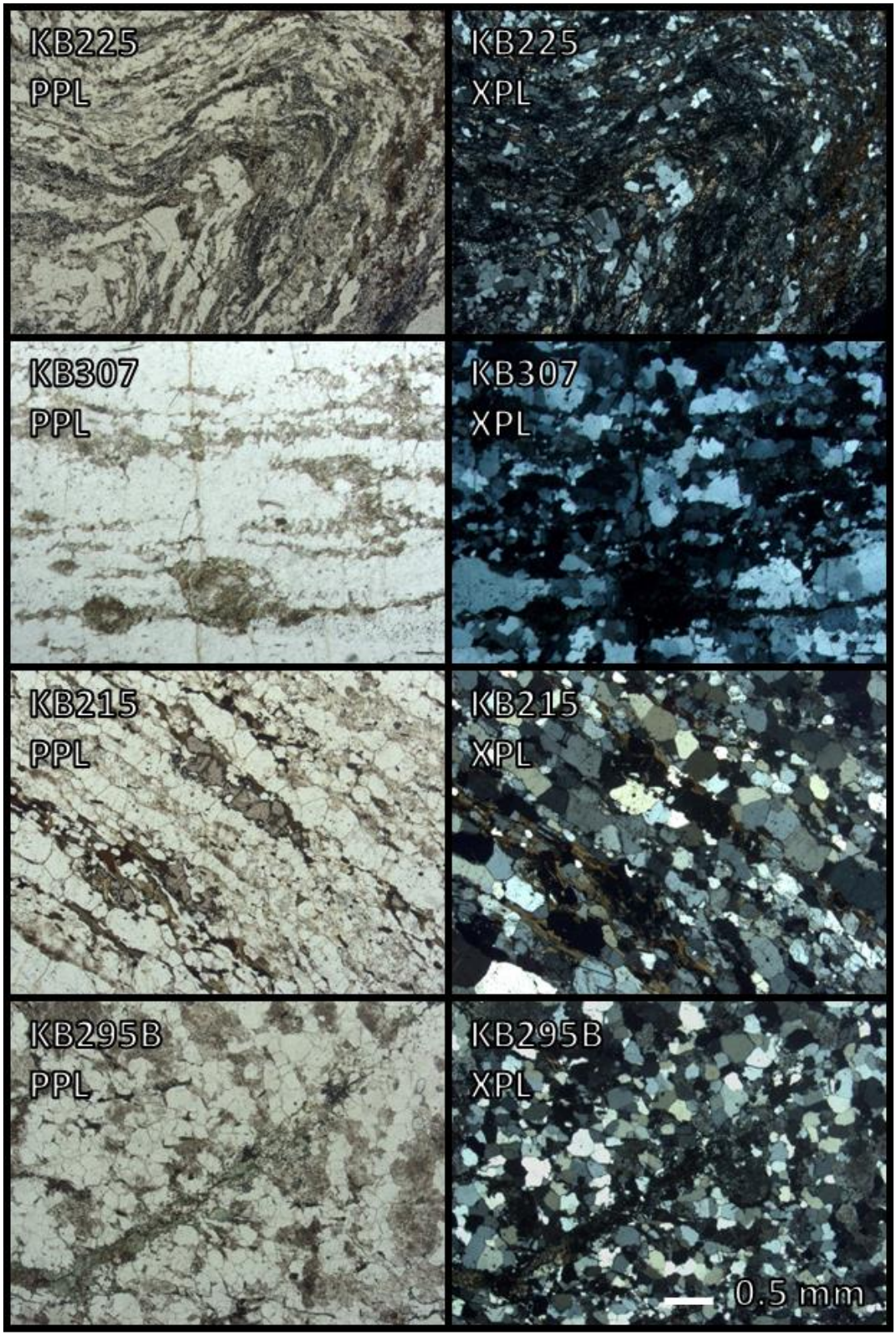

Figure 23. Rare observations in thin sections of the BFSZ. KB255: Folds can rarely be observed in thin section scale. KB307: Only one instance of mantled feldspar porphyroclasts was observed at the micro-scale. KB215: Rarely garnet is present. KB295B: Chlorite is a common late alteration mineral. It cross-cuts the deformational fabric. KB255: 31.12915331°S, 17.93079668°E; KB307: 30.98547366°S, 17.88648566°E; KB215: 30.9765973°S, 17.88977271°E; KB295B: 30.97502268°S, 17.88410981°E.

3. Oxygen Isotope Geochemistry

3.1. Introduction

Oxygen isotopes are useful as a tracer and as a proxy for determining alteration temperatures and water/ rock ratios in shear zones. The high crustal abundance of oxygen makes this a robust method. Oxygen isotope data can be used in combination with geological constraints in order to determine the fluid source, alteration temperature, alteration duration and even the paleoclimate prevalent during hydrothermal fluid – rock exchange (Sharp, 2007). Differences in the concentration of ^{16}O to ^{18}O are expressed mathematically as the $\delta^{18}O$ value (Equation 1) where the standard is SMOW (Standard Mean Oceanic Water) and the unit is per mille (‰).

Equation 1. The $\delta^{18}O$ value:

$$\delta^{18}O = \frac{\left(\frac{^{18}O}{^{16}O}\right)_{sample} - \left(\frac{^{18}O}{^{16}O}\right)_{standard}}{\left(\frac{^{18}O}{^{16}O}\right)_{standard}} * 1000\ ‰$$

The $\delta^{18}O$ values of major oxygen reservoirs are given in Figure 24. Ocean water is the standard (SMOW) has a $\delta^{18}O$ value of ~0‰. Negative $\delta^{18}O$ values only occur in meteoric water. The $\delta^{18}O$ values of the lithosphere are summarised by Eiler (2001). The mantle has a $\delta^{18}O$ value of approximately 5.7‰. Sediments have the highest $\delta^{18}O$ values. Authigenic sedimentary rocks and limestones can have $\delta^{18}O$ values > 30‰. As magmas evolve from a mantle composition to a more felsic composition, typical for continental crust, they are contaminated with sediments to variable degrees and their $\delta^{18}O$ values increase accordingly. Therefore igneous crustal rocks have $\delta^{18}O$ values equivalent to or higher than the mantle. Unaltered metamorphic rocks have $\delta^{18}O$ values similar to their protoliths. Therefore the crust generally has $\delta^{18}O$ values ranging from 5.7‰ to >20‰. Crustal rocks with $\delta^{18}O$ values below 5.7‰ are rare and can only form by high temperature oxygen exchange with fluids. Rocks with negative $\delta^{18}O$ values can only be explained by high temperature interaction with meteoric water.

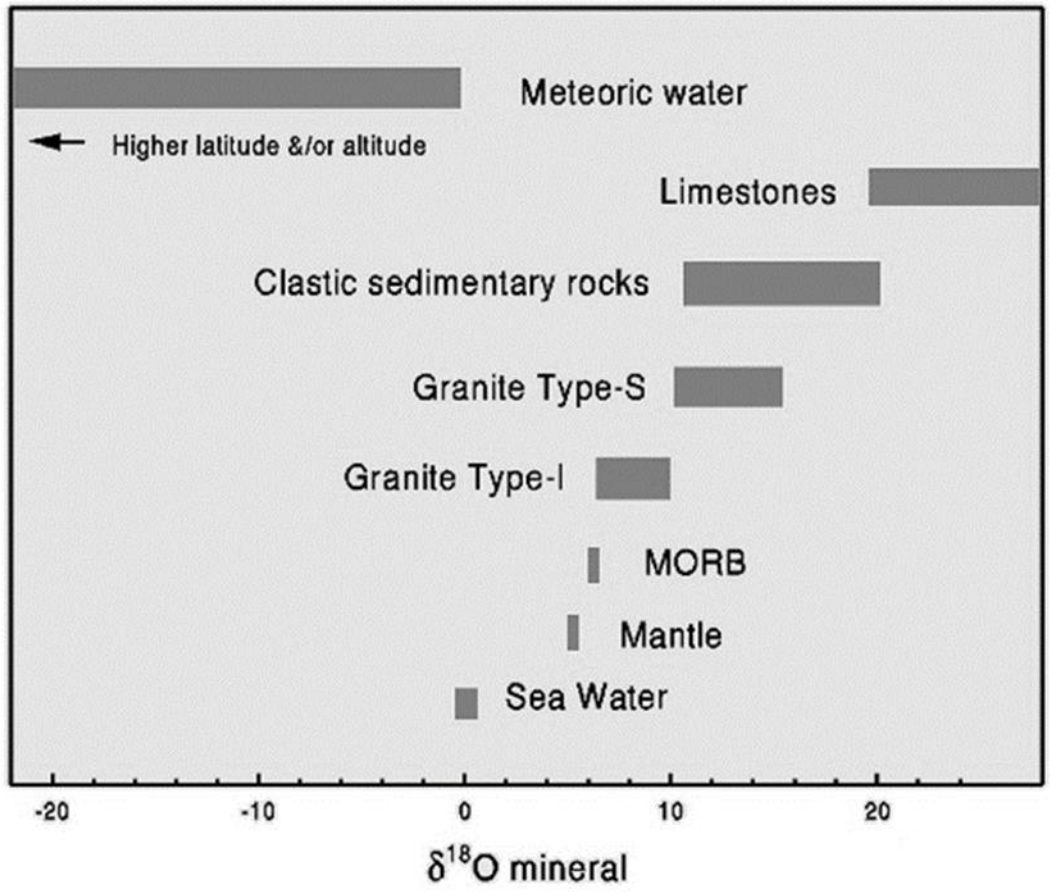

Figure 24. Typical $\delta^{18}O$ ranges of major rock types of the Earths curst (Eiler, 2001) *and for sea water and meteoric water* (Alley and Cuffey, 2001)*. Most crustal rocks are ^{18}O enriched relative to the mantle value of 5.7 ‰. Sediments have high $\delta^{18}O$ values due to incorporation of a high proportion of authigenic minerals. Igneous rocks generally experience and increase of $\delta^{18}O$ values with evolution from the mantle due to contamination with sediments.*

Preferential exchange of oxygen isotopes between phases is called fractionation. The fractionation factor α describes the isotopic equilibrium between two phases where A and B are phases at isotopic equilibrium (Equation 2).

Equation 2.The fractionation factor α between phase A and B:

$$\alpha_{A-B} = \frac{R_A}{R_B} = \frac{\left(\frac{^{18}O}{^{16}O}\right)_A}{\left(\frac{^{18}O}{^{16}O}\right)_B} = \frac{1000+\delta^{18}O_A}{1000+\delta^{18}O_B}$$

The fractionation factor is temperature dependant. The mathematical relationship between the fractionation factor $\alpha_{water\text{-}mineral}$ and temperature for quartz-water and plagioclase-quartz has been determined experimentally and can be mathematically approximated (Clayton et al., 1972; Matsuhisa et al., 1979); Zheng, 1993). Equation 3 A and B and Equation 4 A and B relate $\alpha_{quartz\text{-}water}$ and $\alpha_{quartz\text{-}plagioclase}$ with temperature in Kelvin.

Equation 3 A and B. Mathematical approximation of the relationship between the fractionation factor for quartz – water ($\alpha_{Q\text{-}W}$) and temperature (T, in Kelvin) for a temperature range of 200°C – 500°C and for 500°C – 750°C respectively (Clayton et al., 1972).

$$1000 \ln \alpha_{Q-W} = 3.38 * 10^6 \, T^{-2} - 3.40 \qquad \text{200°C to 500°C}$$

$$1000 \ln \alpha_{Q-W} = 2.51 * 10^6 \, T^{-2} - 1.96 \qquad \text{500°C to 750°C}$$

Equation 4 A and B. Mathematical approximation of the relationship between the fractionation factor albite - water ($\alpha_{Ab\text{-}W}$) and temperature (T, in Kelvin) for a temperature range of 400°C – 500°C and for 500°C – 800°C respectively (Matsuhisa et al., 1979).

$$1000 \ln \alpha_{Ab-W} = 2.39 * 10^6 T^{-2} - 2.51 \qquad \text{400 to 500°C}$$

$$1000 \ln \alpha_{Ab-W} = 1.59 * 10^6 T^{-2} - 1.16 \qquad \text{500 to 800°C}$$

It is worth noting the following about the fractionation factor $\alpha_{water\text{-}mineral}$:

- At lower temperatures the heavy isotopes of oxygen fractionate into the mineral. Therefore a mineral in isotopic equilibrium with water at surface conditions will have a much higher $\delta^{18}O$ value than the water. This leads to high $\delta^{18}O$ values in sediments.
- As temperature increases the fractionation factor $\alpha_{water\text{-}mineral}$ approaches 1. This means that the mineral will reach a $\delta^{18}O$ value close to that of the water at high temperatures.
- Anomalously low $\delta^{18}O$ values in rocks can only be achieved by high temperature alteration with fluid which has an even lower $\delta^{18}O$ value.
- For values of $\alpha < 1.01$, $\Delta \approx 1000 * \ln \alpha$, where Δ is the difference in $\delta^{18}O$ values between 2 phases. If $\alpha = 1.005$ then $\Delta \approx 5‰$.

Not all fractionating processes reach equilibrium, but can be the result of short lived exchange, kinetic exchange or buffering reactions. Differential isotopic exchange creates curved trajectories in mineral-mineral plots which can reveal information on reaction duration, temperature and the equilibrium the system was approaching (Criss et al., 1987; Gregory et al., 1989).

3.2. Analytical Methods

During the course of field work the BFSZ and its wall rock were targeted for sampling. This involved sampling across the shear zone as well as trying to get a regional sample coverage of the Namaqua-Natal Belt and Gariep Supergroup. When found, quartz veins and dykes of the Koegel Fontein Complex were sampled. In total 121 samples were taken. In the field care was taken to sample unweathered rock. If no fresh rock was available, only quartz grains were analysed as quartz is resistant to weathering and Oxygen isotope exchange at surface conditions. Samples were jaw-crushed before hand picking quartz and/or feldspar grains under a microscope. If neither quartz nor feldspar grains could be picked, typically in fine grained samples, a whole rock powder was prepared in a mortar with acetone. Oxygen gas was liberated from the silicates via either laser fluorination or conventional fluorination at the UCT Department of Geological Sciences. Quartz was processed using the laser fluorination line. Feldspar and whole rock powders were processed using the conventional fluorination line. The $\delta^{18}O$ value of the O_2 gas was determined using mass spectroscopy at the UCT Archaeology Department.

Figure 25. The stable isotope lab situated at the UCT Department of Geological Sciences. Left: The conventional fluorination line. Right: The laser fluorination line.

3.2.1. Laser Fluorination

Approximately 2.5 to 3.0 mg of sample was required per oxygen isotope analysis. Quartz grains were handpicked under a microscope. Oxygen gas was extracted and purified via laser fluorination as described by (Harris and Vogeli, 2010). A nickel sample holder with 12 drilled holes was loaded with 10 quartz grains alongside 2 in-house MON GT garnet standards. The samples were dried in a 110°C oven to remove absorbed moisture. The samples and the sample holder were then inserted into the reaction chamber of the laser fluorination line. After pumping out the reaction chamber, BrF_5, a strong oxidation agent, was inserted into the reaction chamber.

Oxygen was liberated from the samples individually. A CO_2 laser heated a sample, providing the activation energy required for oxidation with BrF_5. The products of the oxidation reaction are O_2 (g), fluorine salts, F_2 (g) and Br_2 (g). Essentially, pure O_2 was isolated from the reaction product by passing the gaseous reaction product through a hot KCl filter. The KCl filter retains F_2 (g) and releases Cl_2 (g). The Cl_2 (g) and Br_2 (g) is frozen into a cold finger with liquid nitrogen. The remaining pure O_2 (g) was then frozen into a sample bottle containing a molecular sieve. The sample bottles were then taken to the Archaeology Department of UCT and analysed for $\delta^{18}O$ using a mass spectrometer. The average difference in 216 analyses $\delta^{18}O$ values of the MON GT garnet standard is 0.11‰ and the standard deviation is 0.15‰.

3.2.2. Conventional Fluorination

Approximately 10 mg of feldspar or whole rock powder is required for oxygen liberation using conventional fluorination. Oxygen was liberated from feldspar or whole rock powder and reacted to CO_2 gas using conventional fluorination methods. The conventional fluorination line is located at the UCT Department of Geological Sciences and is described by Harris and Ashwal (2002). The $\delta^{18}O$ of the CO_2 gas was then measured using a mass spectrometer at the UCT Archaeology Department.

In preparation for conventional fluorination, the samples were powdered in a mortar with acetone. The samples were then degassed in a 50°C oven overnight. 8 samples and 2 quartz standards (MQ) are done per run. Approximately 10mg of powdered sample are loaded into nickel reaction tubes and are degassed at 200°C. Oxygen is then liberated from the sample by oxidation with ClF_3 at 550°C for 3h. The reaction vessels are then immersed in N_2 (l) to immobilise excess ClF_3 and unwanted reaction products. The O_2 is converted to CO_2 using a platinated hot carbon rod. The CO_2 was frozen into break seal tubes and sent to the mass spectrometer for oxygen analysis. The long term standard deviation of $\delta^{18}O$ values the MQ quartz standard is 0.15‰.

3.3. Results

A total of 271 analyses were done on the country rock of the Koegel Fontein Complex and on quartz veins. KB samples were sampled and analysed during the current project. KRL and CCK samples are from Curtis et al. (2013) and Curtis (2009). CHK data are unpublished data from Chris Harris. COK data comes from Olianti and Harris (2018). Samples are classified according to age and lithology. An overview of ages and rock types is given in the form of a geological sequence in Table 1. The $\delta^{18}O$ values of the country rock are given in Table 3. Table 4 gives $\delta^{18}O$ values of Pan-African and Cretaceous quartz veins. By plotting the $\delta^{18}O$ values of rocks pre-dating the Pan-African Orogeny in a histogram (Figure 26), two $\delta^{18}O$ peaks, located at ~8‰ and ~0‰ become visible. The highest $\delta^{18}O$ values occur in the Kamiesberg Group and Namibian metasedimentary rocks (the Gariep Supergroup). The lowest $\delta^{18}O$ values occur in sheared gneiss and in Mokolian orthogneiss. There also seems to be a tendency for high $\delta^{18}O$ values in quartz and low $\delta^{18}O$ values in whole rock samples. A histogram of $\delta^{18}O$ values of quartz veins is given in Figure 27. Pan-African veins have $\delta^{18}O$ values of about 6 – 8‰ while Cretaceous quartz veins mostly have $\delta^{18}O < 1$‰ and range from -4 – 11‰.

Table 3. Oxygen isotope analyses of the country rock of the Koegel Fontein Complex. The samples were classified according to age and rock type. Mokolian rocks (2050-900 Ma) pre-date the Namaqua Natal Orogeny (2200-1170 Ma). Mokolian and Namibian (900-542 Ma) rocks pre-date the Pan-African Orogeny (~545). Mokolian orthogneiss includes the Jakkalshoek Granite and the Mesklip Gneiss. The Kamiesberg Group has a sedimentary protolith and is made up of gneiss, schist and quartzite. Most samples of sheared gneiss are sheared Jakkalshoek Granite taken at the BFSZ. Namibian metasedimentary rocks form part of the Gariep Supergroup. KB samples were sampled and analysed during the course of this project. KRL and CCK data comes from Curtis et al. (2013) and Curtis (2009). CHK data are unpublished data from Chris Harris. COK data comes from Olianti and Harris (2018). Latitude and longitude is given in decimal degrees.

Sample	$\delta^{18}O$ Q‰	$\delta^{18}O$ Fsp‰	$\delta^{18}O$ WR‰	Age of Formation	Rock Type	latitude	longitude
CCK02			8.83	Mokolian	Orthogneiss	-31.23578	17.83903
CCK09			5.56	Mokolian	Orthogneiss	-31.10181	18.06233
CCK20			-2.76	Mokolian	Orthogneiss	-31.05042	17.91431
CCK22			-0.20	Mokolian	Orthogneiss	-31.13336	17.91469
CCK27			8.20	Mokolian	Orthogneiss	-31.19803	17.79456
CCK30			3.65	Mokolian	Orthogneiss	-31.19169	17.79322
CCK45			3.24	Mokolian	Orthogneiss	-31.08058	17.71667
CCK46			1.08	Mokolian	Orthogneiss	-31.08156	17.88333
CCK54			2.63	Mokolian	Orthogneiss	-31.02681	17.95067
CHK104	-2.73	-2.21		Mokolian	Orthogneiss	-31.02375	17.92748
CHK106	6.15	6.64		Mokolian	Orthogneiss	-31.19865	18.22422
CHK107		4.67		Mokolian	Orthogneiss	-31.17822	18.11930
CHK109	8.23	7.62		Mokolian	Orthogneiss	-31.15745	18.15060
CHK114	10.74	9.11		Mokolian	Orthogneiss	-31.13705	18.08797
CHK117	5.10	-0.42		Mokolian	Orthogneiss	-31.04073	17.90815
CHK118	5.98	-0.96		Mokolian	Orthogneiss	-31.04252	17.90182
CHK126	0.18	-0.90		Mokolian	Orthogneiss	-30.92478	17.89698
CHK127	7.47	1.18		Mokolian	Orthogneiss	-30.93080	17.89355
CHK129	2.39	5.20		Mokolian	Orthogneiss	-30.93767	17.89237
CHK130	9.25	8.92		Mokolian	Orthogneiss	-30.96695	17.89480
CHK131	7.50	2.21		Mokolian	Orthogneiss	-30.97358	17.90167
CHK134	5.43	-1.43		Mokolian	Orthogneiss	-30.99915	17.92120
CHK138	4.11	2.82		Mokolian	Orthogneiss	-31.04532	17.85583
CHK156		-1.50		Mokolian	Orthogneiss	-31.00877	17.88700
CHK61	9.23	8.98		Mokolian	Orthogneiss	-31.05952	18.01164
CHK62		2.67		Mokolian	Orthogneiss	-31.05952	18.01164
CHK63	10.06	8.95		Mokolian	Orthogneiss	-31.05828	18.03895
CHK72	6.26	5.66		Mokolian	Orthogneiss	-31.07633	17.90952
CHK76	8.39	5.08		Mokolian	Orthogneiss	-30.95691	17.84051
CHK77	8.51	6.91		Mokolian	Orthogneiss	-30.94753	17.84718
CHK96	4.79	6.85		Mokolian	Orthogneiss	-30.96944	17.89650
COK163			3.12	Mokolian	Orthogneiss	-31.04471	17.91248
COK169			0.03	Mokolian	Orthogneiss	-31.05149	17.91491
COK171			1.06	Mokolian	Orthogneiss	-31.03998	17.90879
COK173			3.17	Mokolian	Orthogneiss	-31.05463	17.91640

Sample	$\delta^{18}O$ Q‰	$\delta^{18}O$ Fsp‰	$\delta^{18}O$ WR‰	Age of Formation	Rock Type	latitude	longitude
COK177			-0.09	Mokolian	Orthogneiss	-31.05002	17.91471
COK189	3.94	-0.83		Mokolian	Orthogneiss	-31.05067	17.91682
COK190	6.51	4.25		Mokolian	Orthogneiss	-31.05147	17.91592
KB205	10.59	9.96		Mokolian	Orthogneiss	-31.03008	18.21311
KB214	10.37	7.70		Mokolian	Orthogneiss	-30.97624	17.89068
KB216	8.32	7.00		Mokolian	Orthogneiss	-30.97675	17.88896
KB226	8.30	7.28		Mokolian	Orthogneiss	-30.97066	17.86711
KB227	7.16	6.10		Mokolian	Orthogneiss	-30.96638	17.89370
KB231	-1.06	-1.35		Mokolian	Orthogneiss	-31.01508	17.88362
KB232	10.49	7.94		Mokolian	Orthogneiss	-31.15133	17.93485
KB239	10.30	10.22		Mokolian	Orthogneiss	-31.22283	17.81903
KB240	11.81	7.39		Mokolian	Orthogneiss	-31.20223	17.80003
KB241	9.73	7.53		Mokolian	Orthogneiss	-31.19358	17.79464
KB242	11.99	10.52		Mokolian	Orthogneiss	-31.18649	17.78834
KB243	10.11	8.38		Mokolian	Orthogneiss	-31.18650	17.78860
KB244	9.71	7.32		Mokolian	Orthogneiss	-31.16900	17.77298
KB246	9.52	5.10		Mokolian	Orthogneiss	-31.14720	17.75482
KB247	10.89	6.05		Mokolian	Orthogneiss	-31.13570	17.74457
KB252	9.11	6.76		Mokolian	Orthogneiss	-31.10457	17.73231
KB253	9.37	5.74		Mokolian	Orthogneiss	-31.02146	17.77293
KB254	10.26	8.83		Mokolian	Orthogneiss	-31.12676	17.92941
KB255	10.40	7.68		Mokolian	Orthogneiss	-31.12915	17.93080
KB259	10.55	5.70		Mokolian	Orthogneiss	-31.09936	18.06474
KB260	11.01			Mokolian	Orthogneiss	-31.06723	18.25777
KB261	7.79			Mokolian	Orthogneiss	-31.09136	18.20478
KB265	8.24			Mokolian	Orthogneiss	-31.10621	17.91558
KB266	7.21			Mokolian	Orthogneiss	-31.12945	17.88905
KB267	8.46	-0.60		Mokolian	Orthogneiss	-31.10164	17.89401
KB270	9.40			Mokolian	Orthogneiss	-31.08460	17.88099
KB272	5.74			Mokolian	Orthogneiss	-31.10189	17.91207
KB274		7.97		Mokolian	Orthogneiss	-30.99900	17.86286
KB275	3.42	3.48		Mokolian	Orthogneiss	-30.99679	17.87551
KB276A	0.94	0.90		Mokolian	Orthogneiss	-30.98221	17.88731
KB276B	0.82			Mokolian	Orthogneiss	-30.98221	17.88731
KB277	1.01			Mokolian	Orthogneiss	-30.98047	17.88779
KB278 dark			-2.10	Mokolian	Orthogneiss	-30.97892	17.88773
KB278 light	8.12			Mokolian	Orthogneiss	-30.97892	17.88773
KB279	8.65			Mokolian	Orthogneiss	-30.97877	17.88749
KB280			1.56	Mokolian	Orthogneiss	-30.97877	17.88749
KB281	7.91			Mokolian	Orthogneiss	-30.97657	17.88719
KB282	5.41		2.86	Mokolian	Orthogneiss	-30.97657	17.88719
KB283	7.25			Mokolian	Orthogneiss	-30.97502	17.88411

Sample	$\delta^{18}O$ Q‰	$\delta^{18}O$ Fsp‰	$\delta^{18}O$ WR‰	Age of Formation	Rock Type	latitude	longitude
KB284		2.93		Mokolian	Orthogneiss	-31.10053	17.92543
KB286A	7.17			Mokolian	Orthogneiss	-31.18825	17.92545
KB286B	8.14			Mokolian	Orthogneiss	-31.18825	17.92545
KB290	9.78	5.43		Mokolian	Orthogneiss	-31.11484	17.73712
KB294	10.35			Mokolian	Orthogneiss	-31.08314	17.71954
KB295	3.91			Mokolian	Orthogneiss	-30.97502	17.88411
KB296	6.23		5.00	Mokolian	Orthogneiss	-30.97481	17.88363
KB297		2.82		Mokolian	Orthogneiss	-30.97450	17.88328
KB298A	-1.40		7.36	Mokolian	Orthogneiss	-30.97432	17.88240
KB298B	8.56			Mokolian	Orthogneiss	-30.97432	17.88240
KB299	7.25			Mokolian	Orthogneiss	-30.97390	17.88064
KB301			4.07	Mokolian	Orthogneiss	-30.97365	17.88055
KB303	6.95			Mokolian	Orthogneiss	-30.97264	17.87871
KB304	4.30			Mokolian	Orthogneiss	-30.98425	17.88934
KB305	-0.86			Mokolian	Orthogneiss	-30.98547	17.88649
KB307	1.66			Mokolian	Orthogneiss	-30.98547	17.88649
KB308		2.40		Mokolian	Orthogneiss	-30.99133	17.88010
KB309	0.89			Mokolian	Orthogneiss	-31.01584	17.88326
KB311	0.06			Mokolian	Orthogneiss	-31.01475	17.88383
KB312	6.84			Mokolian	Orthogneiss	-30.91406	17.88022
KB313	7.54	6.22		Mokolian	Orthogneiss	-30.94349	17.85013
KB314	7.30		6.04	Mokolian	Orthogneiss	-30.94788	17.84157
KRL01	7.49	-1.92	0.54	Mokolian	Orthogneiss	-31.02060	17.94586
KRL02	3.62		1.09	Mokolian	Orthogneiss	-31.02162	17.93314
KRL03	5.86		1.86	Mokolian	Orthogneiss	-31.02330	17.92749
KRL04	7.51	5.59	5.73	Mokolian	Orthogneiss	-31.02233	17.91772
KRL05			5.85	Mokolian	Orthogneiss	-31.02150	17.89866
KRL07	0.37	-0.44	-0.19	Mokolian	Orthogneiss	-31.01520	17.88465
KRL09	5.82	5.20	3.02	Mokolian	Orthogneiss	-31.00940	17.87888
KRL10	7.55		7.47	Mokolian	Orthogneiss	-30.99870	17.86281
KRL12			-3.22	Mokolian	Orthogneiss	-31.05071	17.91520
KRL13	4.87		3.65	Mokolian	Orthogneiss	-31.05082	17.91534
KRL14	8.63	4.35	6.18	Mokolian	Orthogneiss	-31.05071	17.91625
KRL15	5.16	1.23	0.99	Mokolian	Orthogneiss	-31.04994	17.91735
KRL18			5.96	Mokolian	Orthogneiss	-31.14362	18.16691
KRL19			6.48	Mokolian	Orthogneiss	-31.14362	18.16691
CCK14			4.61	Mokolian	Kamiesberg Grp	-31.09342	18.01342
KB234A	14.44			Mokolian	Kamiesberg Grp	-31.16567	17.92280
KB235	12.29			Mokolian	Kamiesberg Grp	-31.18046	17.90874
KB236			10.73	Mokolian	Kamiesberg Grp	-31.18044	17.90851
CCK13			10.11	Mokolian	Sheared Gneiss	-31.08467	18.04558
CCK34			-2.96	Mokolian	Sheared Gneiss	-31.15681	17.76306

Sample	$\delta^{18}O$ Q‰	$\delta^{18}O$ Fsp‰	$\delta^{18}O$ WR‰	Age of Formation	Rock Type	latitude	longitude
CHK128	6.23	4.18		Mokolian	Sheared Gneiss	-30.93080	17.89355
CHK132	7.47	2.64		Mokolian	Sheared Gneiss	-30.98223	17.90793
CHK133	6.92	-1.13		Mokolian	Sheared Gneiss	-30.98967	17.91333
CHK152			-0.94	Mokolian	Sheared Gneiss	-30.97952	17.88478
CHK183	7.24	1.59		Mokolian	Sheared Gneiss	-30.97358	17.88052
CHK183	7.24	1.59		Mokolian	Sheared Gneiss	-30.97358	17.88052
CHK184		0.74		Mokolian	Sheared Gneiss	-30.97312	17.88035
CHK73	3.98			Mokolian	Sheared Gneiss	-31.07494	17.90500
COK167			-1.13	Mokolian	Sheared Gneiss	-31.05073	17.91349
COK194	-0.52	-0.63		Mokolian	Sheared Gneiss	-31.05642	17.91640
COK210	0.64		-1.55	Mokolian	Sheared Gneiss	-31.06885	17.92405
KB211			-1.22	Mokolian	Sheared Gneiss	-30.97687	17.88587
KB212	2.37			Mokolian	Sheared Gneiss	-30.97687	17.88587
KB213			2.70	Mokolian	Sheared Gneiss	-30.97635	17.88634
KB215			8.63	Mokolian	Sheared Gneiss	-30.97660	17.88977
KB217			2.69	Mokolian	Sheared Gneiss	-30.97700	17.88797
KB218			6.75	Mokolian	Sheared Gneiss	-30.97704	17.88782
KB219			4.53	Mokolian	Sheared Gneiss	-30.97639	17.88695
KB220			6.80	Mokolian	Sheared Gneiss	-30.97639	17.88695
KB221			3.32	Mokolian	Sheared Gneiss	-30.97456	17.88322
KB223			2.81	Mokolian	Sheared Gneiss	-30.97381	17.88067
KB224			-0.77	Mokolian	Sheared Gneiss	-30.97257	17.87983
KB225	7.47	6.17		Mokolian	Sheared Gneiss	-30.97171	17.87684
KB229			4.98	Mokolian	Sheared Gneiss	-31.01580	17.88393
KB230A			4.81	Mokolian	Sheared Gneiss	-31.01537	17.88400
KB230B	4.64			Mokolian	Sheared Gneiss	-31.01537	17.88400
KB253A			1.01	Mokolian	Sheared Gneiss	-31.02146	17.77293
KB257			8.16	Mokolian	Sheared Gneiss	-31.09936	18.06565
KB300A			-1.69	Mokolian	Sheared Gneiss	-30.97365	17.88055
KB300B	7.73			Mokolian	Sheared Gneiss	-30.97365	17.88055
KB300C		0.90		Mokolian	Sheared Gneiss	-30.97365	17.88055
KB300D	9.32			Mokolian	Sheared Gneiss	-30.97365	17.88055
KB310	-0.70	-0.90		Mokolian	Sheared Gneiss	-31.01434	17.88327
KRL06	7.43		5.58	Mokolian	Sheared Gneiss	-31.02057	17.89270
KRL08			2.48	Mokolian	Sheared Gneiss	-31.01531	17.88423
CCK25			17.39	Namibian	Metasediment	-31.23578	17.83903
CCK28			8.05	Namibian	Metasediment	-31.19803	17.79456
CHK121	14.82			Namibian	Metasediment	-30.94652	17.94718
CHK122	11.81			Namibian	Metasediment	-30.94910	17.94800
CHK123	10.82			Namibian	Metasediment	-30.94963	17.94585
CHK124	11.50			Namibian	Metasediment	-30.92455	17.91452
KB238			16.78	Namibian	Metasediment	-31.23563	17.83897

Table 4. Oxygen isotope analyses of quartz veins. Pan-African veins are massive, large and pre-date the intrusion of the Koegel Fontein Complex. Cretaceous veins are vuggy, less than 10 cm wide and formed during the emplacement of the Koegel Fontein Complex. Latitude and Longitude are given in decimal degrees.

Sample	$\delta^{18}O$ Q‰	$\delta^{18}O$ Fsp‰	$\delta^{18}O$ WR‰	Age of Formation	Rock Type	latitude	longitude
CCK01	10.66			Pan-African	Quartz Vein	-31.15408	18.03333
CCK05	10.22			Pan-African	Quartz Vein	-31.10144	18.06219
CCK16	9.86			Pan-African	Quartz Vein	-31.15214	17.93581
CCK29	10.05			Pan-African	Quartz Vein	-31.19803	17.79456
CCK40	9.60			Pan-African	Quartz Vein	-31.71278	31.07461
CCK49	9.18			Pan-African	Quartz Vein	-31.08317	17.71950
CCK50	5.61			Pan-African	Quartz Vein	-31.08314	17.72008
KB302	7.06			Pan-African	Quartz Vein	-30.97277	17.88005
CCK41	-1.48			Cretaceous	Quartz Vein	-31.07572	17.71319
CCK42	2.21			Cretaceous	Quartz Vein	-31.07858	17.71514
CCK43	-1.39			Cretaceous	Quartz Vein	-31.08058	17.71667
CCK44	-1.73			Cretaceous	Quartz Vein	-31.08058	17.71667
CCK48	-0.88			Cretaceous	Quartz Vein	-31.08156	17.88333
KB246QVA	-0.77			Cretaceous	Quartz Vein	-31.14720	17.75482
KB246QVB	-4.28			Cretaceous	Quartz Vein	-31.14720	17.75482
KB250	-3.49			Cretaceous	Quartz Vein	-31.13570	17.74457
KB251	10.93		-4.05	Cretaceous	Quartz Vein	-31.13570	17.74457
KB256	6.43			Cretaceous	Quartz Vein	-31.12877	17.93552
KB262A	-4.71			Cretaceous	Quartz Vein	-31.10279	17.91141
KB262B	-4.78			Cretaceous	Quartz Vein	-31.10279	17.91141
KB263	9.71			Cretaceous	Quartz Vein	-31.10277	17.91235
KB264	-0.85			Cretaceous	Quartz Vein	-31.10524	17.91526
KB268	-0.74			Cretaceous	Quartz Vein	-31.08460	17.88099
KB271	-1.56			Cretaceous	Quartz Vein	-31.08460	17.88099
KB273	5.41			Cretaceous	Quartz Vein	-31.10189	17.91207
KB288A	-1.68			Cretaceous	Quartz Vein	-31.14882	17.75618
KB288B	3.10			Cretaceous	Quartz Vein	-31.14882	17.75618
KB288C	1.49			Cretaceous	Quartz Vein	-31.14882	17.75618
KB289	0.56			Cretaceous	Quartz Vein	-31.12562	17.74154
KB292	-3.37			Cretaceous	Quartz Vein	-31.08314	17.71954
KB293	-0.33			Cretaceous	Quartz Vein	-31.08314	17.71954
KB306	-4.81			Cretaceous	Quartz Vein	-30.98547	17.88649
KB315	-2.07			Cretaceous	Quartz Vein	-31.11109	17.92765

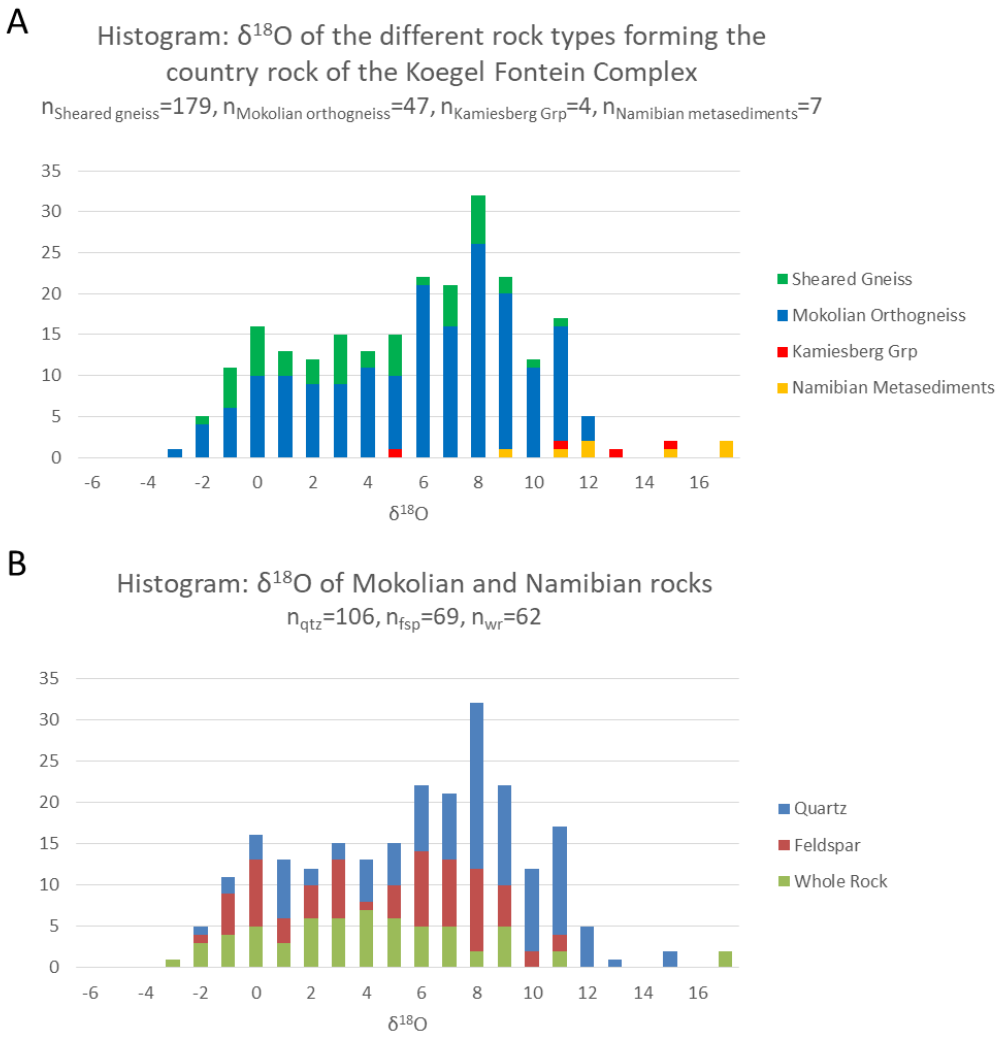

Figure 26. Histogram of $\delta^{18}O$ values of rocks pre-dating the Pan-African orogeny based on Table 3. Two peaks are visible. The high peak is centred at about 8‰ and is made up of predominantly quartz. The low $\delta^{18}O$ peak is centred at about 0‰ and is made up predominantly of feldspar and whole rock analysis. A: Histogram colour-coded according to rock type. B: Histogram showing the distribution of $\delta^{18}O$ in quartz, feldspar and whole rock samples.

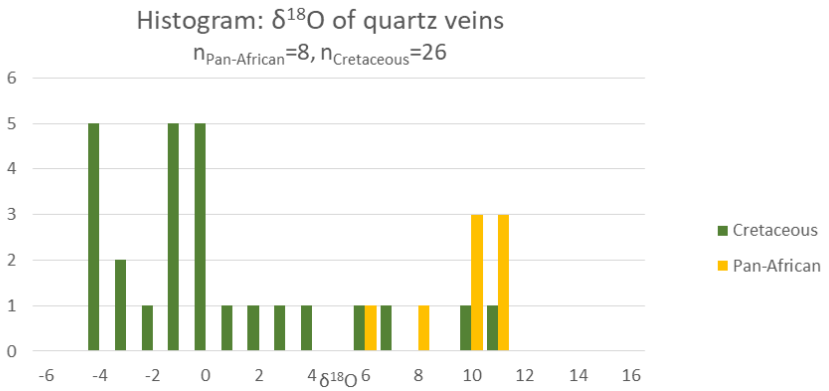

Figure 27. Histogram of quartz veins. Pan-African quartz veins have δ18O values at about 6 – 8‰. Cretaceous quartz veins mostly have δ18O < 1‰ and range from -4 – 11‰.

4. Discussion

4.1. Geological Framework

It has been proposed that low $\delta^{18}O$ magmas and quartz veins of the Koegel Fontein Complex formed due to selective melting of previously ^{18}O depleted crust (Curtis et al., 2013). This model requires a hydrothermal system which predates the Koegel Fontein Complex and which generated extreme ^{18}O depletion in sufficient volumes of rock. In order to place Oxygen isotope data into context, the geology of the study area has to be understood. The relationship between ^{18}O depletion and structures can give an indication to the timing and nature of the hydrothermal system. Alteration temperatures can be used in combination with isotope geochemistry in order to calculate the fluid – rock ratio and to estimate the $\delta^{18}O$ value of the fluid. The following section outlines geological constraints which will be used in combination with isotope geochemistry to determine and as far as possible quantify a proposed hydrothermal system. Figure 28 gives an overview of the area for the following discussion. It shows 3 structural domains which have been defined, the location of two cross-sections (Figure 29) and the location of the detailed map of the BFSZ (Figure 6 and Figure 37).

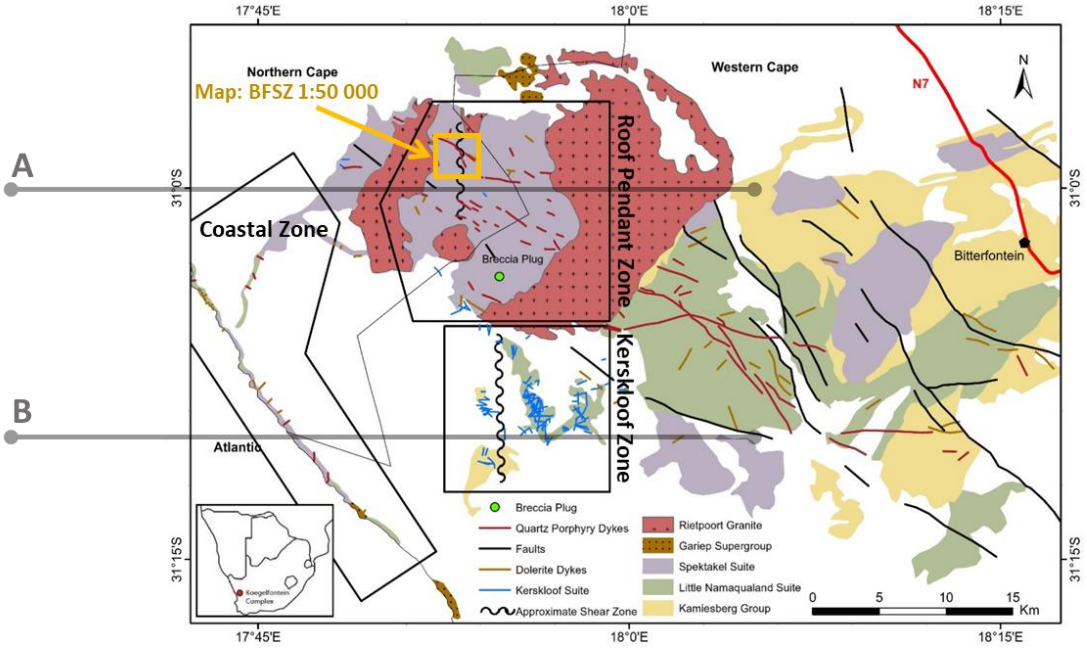

Figure 28. The overview map of the field area with simplified geology (same as Figure 2) with the addition of three zones. The zones are marked by black polygons and are labelled the "Roof Pendant", the "Kerskloof" and the "Coast" zones. Cross-sections were drawn along lines A and B (Figure 29). The location of the map "Brak Fontein Shear Zone 1:50 000" is indicated by the orange rectangle in the "Roof Pendant" zone. This map serves as a frame of reference for the discussion.

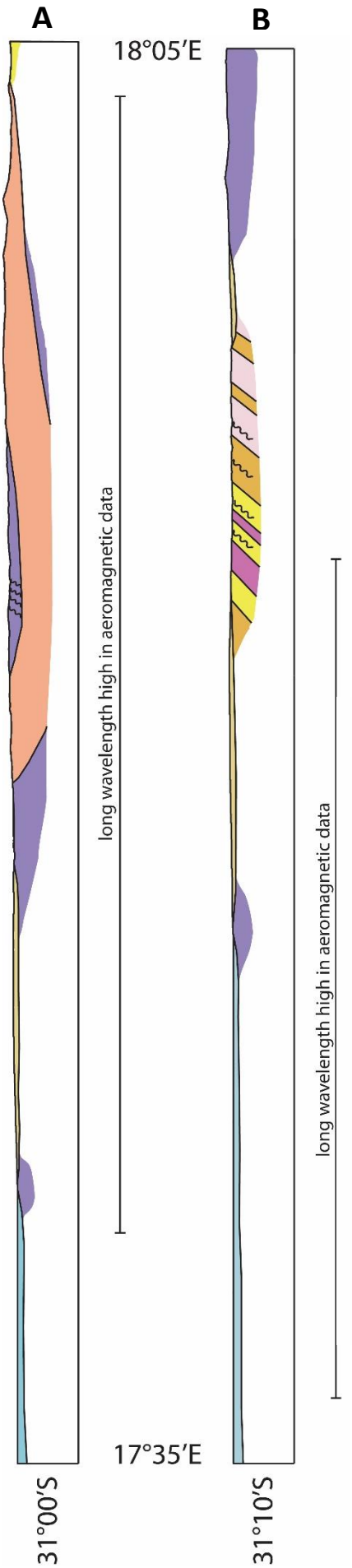

4.1.1. Structural Geology of the Area

The Namaqua-Natal Belt dominates the study area. It is structurally complex and difficult to map due to extensive Neogene cover. Due to ductile deformation and granulite facies metamorphism during the Namaqua-Natal Orogeny, it unlikely that Namaqua-Natal-aged structures had significant permeability during or after deformation. Potentially permeable structures in the Namaqua-Natal Belt post-date the Namaqua-Natal Orogeny. West-dipping Pan-African thrusts occur in the Gariep Supergroup in the northwest of the study area, while west- to southwest-dipping sinistral strike and shear zones occur in the Namaqua-Natal basement. WNW-trending Cretaceous faults and dykes may also be linked to higher permeability.

Two schematic cross sections were drawn along the latitudes of 31°00'S and 31°10'S from 17°35'E to 18°05'E (Figure 29). White space indicates a high uncertainty. Dykes have been omitted from the cross-sections as these are too small to be displayed. The Gariep Supergroup outcrops scarcely and does not occur in either cross-section. The northern cross-section shows the Rietpoort Granite pluton, which intersects the BFSZ, which in turn intersects the Jakkalshoek Granite. The southern-cross section shows variation in the Namaqua-Natal Belt along west-dipping lithological boundaries.

Figure 29. Cross sections of the field area without vertical exaggeration. Due to abundant quaternary cover large areas of the cross section have not been filled in. Lithologies and the BFSZ are generally west-dipping. The Rietpoort Granite is interpreted to be a saucer-shaped pluton of unknown thickness. The location of a deep magnetic high from the geophysical interpretation (Figure 5) is indicated. The locations of the cross-sections are given by lines A and B in Figure 29.

The Rietpoort Granite is interpreted to be a saucer-shaped intrusion with a roof pendant made up of Jakkalshoek Granite. The thickness of the Rietpoort Granite is unknown. The deep magnetic high from the geophysical interpretation (Figure 5) is unlikely to be an artefact of the Rietpoort Granite due to the granite's low magnetic resistivity relative to its country rock and due to a remnant magnetisation in the 1VD filter. A high and highly variable magnetic susceptibility in the BFSZ suggests that altered and/or mineralised Jakkalshoek Granite (as occurs in the BFSZ) may have a highly variable, but on average high magnetic susceptibility which may produce the deep magnetic anomaly. Alternatively the deep magnetic high could be produced by a deep phase of the Koegel Fontein Complex. There is no evidence for mafic underplating in the form of a high in the Bouguer Gravity data.

4.1.2. Pervasive Fabrics and Strain Partitioning

In order to describe the pervasive fabrics in the area, all foliations are plotted on stereonets according to the structural domains defined in Figure 28. Poles to Coenie de Beer's foliation measurements taken from the Koegel Fontein Complex 1:50 000 map (Figure 4) are plotted above poles to my own foliation measurements on lower-hemisphere equal-area stereonets for comparison (Figure 30). The foliation readings from both datasets correspond well. Along the coast the foliations are subhorizontal or shallowly west-dipping, from ~260/60 to ~080/20 averaging ~260/20. The foliations in the roof pendant and in Kerskloof are moderately-to-steeply west-dipping at ~10-90° (averaging 35°) and at ~20-70° (averaging 40°) respectively. There seems to be a gradual change from shallowly west-dipping foliations at the coast, to steeply west-dipping foliations in Kerskloof and the roof pendant. It is noteworthy that the orientation of foliations are the same in the Namaqua-Natal Belt and in the Gariep Supergroup. This was noticed in the field at the contact between the Namaqua-Natal Belt and the Gariep Supergroup, at the coast (Figure 10), where foliations and lineations on in either lithology are parallel, less than 10m apart.

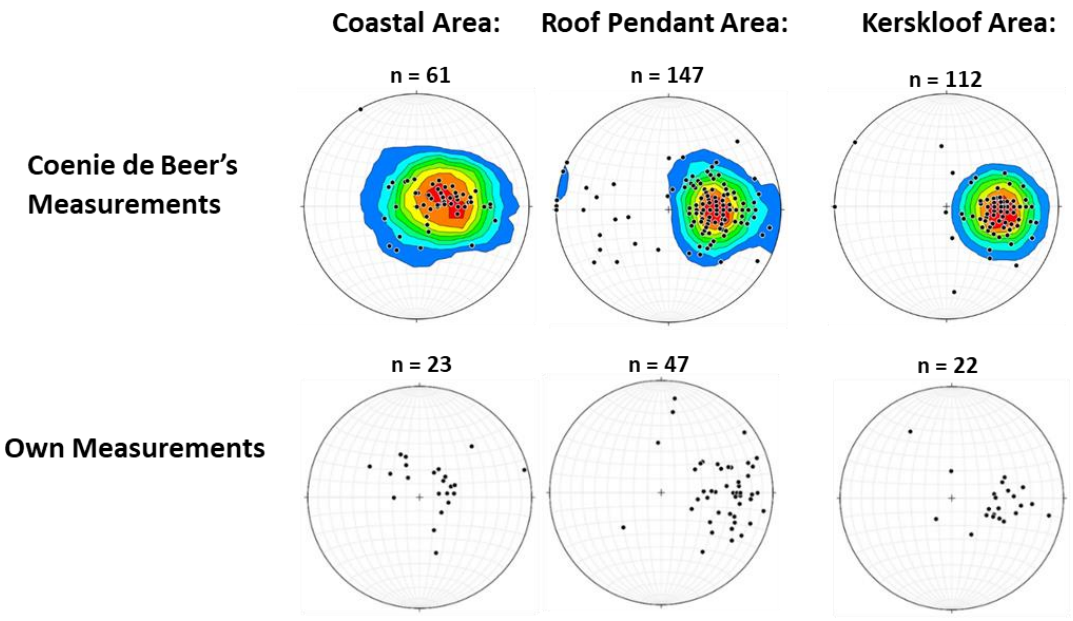

Figure 30. Poles to pervasive foliation of the Namaqua-Natal Belt and the Gariep Supergroup plotted by zones defined in Figure 28. Foliation readings from the map "Koegel Fontein 1:50 000" mapped by Coenie de Beer are shown alongside own readings for comparison. The datasets correspond well. Stereonets are lower-hemisphere equal-area projections.

The fact that pervasive fabrics in the Gariep Supergroup and the Namaqua-Natal Belt have the same orientation suggests that the main tectonic fabric in the area is a result of the Pan-African Orogeny and that the Namaqua-Natal Belt was strongly overprinted or transposed by Pan-African Orogeny along the coast in the study area. The BFSZ has the same orientation and age as the pervasive fabric and is therefore believed to be a manifestation of regional Pan-African strain partitioning. Variability in strain rate, temperature and/ or lithology may have resulted in different degrees of strain partitioning in different areas. North trending fault-like features which occur in the north of aeromagnetic interpretation map (Figure 5) and in the 1:250 000 geological maps are west-dipping thrust faults related to Pan-African deformation. These thrusts are equally areas of high strain partitioning. The thrust faults have a top to the east displacement while BFSZ is a north striking, sinistral, strike-slip shear zone. This may be explained by the regional NW directed shortening being split into a west-shortening thrust component and a NW-shortening strike-slip component manifested in N-trending sinistral shear zones. During the Pan-African Orogeny, NW directed shortening seems to have been accommodated by a combination of pervasive deformation and strain partitioning into strike-slip and thrust components.

4.1.3. Pan-African Orogenic Temperatures

The temperature during deformation has implications for the nature of deformation and the use of Oxygen isotopes. Temperatures of the Pan-African Orogeny are constrained using published data and geothermobarometry. Pseudosections were calculated using Perple_X (Connolly, 2005, 1990; Connolly and Petrini, 2002) using an updated version of the Holland and Powell (2011) dataset (hp11ver.dat). Solution models used in the modelling are the following: Gt(W) for garnet, FspC1(W) for feldspar, Chl(W), Mica(W) and Bi(W) for micas and melt(W) for melt (White et al., 2014). The ten-component MnO–Na2O–CaO–K2O–FeO–MgO–Al2O3–SiO2–H2O–TiO2 (MnNCKFMASHT) model system was used. Previously determined bulk chemistry of 10 samples of the Jakkalshoek Granite and sheared Jakkalshoek Granite in the BFSZ in the roof pendant was used (Mudzanani, 2011). The mean weight percent (wt%) of the major element oxides with the standard deviation (σ) and mean are given in Table 8 (located in the appendix). The mean bulk chemistry of mineral oxides relevant to the MnNCKFMASHT system was normalised and used as an input for Perple_X (Table 5).

A T-H_2O pseudosection was calculated at 5kbar and a P-T pseudosection was calculated assuming H_2O saturation (Figure 31). H_2O oversaturation is a prerequisite for the hydrothermal alteration which shall be proven using Oxygen isotope geochemistry. Fluid-rock exchange may not have occurred at peak metamorphic conditions. The mineralogy may be a result of fluid-rock exchange only if hydrothermal alteration happened at or after peak conditions. Although textural differences occur in the Jakkalshoek Granite inside the BFSZ in comparison to in the wall rock of the shear zone, the mineralogy is identical. The stability field of the Jakkalshoek Granite both inside and out of the BFSZ is indicated by a cross-hatched field. The stability field was constrained by muscovite absence and H_2O saturation. Free H_2O implies sub-solidus conditions because H_2O will be taken up in the melt. The T-H_2O pseudosection illustrates that the rock is saturated with H_2O at 0.3 wt% and that further free H_2O will not have any effect on the mineralogy. The temperature range of 570°C to 680°C is only valid at 5 kbar. The P-T pseudosection gives a P-T stability field for the Jakkalshoek Granite and its deformed variant in the BFSZ.

Kyanite and abundant muscovite occurs to the south of the Rietpoort Granite, in the Kamiesberg Group. The muscovite is attributed to hydration during the Pan-African Orogeny, because the Kamiesberg Group experienced granulite facies metamorphism in the Namaqua-Natal Orogeny. This is supported by the fact that the muscovite foliation has the same orientation as the BFSZ. The presence of muscovite suggests that the Kamiesberg Group's mineralogy is stable at cooler conditions than the mineralogy of the Jakkalshoek Granite.

An approximate P-T path is given in Figure 32. The P-T conditions are constrained to the Jakkalshoek Granite field before the temperature decreased, resulting in the formation of retrograde muscovite in the Kamiesberg Group and the Mesklip Gneiss. The Jakkalshoek presumably remained metastable during cooling and retained its mineralogy. The retrograde P-T path is further constrained by $^{40}Ar/^{39}Ar$ dates near the Salt River in the south of the study area (Frimmel and Frank, 1998). Cleavage muscovite yielded ages of 514 – 495 Ma. These ages might represent cooling instead of peak metamorphic conditions, as closure of muscovite occurs at 410–430°C. During cooling, the pressure decrease was small enough for the P-T conditions to move into the kyanite stability field. The P-T path therefore starts at the high P end of the Jakkalshoek Granite stability field and temperatures during deformation of the Jakkalshoek Granite can be further constrained to have occurred between about 580°C to 690°C. In conclusion the Namaqua-Natal Belt in the field area experienced tectonic and thermal overprint during the Pan-African Orogeny and cooled from a temperature of 580-690°C at approximately 545 Ma to 410-430°C at 514-495 Ma whereas the pressure decrease was small enough for P-T conditions to move into the kyanite stability field. The granitic mineralogy in the sheared Jakkalshoek Granite is preserved, while the Mesklip Gneiss and Kamiesberg Group mineralogically changed during cooling, predominantly by the formation of muscovite, staurolite and kyanite.

Table 5. The bulk chemistry used in pseudosection calculations with Perple_X (Figure 31). These wt% oxides were determined by calculating the mean of previously determined wt% oxides relevant to the MnNCKFMASHT system, normalised to 100%. The original bulk chemistries were sourced from a thesis by Mudzanani (2011)*. Table 8 (in the appendix) gives the original bulk chemistry of 10 samples of the Jakkalshoek Granite in the Roof Pendant of the Rietpoort Granite as well as the normalised mean and standard deviation (σ) of each wt% oxide. The standard deviation shows that the major element chemistry is fairly consistent in the roof pendant area and that using the mean wt% oxide is a good proxy.*

MnO	Na_2O	CaO	K_2O	FeO	MgO	Al_2O_3	SiO_2	TiO_2	H_2O
0.03	2.06	1.23	4.66	2.21	0.37	10.88	58.13	0.43	20

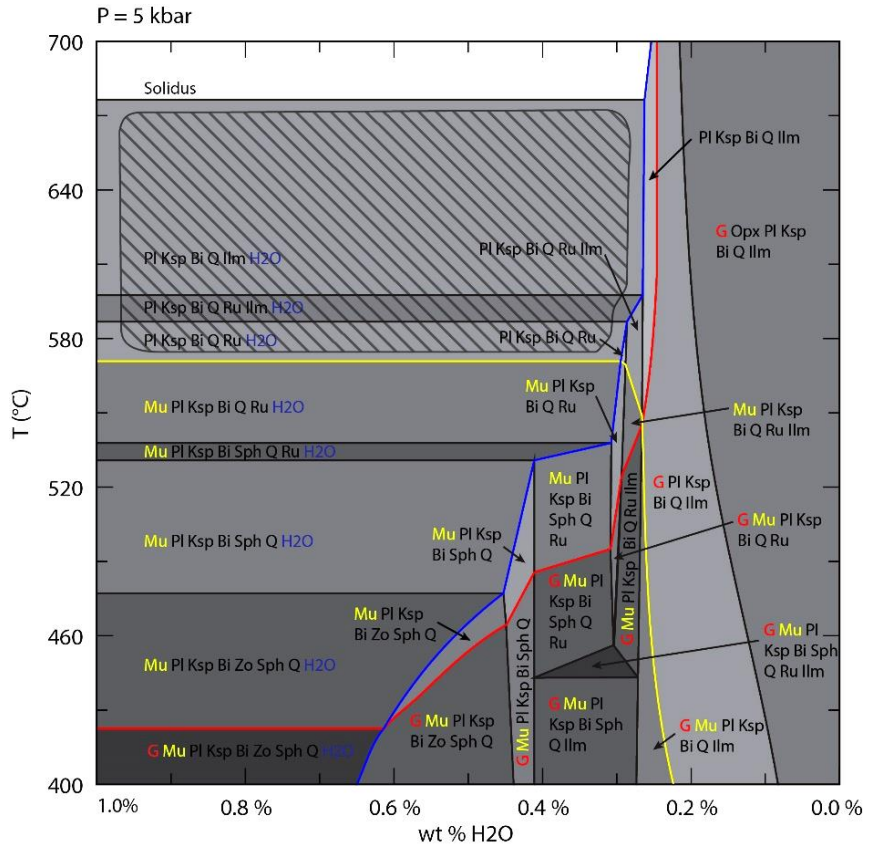

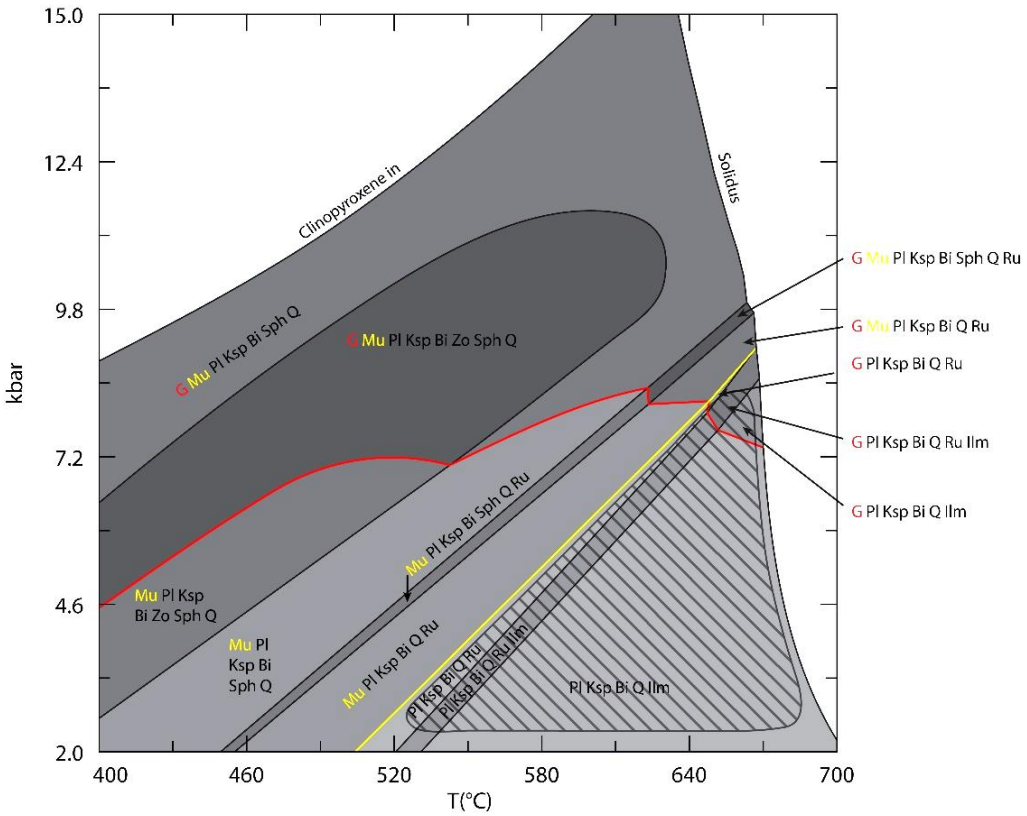

Figure 31. Pseudosections of a representative bulk chemistry of the Jakkalshoek Granite and the BRSZ (Table 5) in the roof pendant of the Rietpoort Granite. Fields with more abundant phases are coloured darker. The Jakkalshoek Granite and the BRSZ plots on the cross-hatched stability field. Absence of muscovite, fluid presence and melt absence were used to constrain the stability field. Free H_2O was present (not necessarily during peak conditions) as is indicated by the following discussion on hydrothermal oxygen exchange. Above: A wt% H_2O - T pseudosection. The BFSZ is fluid saturated with 0.3 wt% H_2O. Below: H_2O saturated P-T pseudosection. The Jakkalshoek Granite and the BFSZ plot in the cross-hatched field due to absence of muscovite.

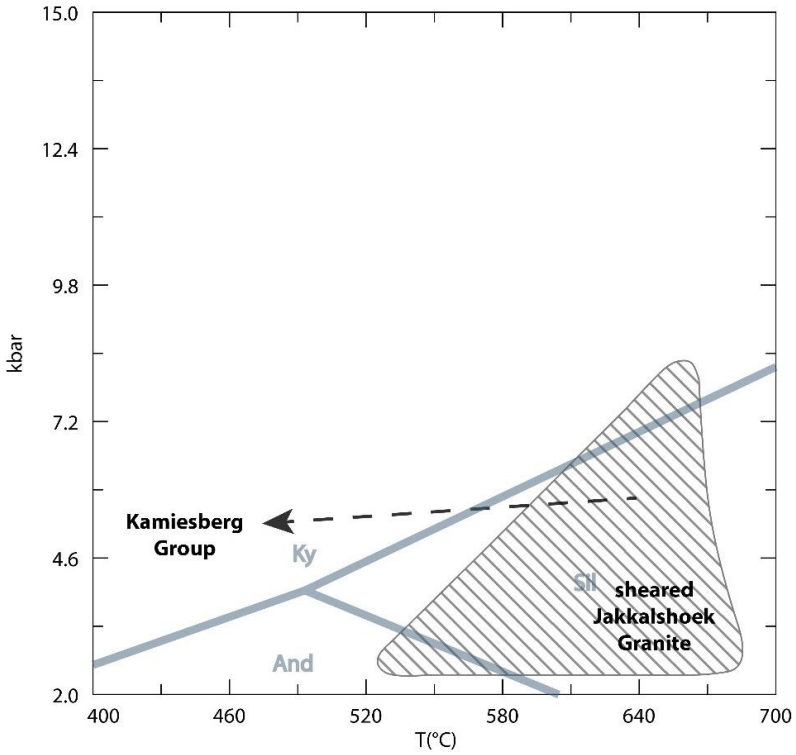

Figure 32. A rough retrograde P-T path for the field area. The BFSZ and its Jakkalshoek Granite wall rock are stable in the cross-hatched field. To the south, the Kamiesberg Group contains abundant muscovite and some vein kyanite. A likely retrograde P-T path goes from the high P end of the Jakkalshoek Granite stability field into the kyanite stability field.

Elastic deformation can be accommodated by three dislocation creep regimes; grain boundary bulging (regime 1), subgrain rotation (regime 2) and grain boundary migration (regime 3). Microstructures can be used to determine a temperature – strain rate dependency (Tullis, 2002). In the BFSZ the quartz is almost completely recrystallized, but probably experienced regime 3 deformation, while the feldspars experienced regime 2 or regime 3 deformation, as described in Figure 22 and Figure 23 in section 2.3. This places the deformation event in the albite regime 2 field or above (Figure 33). These deformation mechanisms are consistent with the temperatures obtained from the pseudosection analysis at reasonable shear strain rates.

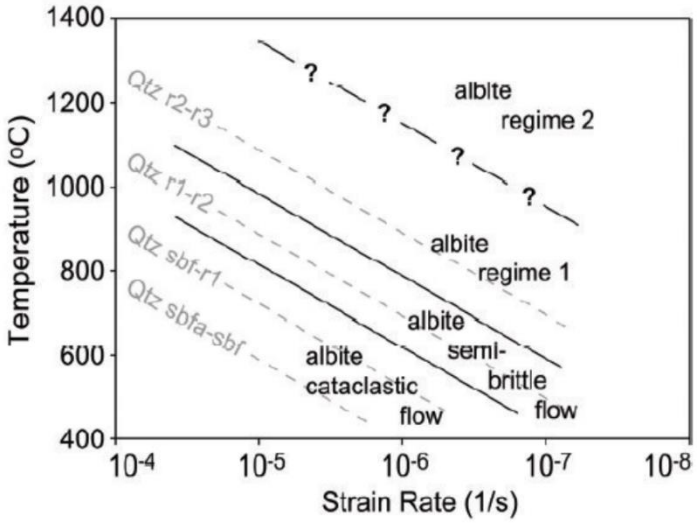

Figure 33. Approximate ductile deformation regimes for albite and quartz dependant on strain rate and temperature (Tullis, 2002). *In the BFSZ quartz is strongly recrystallized and experienced predominantly regime 3 deformation, while feldspars experienced regime 2 or regime 3 deformation, placing the deformation conditions in or above the albite regime 2 field.*

4.2. Variation of ^{18}O Depletion

The following section illustrates how the $\delta^{18}O$ values of quartz veins, quartz grains, feldspar grains and whole rock powders (mostly done on fine grained samples) vary in the country rock of the Koegel Fontein Complex. The relationship between ^{18}O depletion and structures can be used to determine when, how and where fluid-rock exchange occurred.

4.2.1. Oxygen isotopes in Mokolian and Namibian Rocks

All $\delta^{18}O$ values of Mokolian and Namibian Rocks are plotted on an overview map (Figure 34). Quartz, feldspar and whole rock analysis are colour coded blue, red and green respectively. The size reflects the $\delta^{18}O$ value. Large markers indicate low $\delta^{18}O$ values. Small markers are displayed above large markers in order to display the maximum amount of data. A large scatter, including a high proportion of negative $\delta^{18}O$ values is present in the rocks of the roof pendant, particularly near the BFSZ. Some negative $\delta^{18}O$ values occur to the north and south of the roof pendant, along the presumed extension of the BFSZ outside the Rietpoort Granite. Except for an outlier at the coast, the $\delta^{18}O$ values of rocks far removed from the roof pendant and the BFSZ are predominantly above 3‰. Because the $\delta^{18}O$ variation seems non-systematic in map view, the $\delta^{18}O$ values were plotted against longitude (Figure 35) and latitude (Figure 36) in two isotope sections.

The $\delta^{18}O$ value – longitude plot (Figure 35) shows single $\delta^{18}O$ values as points, the weighted average calculated by using 13 values centred on the central value and a schematic cross-section of the geology for comparison. Analysed whole rock powders have the highest $\delta^{18}O$ values, followed by feldspar grains and then quartz grains. There is a negative spike in all three data sets located at the BFSZ and roof pendant. At the negative spike the discrepancy between the $\delta^{18}O$ values of quartz, feldspar and whole rock powders decreases. Plotting the $\delta^{18}O$ values against latitude shows that whole rock powders and feldspar grains have the lowest $\delta^{18}O$ values and quartz grains have the highest $\delta^{18}O$ values. Negative $\delta^{18}O$ values extend outside the roof pendant to the south of the Rietpoort Granite. A sharp spike in the longitude - $\delta^{18}O$ value plot and a gradual decrease of $\delta^{18}O$ values in the latitude - $\delta^{18}O$ value plot suggests that the negative $\delta^{18}O$ value anomaly is an elongated, north trending feature. This coincides with the BFSZ and to a lesser degree with the roof pendant of the Rietpoort Granite.

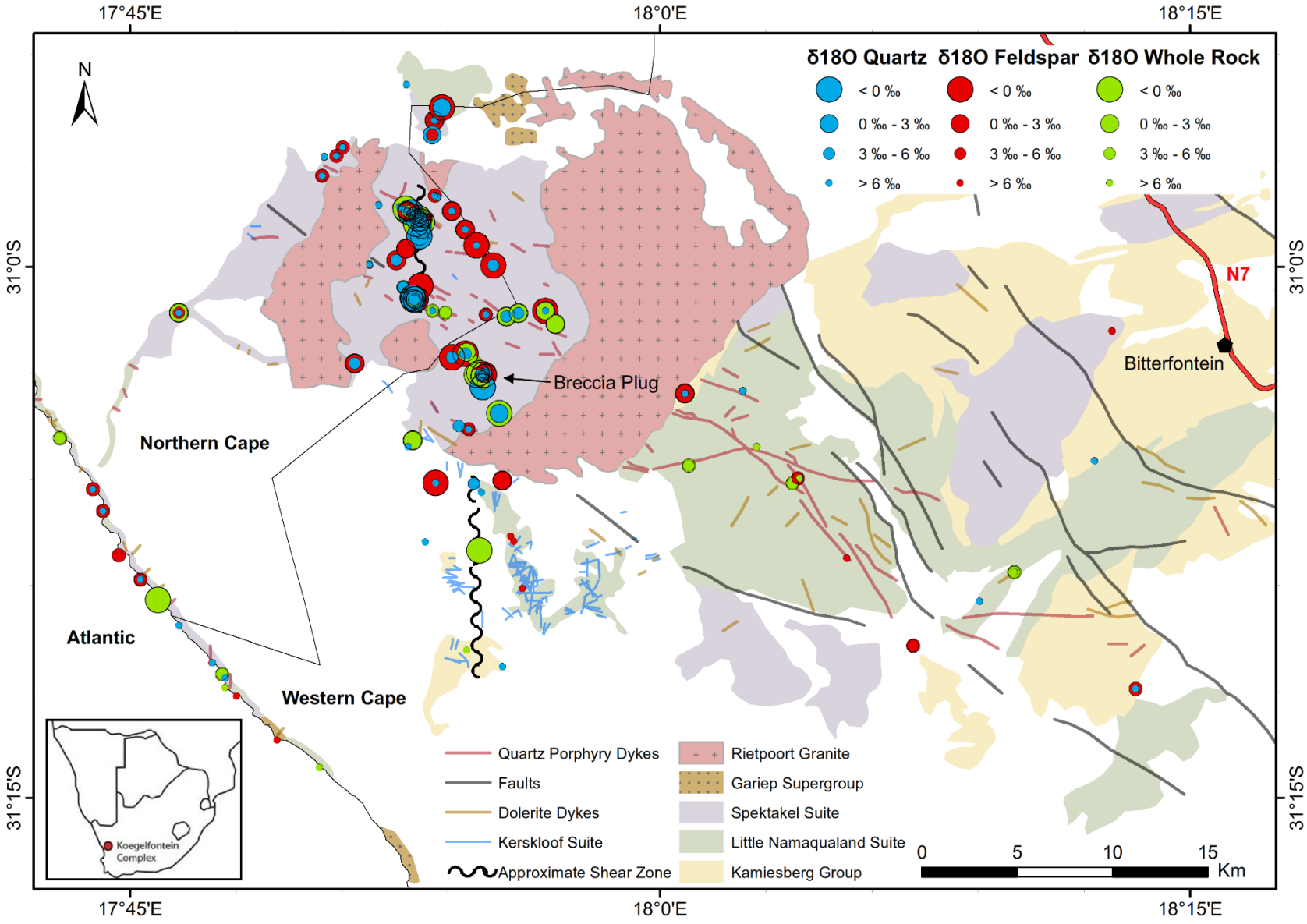

Figure 34. Regional Oxygen isotope variation in the country rock of the Koegel Fontein Complex. Oxygen isotope analyses are displayed as shown on the legend. High $\delta^{18}O$ values are placed above low $\delta^{18}O$ values to reduce data being covered by overlying data points. The lowest $\delta^{18}O$ values occur in the roof pendant, along the BFSZ. Some negative $\delta^{18}O$ values occur in the southern extension of the shear zone, in Kerskloof. One negative $\delta^{18}O$ value occurs along the coast.

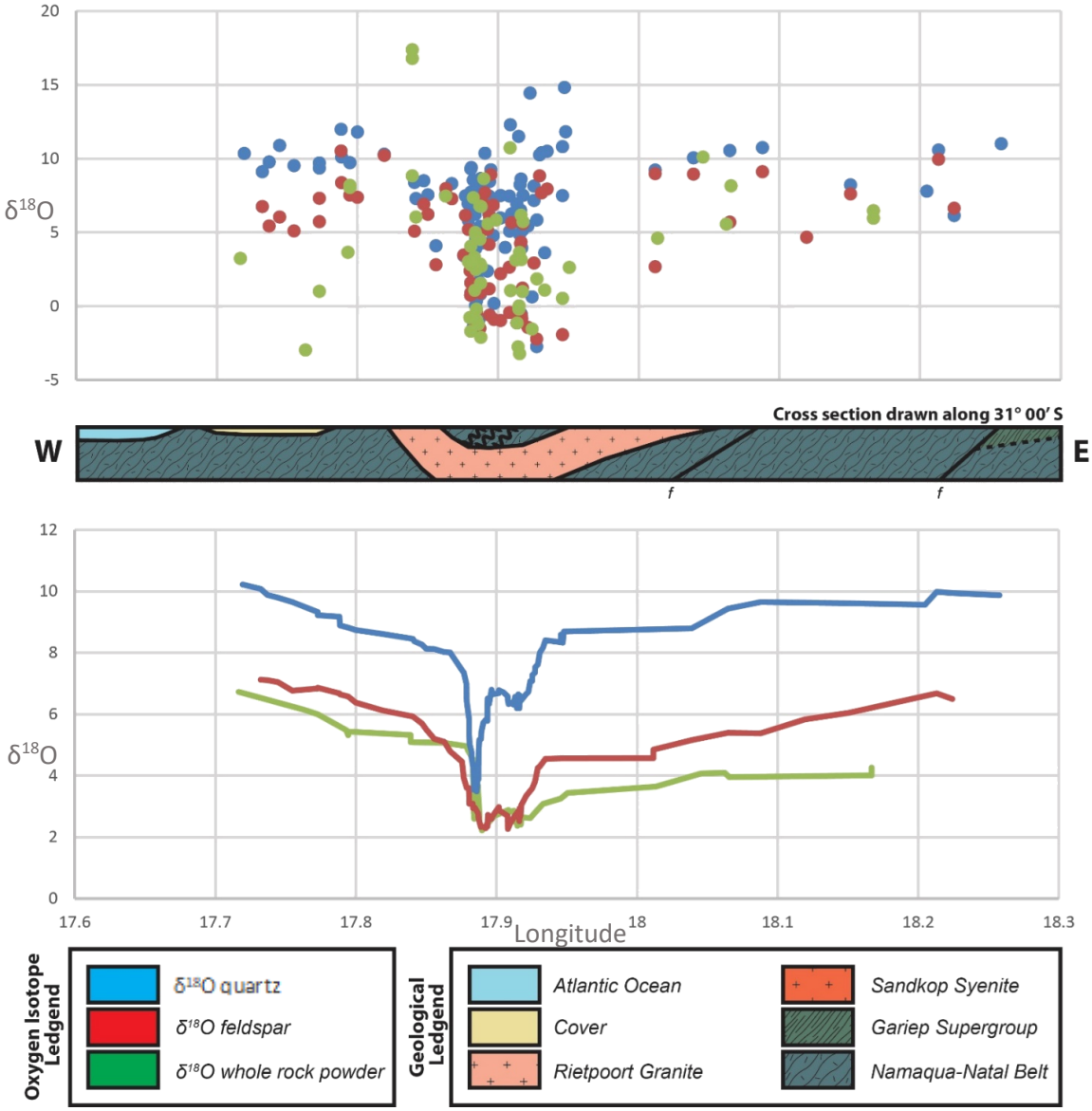

Figure 35. Plotting the $\delta^{18}O$ values against longitude shows a sharp negative spike at the longitude of the BFSZ and the roof pendant of the Rietpoort Granite. Top: All $\delta^{18}O$ values of quartz, feldspar and whole rock plotted against longitude. Centre: A schematic cross-section is given as a reference to the Oxygen isotope section. Bottom: the weighted average of 13 samples centred on the central sample.

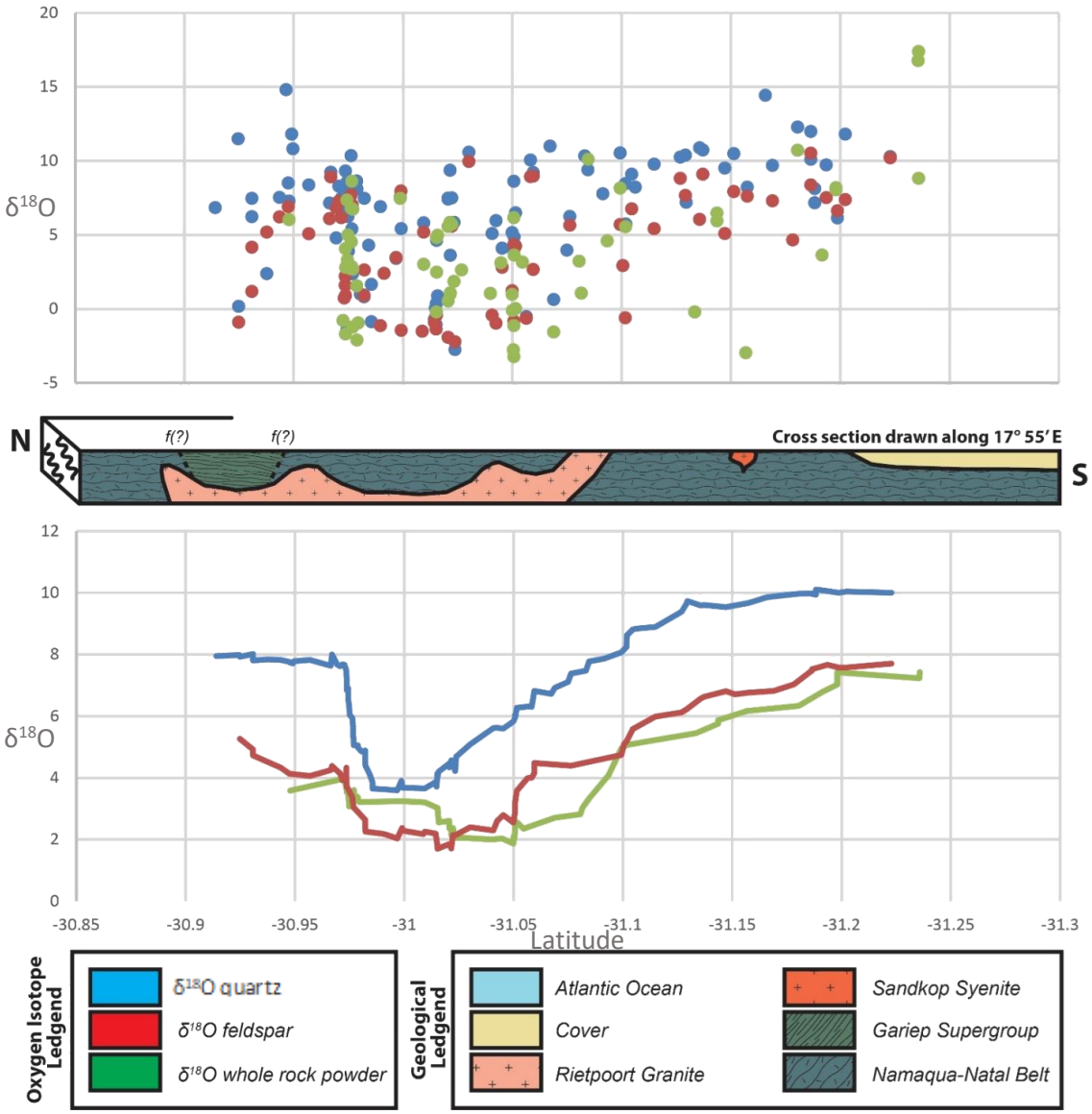

Figure 36. The $\delta^{18}O$ – latitude plot does not have a sharp negative spike like the $\delta^{18}O$ – longitude plot has (Figure 35). This implies an asymmetry in the distribution of $\delta^{18}O$ values. It seems that low $\delta^{18}O$ values are associated with a north-trending feature. Top: All $\delta^{18}O$ values of quartz, feldspar and whole rock plotted against longitude. Centre: A schematic cross-section is given as a reference to the Oxygen isotope section. Bottom: the weighted average of 13 samples centred on the central sample.

4.2.2. Oxygen isotopes in the Brak Fontein Shear Zone

The $\delta^{18}O$ values are plotted on the structural map of the BFSZ (Figure 37). There is a large variation of $\delta^{18}O$ values, however negative $\delta^{18}O$ values occur only in or close to the mylonite of the BFSZ. Plotting the $\delta^{18}O$ values of the BFSZ against longitude and latitude (Figure 38) confirms that there is a relationship between the shear zone and $\delta^{18}O$ values. The wall rock has $\delta^{18}O$ values of 6‰ to 10‰ while the shear zone itself have a large scatter of $\delta^{18}O$ values, from -2‰ to 10‰. The mineralogy, strain and Oxygen isotopes seem highly variable inside the shear zone. There are $\delta^{18}O$ value variations even in centimetre-scale (Figure 39). Negative $\delta^{18}O$ values in the BFSZ are evidence for the infiltration of meteoric water (as described in section 3.1).

Fluid infiltration in fault zones has been described by (Faulkner et al., 2010). Permeability in faults is generally heterogeneous due to a complex arrangement of often impermeable core zones and permeable damage zones. At upper crustal levels, fluid is often at hydrostatic pressure due to a higher likelihood of interconnected fluid pathways to the surface. The BFSZ is located deeper in the crust, at or below the brittle – ductile transition zone. Here permeability decreases, fluid becomes isolated from the surface and fluid pressures approach lithostatic pressure. The remaining fluid becomes overpressured (with respect to hydrostatic pressure) and downwards fluid movement should theoretically be impossible.

Penetration of surface water into the ductile crust is controversial, but evidence does for deep penetration of fluids does exist. Deuterium isotopes with meteoric δD values (Menzies et al., 2014) and hydrocarbons of sedimentary origin in basement rocks (Munz et al., 1995) give evidence for the introduction of surface waters into the ductile crust. Bimodal distributions of homogenisation temperatures in fluid inclusions indicate that fluid is pumped down, isolated and pressurised (Yardley et al., 2000). Variable strain rates may have made the BFSZ experience intermittent brittle deformation, allowing for short lived fluid infiltration. A possible mechanism for deep penetration of surface fluids is seismic pumping (McCaig, 1988).

The ^{18}O depletion in the BFSZ may be an example of surface water penetrating into the ductile crust. No evidence was found for an initial phase of brittle deformation, though it is difficult to rule out this hypothesis as the ductile overprint could effectively disguise the signature of brittle deformation. The addition of water to a shear zone can greatly affect its rheological properties and has implications for the evolution of such structures.

$\delta^{18}O$: Brak Fontein Shear Zone 1:5 000

Poles to Foliation (n = 35)
Lower hemisphere equal area projection

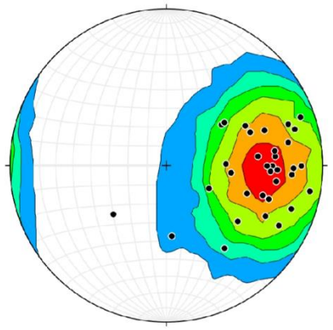

$\delta^{18}O$ Qtz grains (n = 22)

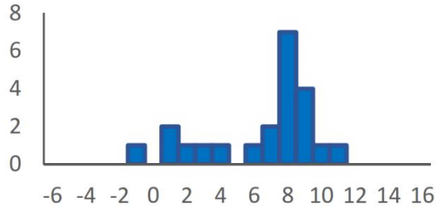

$\delta^{18}O$ Fsp grains (n = 9)

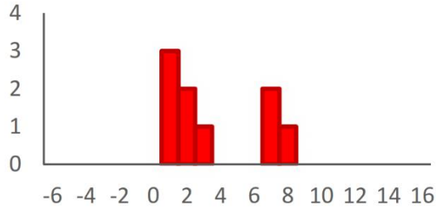

$\delta^{18}O$ WR grains (n = 18)

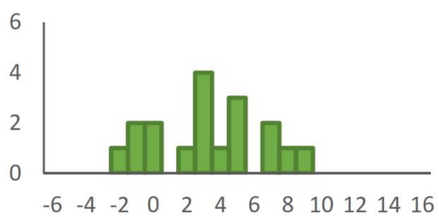

$\delta^{18}O$ Qtz

- < 0 ‰
- 0 - 6 ‰
- > 6 ‰

$\delta^{18}O$ Fsp

- < 0 ‰
- 0 - 6 ‰
- > 6 ‰

$\delta^{18}O$ WR

- < 0 ‰
- 0 - 6 ‰
- > 6 ‰

N

WGS 1984

- Foliation
- Form Lines
- Quartzite
- Granitic Gneiss
- Mylonite
- Quartz Porphyry Dyke

0 50 100 200 300 m

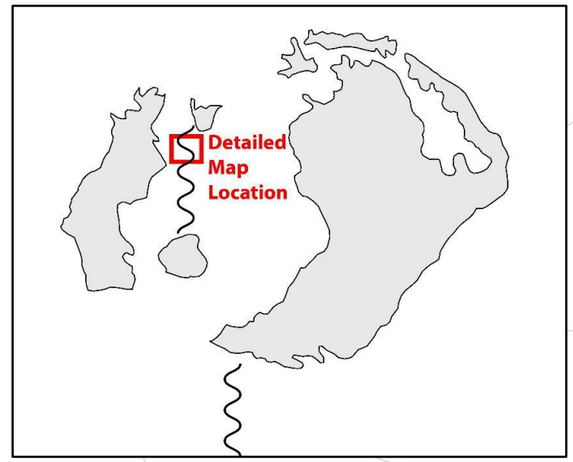

Figure 37. Oxygen isotopes in the BFSZ. Negative $\delta^{18}O$ values occur in the shear zone while $\delta^{18}O$ values above 6‰ occur in the wall rock. There is a large spread of $\delta^{18}O$ values in the high strain areas. Histograms indicate that whole rock powders of fine grained mylonite have the lowest $\delta^{18}O$ values while quartz grains have the highest $\delta^{18}O$ values.

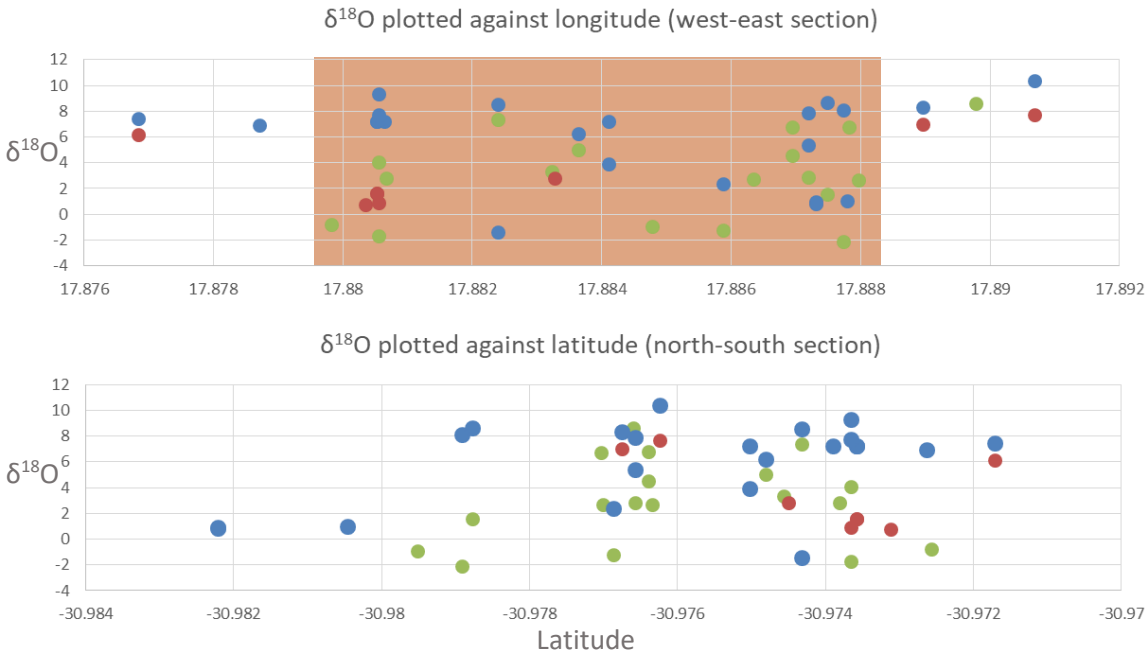

Figure 38. The $\delta^{18}O$ of quartz (blue), feldspar (red) and whole rock powders (green) in the BFSZ plotted against longitude and latitude. Above: The $\delta^{18}O$ – longitude section transects the BFSZ. The approximate location of the BFSZ is indicated by brown shading. The wall rock of the shear zone has normal $\delta^{18}O$ values of above 6‰. A high variation of $\delta^{18}O$ values occurs inside the shear zone, with $\delta^{18}O$ values as low as -2‰. Below: The $\delta^{18}O$ – latitude plot does not have any trends. This is expected because this section has the same strike as the BFSZ.

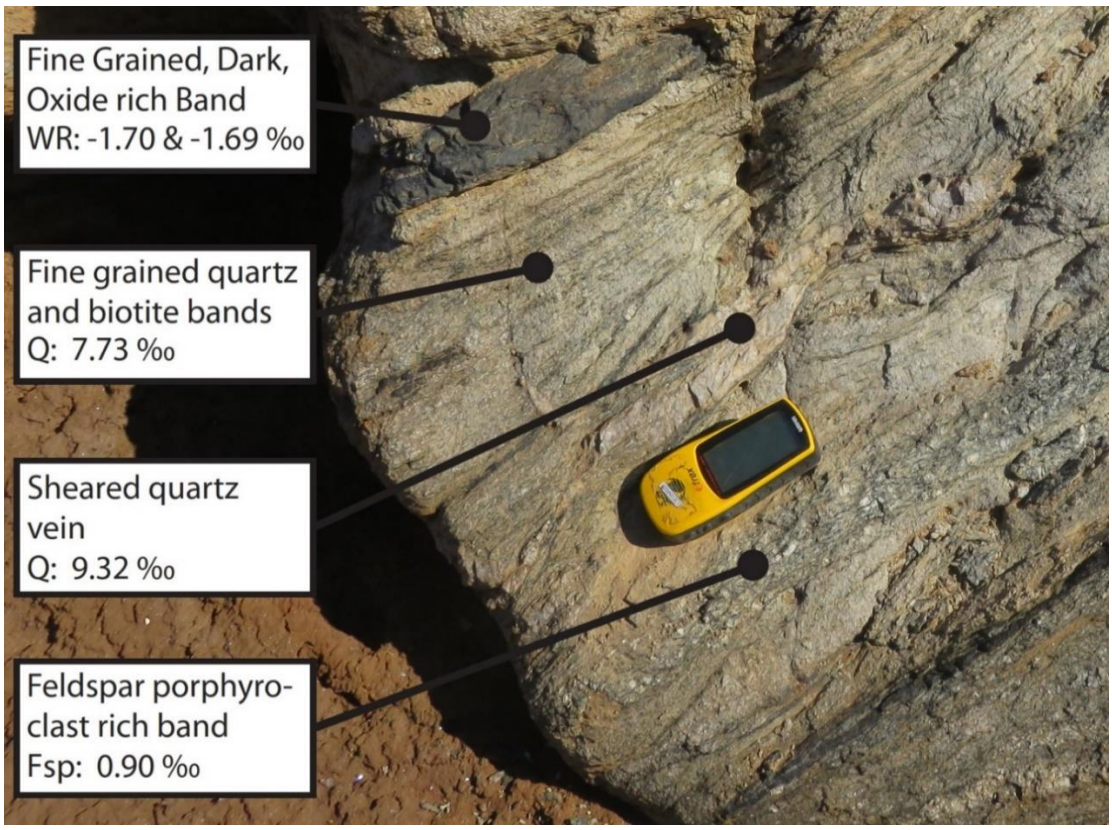

Figure 39. In the BFSZ $\delta^{18}O$ values, mineralogy and strain are highly heterogeneous, even in cm-scale.

4.2.3. Oxygen isotopes in Quartz Veins

Two populations of quartz veins were analysed. Pan-African veins contain massive quartz, are several meters wide or larger and can extend for tens of kilometres. Cretaceous veins are generally less than 10cm wide, are vuggy and have euhedral quartz crystals which protrude into the centre of the vein (Figure 20). Plotting the $\delta^{18}O$ values of quartz veins on histograms (Figure 26) reveals that the Pan-African veins have $\delta^{18}O$ values of 6‰ to 12‰ while the $\delta^{18}O$ values of Cretaceous veins ranges from -4‰ to 12‰. High $\delta^{18}O$ values in Pan-African veins and low $\delta^{18}O$ values in Cretaceous veins may lead one to the conclusion that the ^{18}O depletion is Cretaceous in age and that the low $\delta^{18}O$ values in the BFSZ formed due to Cretaceous fluids passing through a dormant shear zone. This scenario is unlikely, because low $\delta^{18}O$ veins are almost entirely absent from the BFSZ and because the shear zone was completely recrystallized after deformation and therefore was unlikely to be permeable during the Cretaceous. Furthermore the absence of brittle overprint in the BFSZ rules out brittle reactivation during Cretaceous extension. A more plausible scenario is that ^{18}O-depletion predates the Cretaceous and occurred in, but is perhaps not limited to the BFSZ. During the emplacement of the Koegel Fontein Complex the ^{18}O depleted county rock was dehydrated and melted, forming low $\delta^{18}O$ magmas (Curtis et al., 2013) and mobilising low $\delta^{18}O$ fluid, which resulted in the formation of low $\delta^{18}O$ quartz veins and a breccia plug (Olianti and Harris, 2018). Therefore a Cretaceous hydrothermal system mobilised low $\delta^{18}O$ fluid by dehydration of previously ^{18}O-depleted crust.

4.3. Fluid-Rock Exchange

Cretaceous low $\delta^{18}O$ quartz veins, a breccia plug and low $\delta^{18}O$ magmas are a result of dehydration melting of previously ^{18}O-depleted rock (Curtis et al., 2013; Olianti and Harris, 2018). The following section uses data from samples believed to be far removed from Cretaceous ^{18}O-depletion to constrain and as far as possible quantify the initial ^{18}O-depletion event. Samples of Jakkalshoek Granite, Mesklip Gneiss and the BFSZ, which were analysed for $\delta^{18}O_{Quartz}$ and $\delta^{18}O_{Feldspar}$ or for $\delta^{18}O_{Quartz}$ and $\delta^{18}O_{Whole\ Rock}$ (matrix) are plotted on a $\delta^{18}O_{Quartz} - \delta^{18}O_{Feldspar}$ plot (Figure 40). The $\delta^{18}O_{Whole\ Rock}$ data represents the bulk rock $\delta^{18}O$ value, which is predominantly made up of a feldspar and a quartz component. Temperature contours for O-isotopic equilibrium between quartz and albite are plotted using Equation 2, Equation 3 and Equation 4.

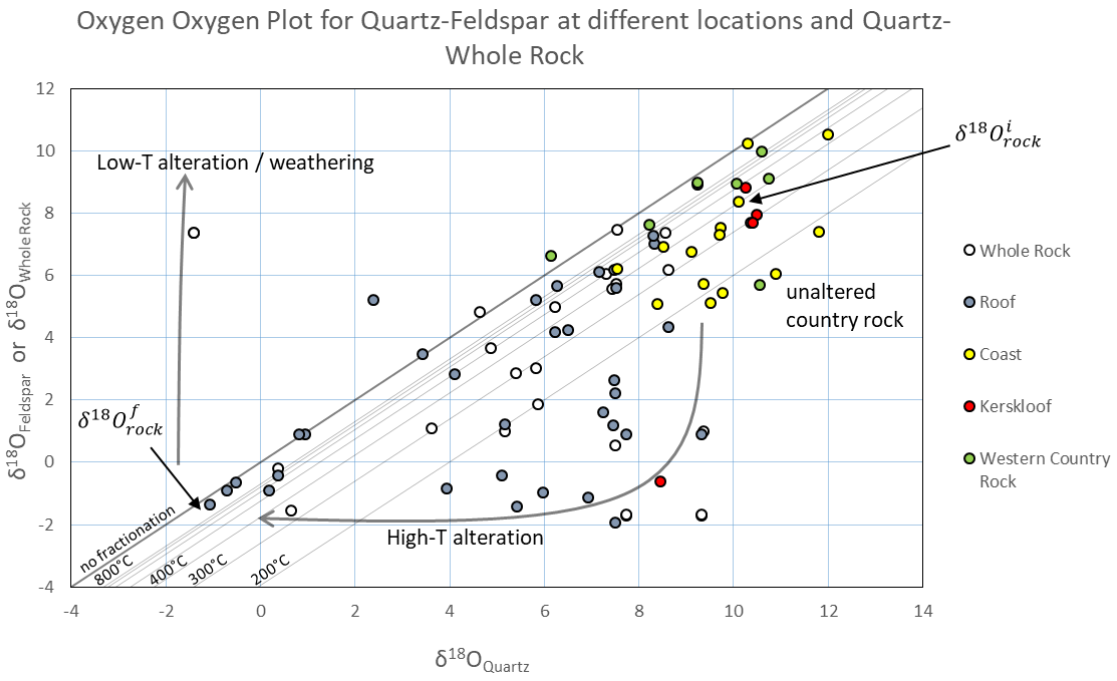

Figure 40. Mineral-mineral plot with $\delta^{18}O_{Feldspar}$ and $\delta^{18}O_{Whole\ Rock}$ plotted against $\delta^{18}O_{Quartz}$. Unaltered mineral pairs have high $\delta^{18}O_{Feldspar}$ and $\delta^{18}O_{Quartz}$ values. Low $\delta^{18}O_{Feldspar}$ and $\delta^{18}O_{Quartz}$ values are a result of hydrothermal fluid – rock exchange with low $\delta^{18}O$ fluids. The Oxygen isotope – quartz – feldspar – water equilibrium system is dependent on $\delta^{18}O_{Feldspar}$, $\delta^{18}O_{Quartz}$, $\delta^{18}O_{fluid}$ and the alteration temperature. The mathematical equilibrium relationship between these variables is approximated by Clayton et al. (1972) and Matsuhisa et al. (1979) and is given by Equation 3 and Equation 4. Oxygen isotope data is plotted on a graph with alteration temperature contours. Mineral pairs below the 300°C alteration temperature contour have not reached Oxygen isotope equilibrium. Differential kinetic oxygen exchange between quartz and feldspar creates clockwise curved trajectories described by Criss et al. (1987 and Gregory et al. (1989).

If samples are in isotopic equilibrium, they are expected to fall on a straight line with a gradient of one. Alteration is expected to occur along clockwise curved trajectories in $\delta^{18}O_{quartz}$ – $\delta^{18}O_{feldspar}$ space, from a point on the high end to a point on the low end of the equilibrium line (Figure 40). This is due to the kinetic resistance to oxygen exchange in quartz relative to feldspar (Criss et al., 1987; Gregory et al., 1989). In samples below 300°C, feldspar and quartz are not at isotopic equilibrium. Here feldspar is closer to isotopic equilibrium than quartz and the temperature contours cannot be used. This is illustrated by the high temperature alteration arrow. The geographic locations of the plotted samples are indicated in the legend. The strongest ^{18}O-depletion occurred in the Jakkalshoek Granite of the roof pendant of the Rietpoort Granite, which is the location of the BFSZ.

The plotted samples have a mineralogy dominated by of feldspar, followed by quartz. From Figure 40 it can be determined that feldspar has an initial $\delta^{18}O$ value of 8‰ and a final $\delta^{18}O$ value of -2‰ while quartz has an initial $\delta^{18}O$ value of 10‰ and a final $\delta^{18}O$ value of -1.6‰. The approximation can be made that $\delta^{18}O_{rock}{}^{i} \approx 8‰$ and $\delta^{18}O_{rock}{}^{f} \approx -2‰$, because the dominant mineral in the samples is feldspar. Furthermore the possible temperature of fluid – rock exchange is constrained by the highest possible temperature, estimated to be 690°C, as estimated in section 4.1.3, and the lowest temperature where oxygen exchange between the fluid and the rock is kinetically feasible, estimated to be >300°C. These assumptions can be used to calculate the water – rock ratio (W/R) in order to estimate how much fluid passed through the system.

Equation 5. Formula for calculating the molar water/ rock ratio in a closed system. Superscript "i" and "f" indicate initial and final respectively (Sharp, 2007).

$$\frac{W}{R}_{closed\ system} = \frac{\delta^{18}O^{f}_{rock} - \delta^{18}O^{i}_{rock}}{\delta^{18}O^{i}_{water} - \left(\delta^{18}O^{f}_{rock} - \Delta_{rock-water}\right)}$$

Equation 6. Formula for calculating the molar water/ rock ratio in an open system. Superscript "i" and "f" indicate initial and final respectively (Sharp, 2007).

$$\frac{W}{R}_{open\ system} = \ln\left[\frac{\delta^{18}O^{i}_{fluid} + \Delta_{r-w} - \delta^{18}O^{i}_{rock}}{\delta^{18}O^{i}_{fluid} - \left(\delta^{18}O^{f}_{rock} - \Delta_{r-w}\right)}\right]$$

W/R is calculated using Equation 5 for a closed system (a single – pass system where fluid equilibrates with the rock and is expelled) and Equation 6 for an open system (multi – pass system where new fluid continuously exchanges with the rock) assuming that $\Delta_{rock\text{-}water} \approx \Delta_{albite\text{-}water}$ (calculated using Equation 4). The W/R is modelled for a temperature range of 400°C to 700°C and for $\delta^{18}O_{fluid}{}^{i}$ values of 0‰ to -30‰ assuming $\delta^{18}O_{rock}{}^{i} \approx 8‰$ and $\delta^{18}O_{rock}{}^{f} \approx -2‰$ for a closed and open system (Table 6 A and B). The fields of the tables have been coloured green, for a low W/R (0.35), yellow for an intermediate W/R (0.7) and red for a high W/R (1.4) for easier interpretation. N/A indicates that the $\delta^{18}O_{rock}{}^{f}$ is impossible to achieve with the predefined conditions. The results show that the W/R_{closed} is larger than W/R_{open}, which is expected, but in reality the rocks probably experienced a mixture of closed (single – pass) and open (multi – pass) fluid infiltration.

Table 6. The W/R required for a change from $\delta^{18}O_{rock}^{i} \approx 8$ ‰ to $\delta^{18}O_{rock}^{f} \approx -2$ ‰ for a temperature range of 400°C to 700°C and for a $\delta^{18}O_{fluid}^{i}$ range from -30 ‰ to 0‰ in an open system and a closed system. Green represents low W/R, which is more likely and red indicates a high W/R, which is less likely. N/A is impossible to achieve.

$W/R_{\text{closed system}}$ for $\delta^{18}O_{Rock}^{i} \approx 8‰ \rightarrow \delta^{18}O_{Rock}^{f} \approx -2‰$ **A**

T	$\Delta_{Rock-Water}$	$\delta^{18}O_{fluid}^{i}$								
		-30 ‰	-20 ‰	-10 ‰	-8 ‰	-5 ‰	-4.5 ‰	-3.5 ‰	-2.9 ‰	-2.5 ‰
400°C	2.76	0.40	0.66	1.91	3.09	41.67	N/A	N/A	N/A	N/A
500°C	1.50	0.38	0.61	1.54	2.22	6.67	10.00	N/A	N/A	N/A
600°C	0.93	0.37	0.59	1.41	1.97	4.83	6.37	17.54	N/A	N/A
700°C	0.52	0.36	0.57	1.34	1.82	4.03	5.05	10.20	26.32	N/A

$W/R_{\text{open system}}$ for $\delta^{18}O_{Rock}^{i} \approx 8‰ \rightarrow \delta^{18}O_{Rock}^{f} \approx -2‰$ **B**

T	$\Delta_{Rock-Water}$	$\delta^{18}O_{fluid}^{i}$								
		-30 ‰	-20 ‰	-10 ‰	-8 ‰	-5 ‰	-4.5 ‰	-3.5 ‰	-2.9 ‰	-2.5 ‰
400°C	2.76	0.33	0.50	1.07	1.41	3.75	N/A	N/A	N/A	N/A
500°C	1.50	0.32	0.47	0.93	1.17	2.04	2.40	N/A	N/A	N/A
600°C	0.93	0.31	0.46	0.88	1.09	1.76	2.00	2.92	N/A	N/A
700°C	0.52	0.31	0.45	0.85	1.04	1.62	1.80	2.42	3.31	N/A

Table 6 A and B only approximate reality, but they demonstrate that there is a trade-off between temperature, $\delta^{18}O_{fluid}^{i}$ and W/R. A low W/R primarily requires low $\delta^{18}O_{fluid}^{i}$ and, to a lesser degree, high temperature. For example, a W/R < 0.5 can be achieved if $\delta^{18}O_{fluid}^{i} \approx -30‰$ for an open or closed system or if $\delta^{18}O_{fluid}^{i} \approx -20‰$ and T > 400°C for an open system. Low W/R ratios are more easily reached, because high W/R ratios require sufficient permeability, fluid flux, temperature and duration of fluid – rock exchange. The ^{18}O-depletion in the Jakkalshoek Granite and BFSZ requires a temperature which is high enough for oxygen exchange, conditions that are right for a hydrothermal system to allow for sufficient W/R ratios and a $\delta^{18}O_{fluid}^{i}$ that is sufficiently low. At some point in geological history all conditions must have been suitable to create ^{18}O-depletion in the BFSZ.

4.4. Timing of ^{18}O-Depletion

For ^{18}O-depletion to occur in the BFSZ, a hydrothermal system must have allowed for an adequate W/R ratio, $\delta^{18}O_{fluid}^{i}$ was sufficiently low and the geothermal gradient was high enough for oxygen exchange. The only plausible timing of a hydrothermal system is either during the emplacement of the Koegel Fontein Complex, or during Pan-African Orogeny. Literature examples of realistic W/R ratios for intrusion related hydrothermal systems exist for the Silver Creek, Porphyry copper deposit and the Skaergaard intrusion. At Silver Creek, W/R ranges from 1.10 to 0.54 in the central part of the hydrothermal system and from 0.41 to <0.01 in the margins of the hydrothermal system (Larson and Zimmerman, 1991). At Skaergaard W/R = 0.52 in the upper part the intrusion, W/R = 0.88 in the basalt country rock and W/R = 0.003 in the impermeable granitic gneiss country rock, which lies unconformably below the basalt (Norton and Taylor, 1979). These examples suggest that a hydrothermal system caused by the intrusion of the Koegel Fontein Complex could theoretically create a W/R of up <1.5, however the lack of ^{18}O-depletion in the Rietpoort Granite makes this scenario unlikely. Furthermore, the Jakkalshoek Granite and the BFSZ is unfractured and impermeable and W/R of ~0.003 may be expected by analogy with the granitic gneiss country rock of the Skaergaard intrusion. Examples of W/R ratios for deep fluid migration in shear zones is given for shear zones in the French Pyrenees, where deformation occurred at 400-450°C. Extensive fluid infiltration and muscovite mineralisation resulted in a W/R ≈ 10^3 (Mccaig et al., 1990). This high W/R ratio suggests that fluid infiltration in the BFSZ during the Pan-African Orogeny may have created significant W/R ratios. The required W/R ratio is also strongly controlled by $\delta^{18}O_{fluid}^{i}$, which is a result of the paleoclimate and paleolatitude of BFSZ during ^{18}O-depletion.

The only mechanism to create negative $\delta^{18}O$ values in rocks is high temperature oxygen exchange with negative $\delta^{18}O$ fluid. The only source of water with negative $\delta^{18}O$ values is meteoric water. This is due to preferential evaporation of H_2O molecules containing ^{16}O and ^{1}H from the oceans, which have a $\delta^{18}O$ value of 0‰. Fractionation during evaporation is temperature dependant leading to low $\delta^{18}O$ values in meteoric water at high latitudes. During transport in the atmosphere, the H_2O containing ^{18}O and ^{2}H is preferentially rained out. This leads to ^{16}O and ^{1}H enrichment in meteoric water at high altitudes and in the centre of continents. The only present-day locations where precipitation has a $\delta^{18}O$ < -20‰ are the polar ice caps in Antarctica and Greenland (Alley and Cuffey, 2001).

The $\delta^{18}O$ value of the oceans is buffered at mid ocean ridges and has therefore been near 0‰ since the onset of plate tectonics, with the exception of short-lived effects, such as global glaciations (Gregory and Taylor, 1981). During ordinary climatic conditions, the current day relationship between latitude and $\delta^{18}O$ value of precipitation can be used to estimate the $\delta^{18}O$ value of precipitation at a given time using paleolatitude. Very low $\delta^{18}O$ values in precipitation (<-30‰) occurred during global glaciations, where high altitude ice caps covered most of the planet. The paleolatitude of the Kalahari Craton and cold periods are given in Figure 41 for a reconstruction of $\delta^{18}O$ values of meteoric water.

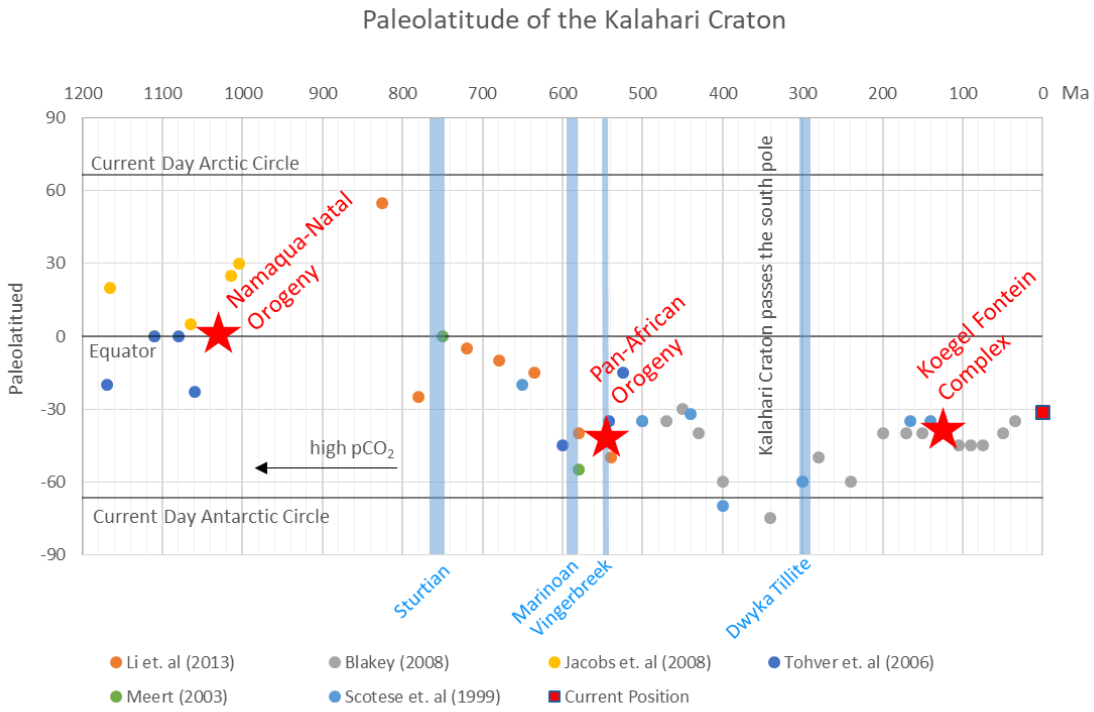

Figure 41. Paleolatitude of the Kalahari Craton from various paleomagnetic reconstructions (Blakey, 2008; Jacobs et al., 2008; Li et al., 2013; Meert, 2003; Scotese et al., 1999; Tohver et al., 2006). *The paleolatitude is accurate within 5° latitude. The timing of global glaciations* (Frimmel et al., 2002; Germs and Gaucher, 2012) *are indicated in blue shading. Although not a global glaciation, the formation of the Dwyka Tillite* (Bangert et al., 1999) *coincides with high latitudes, but no accompanying tectonic event occurred, which may have driven a hydrothermal system.*

Notably meteoric water with $\delta^{18}O < -30$ ‰ can be expected during the 549-545 Ma Vingerbreek global glaciation, which coincides with early Pan-African deformation. This would imply that W/R < 0.4, which is achievable in the BFSZ during deformation. Meteoric water during the emplacement of the Koegel Fontein Complex had higher $\delta^{18}O$ values. During the Cretaceous, the paleolatitude of the Kalahari Craton was similar to the current latitude. Furthermore, the Cretaceous is known as a generally warm period. Therefore the precipitation during the emplacement of the Koegel Fontein Complex in the Cretaceous has a possible $\delta^{18}O$ value range of -8‰ to 0 ‰. Assuming the lowest reasonable $\delta^{18}O$ value in precipitation, a W/R of 1 to 3 would be required. Considering that the grains were strongly recrystallized in the BFSZ after Pan-African deformation and that there is no sign of brittle reactivation of the BFSZ, the permeability in the BFSZ was probably too low to allow a W/R of 1. In conclusion, ^{18}O-depletion must have occurred during the Gaskiers Glaciation during the early stages of the Pan-African Orogeny.

4.5. Selective Dehydration of Previously ^{18}O-Depleted Rock

Not all low $\delta^{18}O$ rocks are related to the Pan-African Orogeny and the BFSZ. Low $\delta^{18}O$ magmas, quartz veins and breccia rock as well as small volumes of ^{18}O depleted Cretaceous dykes have been described and attributed to a Cretaceous hydrothermal system (Curtis et al., 2013). Olianti and Harris (2018) concluded that Cretaceous low $\delta^{18}O$ rocks are the result of remobilisation and selective melting of previously ^{18}O-depleted rock during the emplacement of the Koegel Fontein Complex. They suggested that initially the basement gneiss was ^{18}O-depleted during the ~547 Ma Vingerbreek Glaciation during the Pan-African Orogeny.

My results agree with an initial ^{18}O-depletion during the Vingerbreek Glaciation, followed by remobilisation of low $\delta^{18}O$ fluids during the emplacement of the Koegel Fontein Complex. The age of Cretaceous low $\delta^{18}O$ quartz veins is constrained to 130-135 Ma by cross-cutting field relationships (Figure 20), but ^{18}O-depletion in the BFSZ did not occur in the Cretaceous because a sufficient W/R ratio could not be achieved due to low permeability. Evidence for low permeability is given by 1) strong recrystalisation and annealing after deformation in the BFSZ, 2) the lack of brittle overprint in the BFSZ, 3) the absence of fractures in the Jakkalshoek Granite, even at the contact to the Rietpoort Granite, ruling out a Yellowstone – style caldera collapse and 4) the absence of Cretaceous low $\delta^{18}O$ quartz veins in the BFSZ.

The major difficulty with Pan-African ^{18}O-depletion is explaining how low $\delta^{18}O$ meteoric water could penetrate into the BFSZ, which experienced deformation at or below the brittle-ductile transition zone. Ductile deformation should eliminate pore space, reduce permeability and overpressure fluids. Penetration of meteoric fluids into the BFSZ can be explained in two ways:

- Variable strain rates and seismic pumping may have caused meteoric water to infiltrate the ductile zone. Although controversial, a number of studies have used isotopes, chemistry and fluid inclusions to show that it is possible (Mccaig et al., 1990; Menzies et al., 2014; Munz et al., 1995; Yardley et al., 2000).
- The BSFZ may have undergone an earlier phase of brittle deformation allowing for fluid infiltration and ^{18}O-depletion before experiencing ductile overprint.

In the instance of the BFSZ, a combination of Pan-African deformation and fluid infiltration accompanied by a global glaciation gave rise to negative $\delta^{18}O$ values. The ^{18}O-depleted rock was selectively dehydrated and melted during the emplacement of the Koegel Fontein Complex, forming a Cretaceous hydrothermal system.

5. Conclusion

1. During the ~545 Ma Pan-African Orogeny stress was accommodated in the Gariep Supergroup and the Namaqua-Natal Belt by the formation of west-dipping thrusts, west-dipping sinistral strike slip shear zones and a west dipping pervasive fabric. During deformation the Namaqua-Natal Belt experienced temperatures exceeding 550°C. In the Jakkalshoek Granite a granitic mineralogy is preserved, even in the BFSZ, where there is isotopic evidence for hydrothermal alteration. During retrograde metamorphism, the Kamiesberg Group and Mesklip Gneiss was mineralogically changed as indicated by the occurrence of kyanite and abundant muscovite, which forms a pervasive west-dipping cleavage, suggesting cooler temperatures.
2. Glacial diamictite and cap carbonates of the Gariep Group were deposited onto the Namaqua-Natal Belt. These deposits are evidence a disputed number of Neoproterozoic global glaciations. Cold climates and possibly high altitude ice caps are the required conditions for extremely low $\delta^{18}O$ values in precipitation. Notably the 549-545 Ma Vingerbreek Glaciation coincides with the Pan-African Orogeny.
3. Low $\delta^{18}O$ meteoric fluids infiltrated the BFSZ at high temperatures leading to $\delta^{18}O$ values as low as -2.1‰ in quartz grains, feldspar grains and mylonite whole rock samples. A W/R ratio > 0.3 suggests that significant amount of fluid infiltrated the BFSZ. Fluid – rock exchange in the BFSZ may be evidence for fluid infiltration in ductile shear zones. Alternatively, fluid – rock exchange may have occurred before peak temperatures when the BFSZ may have experienced brittle deformation. Retrograde metasomatism, seen extensively in the Kamiesberg Group and Mesklip Gneiss, does not seem to be related to ^{18}O-depletion.
4. This work supports the previous theory that ^{18}O-depletion initially occurred during a ~547 Ma global glaciation and that low $\delta^{18}O$ rocks and quartz veins of the Koegel Fontein Complex (~134 Ma) are a result of selective dehydration and melting of previously ^{18}O-depleted crust (Curtis et al., 2013; Olianti and Harris, 2018). The age of Cretaceous low $\delta^{18}O$ quartz veins is constrained by cross-cutting field relationships, however ^{18}O-depletion in the BFSZ did not occur in the Cretaceous due to the lack of permeability as indicated by annealing and recrystalisation, the lack of brittle overprint and the absence of Cretaceous quartz veins. The BFSZ must have experienced ^{18}O-depletion while the shear zone was active during the ~545 Pan-African Orogeny, which coincides with the 549-545 Ma Vingerbreek glaciation.

References

Alley, R.B., Cuffey, K.M., 2001. Oxygen - and Hydrogen - Isotopic Ratios of Water in Precipitation: Beyond Paleothermometry. Rev. Mineral. Geochemistry 43, 527–553.

Bangert, B., Stollhofen, H., Lorenz, V., Armstrong, R., 1999. The geochronology and significance of ash- fall tuffs in the glaciogenic Carboniferous- Permian Dwyka Group of Namibia and South Africa. J. African Earth Sci. 29, 33–49. doi:10.1016/S0899-5362(99)00078-0

Bial, J., Büttner, S.H., Schenk, V., Appel, P., 2015. The long-term high-temperature history of the central Namaqua Metamorphic Complex : Evidence for a Mesoproterozoic continental back-arc in southern Africa. Precambrian Res. 268, 243–278. doi:10.1016/j.precamres.2015.07.012

Blakey, R.C., 2008. Gondwana paleogeography from assembly to breakup - A 500 m.y. odyssey. Geol. Soc. Am. Spec. Pap. 441, 1–28. doi:10.1130/2008.2441(01).

Chief Directorate: Surveys and Mapping, 2003a. 3017DC Nariep.

Chief Directorate: Surveys and Mapping, 2003b. 3018CC Rietpoort.

Chief Directorate: Surveys and Mapping, 2003c. 3118AA Komkans.

Chief Directorate: Surveys and Mapping, 2003d. 3117BA&BB Ruitersvlei.

Chief Directorate: Surveys and Mapping, 1970. 3017DD Kotzesrus.

Clayton, R.N., O'Neil, J.R., Mayeda, T.K., 1972. Oxygen Isotope Exchange between Quartz and Water. J. Geophys. Res. 77, 3057–3067.

Connolly, J.A.D., 2005. Computation of phase equilibria by linear programming: A tool for geodynamic modeling and its application to subduction zone decarbonation. Earth Planet. Sci. Lett. 236, 524–541.

Connolly, J.A.D., 1990. Multivariable phase diagrams; an algorithm based on generalized thermodynamics. Am. J. Sci. 290, 666–718.

Connolly, J.A.D., Petrini, K., 2002. An automated strategy for calculation of phase diagram sections and retrieval of rock properties as a function of physical conditions. J. Metamorph. Geol. 20, 697–708.

Criss, R.E., Gregory, R.T., Taylor, H.P., 1987. Kinetic theory of oxygen isotopic exchange between minerals and water. Geochim. Cosmochim. Acta 51, 1099–1108.

Curtis, C., 2009. Stable isotope and whole rock geochemical study of the Cretaceous Koegel Fontein Complex: magma characterisation, evidence for constraints for low–δ18O magmas.

Curtis, C.G., Harris, C., Trumbull, R.B., De Beer, C., Mudzanani, L., 2013. Oxygen isotope diversity in the anorogenic Koegel Fontein complex of South Africa: A case for basement control and selective melting for the production of low-δ18O magmas. J. Petrol. 54, 1259–1283. doi:10.1093/petrology/egt011

Curtis, C.G., Trumbull, R.B., de Beer, C.H., Harris, C., Reid, D.L., Romer, R.L., 2011. Geochemistry of the Early Cretaceous Koegel Fontein Anorogenic Igneous Complex, South Africa. South African J. Geol. 114, 1–26. doi:10.2113/gssajg.114.2.000

de Beer, C.H., 2010. 3017 Garies. Council for Geoscience: 1:250 000 Geological Series.

de Beer, C.H., 2001. 3118 Calvinia. Council for Geoscience: 1:250 000 Geological Series.

Eiler, J.M., 2001. Oxygen Isotope Variations of Basaltic Lavas and Upper Mantle Rocks. Rev. Mineral. Geochemistry 43, 319–364.

Faulkner, D.R., Jackson, C.A.L., Lunn, R.J., Schlische, R.W., Shipton, Z.K., Wibberley, C.A.J., Withjack, M.O., 2010. A review of recent developments concerning the structure, mechanics and fluid flow properties of fault zones. J. Struct. Geol. 32, 1557–1575. doi:10.1016/j.jsg.2010.06.009

Fölling, P.G., Frimmel, H.E., 2002. Chemostratigraphic correlation of carbonate successions in the Gariep and Saldania Belts, Namibia and South Africa. Basin Res. 14, 69–88. doi:10.1046/j.1365-2117.2002.00167.x

Frimmel, H.E., Fölling, P.G., Diamond, R., 2001. Metamorphism of the Permo-Triassic Cape Fold Belt and its basement, South Africa. Mineral. Petrol. 73, 325–346.

Frimmel, H.E., Fölling, P.G., Eriksson, P.G., 2002. Neoproterozoic tectonic and climatic evolution recorded in the Gariep Belt , Namibia and South Africa. Basin Res. 14, 55–67.

Frimmel, H.E., Frank, W., 1998. Neoproterozoic tectono-thermal evolution of the Gariep Belt and its basement , Namibia and South Africa. Precambrian Res. 90, 1–28.

Germs, G.J.B., Gaucher, C., 2012. NATURE AND EXTENT OF A LATE EDIACARAN (CA . 547 MA) GLACIGENIC EROSION SURFACE IN SOUTHERN AFRICA. South African J. Geol. 115, 91–102. doi:10.2113/gssajg.115.91

Gregory, R.T., Criss, R.E., Taylor, H.P., 1989. Oxygen Isotope Exchange Kinetics of Mineral Pairs: Applications to Problems of Hydrothermal Alteration of Igneous Rocks and Precambrian Iron Formations. Chem. Geol. 75, 1–42.

Gregory, R.T., Taylor, H.P., 1981. An Oxygen Isotope Profile in a Section of Cretaceous Oceanic Crust, Samail Ophiolite, Oman: Evidence for d18O Buffering of the Oceans by Deep (>5 km) Seawater-Hydrothermal Circulation at Mid-Ocean Ridges. J. Geophys. Res. 86, 2737–2755.

Harris, C., 1995. Oxygen isotope geochemistry of the Mesozoic anorogenic complexes of Oxygen isotope geochemistry of the Mesozoic anorogenic complexes of Damaraland , northwest Namibia : evidence for crustal contamination and its effect on silica saturation. Contrib. to Miner. Petrol. 122, 308–321. doi:10.1007/s004100050130

Harris, C., Ashwal, L.D., 2002. The origin of low δ18O granites and related rocks from the Seychelles. Contrib. to Miner. Petrol. 143, 366–376. doi:10.1007/s00410-002-0349-6

Harris, C., Vogeli, J., 2010. Oxygen isotope composition of garnet in the Peninsula Granite, Cape Granite Suite, South Africa: Constraints on melting and emplacement mechanisms. South African J. Geol. 113, 385–397. doi:10.2113/gssajg.113.4.401

Hoffman, P.F., Schrag, D.P., 2002. The snowball Earth hypothesis : testing the limits of global change. Terra Nov. 14, 129–155. doi:10.1080/713604466

Holland, T.J.B., Powell, R., 2011. An improved and extended internally consistent thermodynamic dataset for phases of petrological interest, involving a new equation of state for solids. J. Metamorph. Geol. 29, 333–383.

Jacobs, J., Pisarevsky, S., Thomas, R.J., Becker, T., 2008. The Kalahari Craton during the assembly and dispersal of Rodinia. Precambrian Res. 160, 142–158. doi:10.1016/j.precamres.2007.04.022

Larson, P.B., Zimmerman, B.S., 1991. Variations in δ18O values , water frock ratios , and water flux in the Rico paleothermal anomaly , Colorado. Geochemical Soc. Spec. Publ. 3, 463–469.

Li, Z.-X., Evans, D.A.D., Halverson, G.P., 2013. Neoproterozoic glaciations in a revised global palaeogeography from the breakup of Rodinia to the assembly of Gondwanaland. Sediment. Geol. 294, 219–232. doi:10.1016/j.sedgeo.2013.05.016

Macey, P.H., Minnaar, H., 2010. 3018 Loeriesfontein. Council for Geoscience: 1:250 000 Geological Series.

Marsh, J.S., 1973. Relationships between Transform Directions and Alkaline Igneous Rock Lineaments in Africa and South America. Earth Planet. Sci. Lett. 18, 317–323.

Matsuhisa, Y., Goldsmith, J.R., Clayton, R.N., 1979. Oxygen isotopic fractionation in the system quartz-albite-anorthite-water. Geochim. Cosmochim. Acta 43, 1131–1140.

Maus, S., Barckhausen, U., Berkenbosch, H., Bournas, N., Brozena, J., Childers, V., Dostaler, F., Fairhead, J., Finn, C., von Frese, R., Gaina, C., Golynsky, S., 2009. A 2-arc min resolution Earth Magnetic Anomaly Grid compiled from satellite, airborne, and marine magnetic measurements. Geochemistry Geophys. Geosystems, Tech. Br. 10, 1–12.

McCaig, A.M., 1988. Deep fluid circulation in fault zones. Geology 16, 867–870.

Mccaig, A.M., Wickham, S.M., Taylor, H.P., 1990. Deep fluid circulation in alpine shear zones , Pyrenees , France : field and oxygen isotope studies. Contrib. to Miner. Petrol. 106, 41–60.

Meert, J.G., 2003. A synopsis of events related to the assembly of Eastern Gondwana. Tectonophysics 362, 1–40. doi:10.1016/S0040-1951(02)00629-7

Menzies, C.D., Teagle, D.A.H., Craw, D., Cox, S.C., Boyce, A.J., Barrie, C.D., Roberts, S., 2014. Incursion of meteoric waters into the ductile regime in an active orogen. Earth Planet. Sci. Lett. 399, 1–13. doi:10.1016/j.epsl.2014.04.046

Milner, S.C., le Roux, A.P., O'Connor, J.M., 1995. Age of Mesozoic igneous rocks in northwestern Namibia, and their relationship to continental breakup. J. Geol. Scociety, London 152, 97–104.

Mudzanani, L., 2011. Origin of low d18O in the Koegel Fontein Complex roof zone. University of Cape Town.

Munz, I.A., Yardley, B.W.D., Banks, D.A., Wayne, D., 1995. Deep penetration of sedimentary fluids in basement rocks from southern Norway : Evidence from hydrocarbon and brine inclusions in quartz veins. Geochim. Cosmochim. Acta 59, 239–254.

Norton, D., Taylor, H.P., 1979. Quantitative Simulation of the Hydrothermal Systems of Crystallizing Magmas on the Basis of Transport Theory and Oxygen Isotope Data : An analysis of the Skaergaard Intrusion. J. Petrol. 20, 421–486.

Olianti, C.A.E., Harris, C., 2018. A low- δ 18 O intrusive breccia from Koegel Fontein , South Africa : Remobilisation of basement that was hydrothermally altered during global glaciation ? Lithos 300, 33–50. doi:10.1016/j.lithos.2017.12.006

Scotese, C.R., Boucot, A.J., Mckerrow, W.S., 1999. Gondwanan palæogeography and palæoclimatology. J. African Earth Sci. 28, 99–114. doi:10.1016/S0899-5362(98)00084-0

Sharp, Z., 2007. Principles of Stable Isotope Geochemistry. Pearson Education, Inc. Pearson.

Tohver, E., Agrella-Filho, M.S. D', Trindade, R.I.F., 2006. Paleomagnetic record of Africa and

South America for the 1200-500 Ma interval, and evaluation of Rodinia and Gondwana ... Paleomagnetic record of Africa and South America for the 1200 – 500 Ma interval, and evaluation of Rodinia and Gondwana assemblies. Precambrian Res. 147, 193–222. doi:10.1016/j.precamres.2006.01.015

Trumbull, R.B., Harris, C., Frindt, S., Wigand, M., 2004. Oxygen and neodymium isotope evidence for source diversity in Cretaceous anorogenic granites from Namibia and implications for A-type granite genesis. Lithos 73, 21–40. doi:10.1016/j.lithos.2003.10.006

Trumbull, R.B., Reid, D.L., De Beer, C., van Acken, D., Romer, R.L., 2007. Magmatism and continental breakup at the west margin of southern Africa: A geochemical comparison of dolerite dikes from northwestern Namibia and the Western Cape. South African J. Geol. 110, 477–502. doi:10.2113/gssajg.110.2-3.477.

Tullis, J., 2002. Deformation of Granitic Rocks: Experimental Studies and Natural Examples. Rev. Mineral. Geochemistry 51, 51–95.

White, R.W., Powell, R., Holland, T.J.B., Johnson, T.E., Green, E.C.R., 2014. New mineral activity–composition relations for thermodynamic calculations in metapelitic systems. J. Metamorph. Geol. 32, 261–286.

Will, T.M., Frimmel, H.E., 2013. The Influence of Inherited Structures on Dike Emplacement during Gondwana Breakup in Southwestern Africa. J. Geol. 121, 455–474. doi:10.1086/671398

Yardley, B., Gleeson, S., Bruce, S., Banks, D., 2000. Origin of retrograde fluids in metamorphic rocks. J. Geochemical Explor. 69, 281–285.

Zheng, Y.-F., 1993. Calculation of oxygen isotope fractionation in anhydrous silicate minerals. Geochim. Cosmochim. Acta 57.

Appendix

Table 7. Magnetic susceptibility of the samples measured by lithology. Each sample was measured 8 times with a hand-held magnetic susceptibility meter. The mean and standard deviation (σ) of the magnetic susceptibility is given for 8 analyses per sample. BR = breccia plug, GN = Jakkalshoek Gneiss, QP = quartz porphyry dyke, RG = Rietpoort Granite and SZ = Brak Fontein Shear Zone.

Sample	Lithology	Mean	σ
COK164	BR	1.36	0.047893
COK175	BR	0.95	0.272958
COK205	BR	0.25	0.055143
KB246	GN	0.89	0.119791
KB244	GN	2.90	2.200426
unnamed coastal gneiss	GN	4.66	1.591673
KB288A	GN	1.04	0.304551
KB269	GN	0.32	0.081548
KB285	GN	0.11	0.03935
KB317	GN	4.11	1.696902
KB235	GN	0.39	0.063332
CHK136	QP	2.89	0.623353
CHK137	QP	0.35	0.250047
CHK78	RG	2.95	0.20718
CHK74	RG	1.17	0.057009
CHK101	RG	0.50	0.107464
CHK59	RG	1.76	0.145897
KB267	SZ	0.26	0.077539
KB286	SZ	0.82	0.551565
KB314	SZ	0.33	0.086057
KB299	SZ	1.14	0.226777
KB310	SZ	20.93	3.995857
KB295	SZ	1.15	2.090307
KB276	SZ	4.80	0.934779
KB290	SZ	0.07	0.020272
KB255	SZ	6.27	1.206554

Table 8. Normalised bulk chemistry of Jakkalshoek Granite from the roof pendant of the Rietpoort Granite previously analysed by Mudzanani (2011). *The normalised mean of wt% oxides and standard deviation of wt% oxides is given. The mean wt% oxides were used for determining a normalised bulk relevant to the MnNCKFMASHT system (Table 5) which was used to calculate pseudosections in Perple_X (Figure 31).*

Sample	SiO_2	TiO_2	Al_2O_3	Fe_2O_3	MnO	MgO	CaO	Na_2O	K_2O	P_2O_5	SO_3	Comments
KRL01	68.26	0.83	14.44	4.87	0.06	0.72	2.03	3.04	5.45	0.30	0.02	augen gneiss
KRL02	75.94	0.47	11.16	3.20	0.03	0.33	0.86	2.54	5.27	0.17	0.02	augen gneiss
KRL03	70.04	0.70	13.46	5.34	0.05	0.63	2.13	2.52	4.83	0.27	0.02	augen gneiss
KRL04	70.77	0.46	14.19	3.34	0.03	0.52	1.59	2.42	6.49	0.17	0.02	augen gneiss
KRL05	78.20	0.20	11.44	1.52	0.00	0.01	0.36	1.73	6.49	0.02	0.02	augen gneiss
KRL06	71.54	0.56	13.27	4.21	0.05	0.44	1.73	2.55	5.43	0.20	0.02	sheared gneiss
KRL07	70.37	0.61	14.60	3.38	0.05	0.43	1.62	2.35	6.33	0.23	0.02	augen gneiss
KRL08	74.00	0.28	13.77	1.61	0.01	0.32	0.92	2.94	6.07	0.06	0.02	sheared gneiss
KRL09	70.01	0.54	14.58	3.44	0.04	0.56	1.58	2.97	6.05	0.20	0.02	augen gneiss
KRL10	69.83	0.69	13.59	4.89	0.06	0.58	2.41	2.48	5.18	0.27	0.02	augen gneiss
mean	71.89	0.54	13.45	3.58	0.04	0.45	1.52	2.55	5.76	0.19	0.02	normalised to 100
σ	2.98	0.18	1.16	1.24	0.02	0.19	0.60	0.36	0.57	0.08	0.00	standard deviation

Koegel Fontein Complex
1 : 50 000

Field maps 3117 BA BB Ruitersvlei and 3017 DD Kot esrus mapped by Coenie De Beer (CGS) and digitised by Benjamin Whitehead

GEOLOGICAL LEGEND

METAMORPHIC, SEDIMENTARY AND VOLCANIC ROCKS | IGNEOUS ROCKS

GROUP | FORMATION

QUATERNARY

Q

PALAEOGENE

Tbf Olivine melilitite and nephelinite plug

[EARLY] CRETACEOUS

Tsa Sandkopsdrif Complex*

BIESJES FONTEIN SUITE*

Kr Rietpoort Granite*

Kkr Kruisvlei Quartz Porphyry* — 133.6±1.3 Ma (U-Pb SHRIMP Zircon, De Beer and Armstrong, 1998)

Kb Breccia Plug

Kke Kerskloof Bostonite*

Krb Ribbokrug Alkali Syenite

Kro Rooivlieitjie Granite*

Ksa Sandkop Syenite* — 144±2 Ma (U-Pb SHRIMP Zircon, De Beer and Armstrong, 1998)

KOEGEL FONTEIN COMPLEX

Kf FALSE BAY DOLERITE SUITE

NAMIBIAN

GARIEP SUPERGROUP

VANRHYNSDORP

Nar Arkose, grit, siltstone, vein quartz conglomerate, phyllite

GIFBERG

Nwi Limestone and dolomitic marble

Arondegas*

Aties*

Wildouw*

Karoetjes Kop*

MOKOLIAN

Nkr Conglomerate, diamictite, quartzite, biotite schist

Ngar Garies Granite*

Nbk Bloukop Granite*

Nkh Kliphoek Granite*

Njk Jakkalshoek Granite*

1065±2 Ma (U-Pb TIMS Zircon, Thomas et al., 1996)

SPEKTAKEL SUITE

KAMIESBERG **

Mks Quartz-muscovite-biotite-garnet ±kyanite±staurolite schist

Mkp Metapelitic gneiss, biotite gneiss

Mkq Metaquartzite (feldspathic, glassy, ferruginous), leucogneiss

Nme Meesklip Gneiss*

Grey leucogneiss and biotite gneiss, augen gneiss

Nhb Hunboom Gneiss*

±1170 Ma (pro) (U-Pb SHRIMP Zircon, De Beer and Armstrong, unpublished data)

LITTLE NAMAQUALAND SUITE

* Not approved by SACS

** Age uncertain, formations not in stratigraphic order

LITHOLOGY

Q	Quarternary Cover
Tbf	Olivine melilitite and nephelinite plug
Kr	Alkali feldspar leucogranite
Kkr	Quartz porphyry dyke
Kke	Microsyenite, quartz-microsyenite
Kb	Plug forming breccia rock
Krb	Aegerine syenite and/or fenite
Kro	Coarse alkali feldspar leucogranite
Ksa	Quartz-hornblende syenite, quartz-biotite syenite
Kf	Dolerite
Nar	Arkose, grit, siltstone, vein quartz conglomerate, phyllite
Nat	White quartzite, graphitic phyllite, iron gossans
Nwi	Limestone and dolomitic marble
Nkr	Conglomerate, diamictite, quartzite, biotite schist
Ngar	Mesocratic to leucocratic, equigranular to small porphyritic, schlieric granite
Nbk	Blue-grey megacrystic granite
Nkh	Grey-green, megacrystic granite
Njk	Leucocratic, megacrystic granite to gneissic granite
Mk	See legend
Nme	Pink augen gneiss, equigranular gneiss and leucogneiss
Nhb	Grey equigranular biotite and quartz-feldspar gneiss, augen gneiss

Structural Symbols

Lineation — Foliation — Shear Zone — Fault — Vein

N

April 2017

WGS 1984

0 5 10 Km

17 40 | 17 45 | 17 50 | 17 55 | 18 0

31 0 S | 31 5 S | 31 10 S | 30 50 S | 30 55 S